

**Structural and functional studies of α M-conotoxin
RIIK interaction with *Shaker*-related potassium
channels from trout fish (*TSha1*)**

Dissertation zur Erlangung des Grades eines Doktors der Naturwissenschaften

-Dr. rer. nat.-

dem Fachbereich Biologie/Chemie der

Universität Bremen

vorgelegt von

Ahmed Nafi' (Sulaiman) Al-Sabi'

Bremen

November 2004

Die vorliegende Arbeit wurde in der Zeit von Oktober 2001 bis November 2004 am Max-Planck-Institut für Experimentelle Medizin in Göttingen angefertigt.

1. Gutachter: Prof. Dr. Venugopalan Ittekkot

2. Gutachter: Prof. Dr. Heinrich Terlau

Tag des Promotionskolloquiums: 04. November 2004



To my father & mother

sisters & brothers

LIST OF CONTENTS

LIST OF CONTENTS	i
LIST OF TABLES AND FIGURES	iv
ABBREVIATIONS	vi
CHAPTER ONE: INTRODUCTION	1
1.1. Voltage-gated ion channels	1
1.1.1. Voltage-gated potassium channels (VGKC)	3
1.1.2. Structural and functional studies of VGKC	6
1.2. Conopeptides	8
1.2.1. Cone snails: the source of conopeptides	8
1.2.2. Conopeptides and conotoxins	10
1.2.3. Conotoxins targeting VGKC and dyad hypothesis	12
1.3. Objectives	15
CHAPTER TWO: MATERIALS AND METHODS	16
2.1. Electrophysiological methods	16
2.1.1. <i>Xenopus</i> oocyte preparation	16
2.1.1.1. <i>Xenopus</i> oocyte solutions	16
2.1.1.2. <i>Xenopus</i> oocytes handling	16
2.1.2. Two-electrode voltage clamp (TEVC)	20
2.1.2.1. Instrumentation	21
2.1.2.2. Micropipettes and electrodes	22
2.1.2.3. TEVC stimulation protocols	23
2.1.2.3.1. Single pulse (I-V) protocol	23
2.1.2.3.2. Double pulse (DP) protocol	24
2.1.2.3.3. Leakage and capacitive current correction	24
2.2. Molecular Biology	25
2.2.1. Vector ligation	26
2.2.2. <i>TShal</i> DNA Transformation	27
2.2.3. Bacterial culture	27
2.2.4. Plasmid isolation	28

2.2.5. Restriction enzyme digestion	28
2.2.6. Agarose gel electrophoresis	28
2.2.7. Mutagenic primer design and PCR amplification	29
2.2.8. Plasmid transformation	30
2.2.9. Plasmid isolation and linearization	30
2.2.10. <i>In vitro</i> transcription	32
2.3. Data analysis	33
CHAPTER THREE: RESULTS	36
3.1. \squareM-R111K interacting with <i>Shaker</i>-type K⁺ channels	36
3.1.1. \square M-R111K specificity interacts with <i>TShal</i> channels	36
3.1.1.1. Determining IC ₅₀ of open state block	36
3.1.1.2. Interaction at different extracellular K ⁺ concentrations	36
3.1.2. \square M-R111K interacts with mammalian Kv1.2	38
3.1.2.1. Determining IC ₅₀ of open state block of Kv1.2	39
3.1.2.2. Inhibition of Kv1.2 mediated currents is state dependent	40
3.2. Alanine scanning mutagenesis	44
3.2.1. Identification of the residues important for \square M-R111K	44
3.2.2. Evaluation of additional substitution mutations at Leu1	47
3.2.3. \square M-R111K analogs affect the binding kinetics	49
3.2.4. \square M-R111K mutants do not interact with Nav1.4 sodium channel	53
3.3. Mutant cycle analysis	55
3.3.1. <i>TShal</i> mutant channels	56
3.3.2. Determining IC ₅₀ values of the mutant cycle analysis	59
3.3.3. Docking model of \square M-R111K interaction with <i>TShal</i>	63
CHAPTER FOUR: DISCUSSION	64
4.1. \squareM-R111K: a peptide blocking K⁺ channels	64
4.1.1. \square M-R111K specificity interacts with the pore <i>TShal</i> channels	64
4.1.2. \square M-R111K binding is altered by [K ⁺] _o	64
4.1.3. \square M-R111K: first conotoxin targeting mammalian Kv1.2	65
4.1.4. \square M-R111K mutants affect kinetics of binding	67

4.1.5. \square M-R111K mutants do not interact with Nav1.4 sodium channel	68
4.2. \squareM-R111K: novel structure among conotoxins	69
4.2.1. Structure of \square M-conotoxin R111K	69
4.2.2. Comparison between \square M-R111K and members of M-superfamily	69
4.3. Identification of \squareM-R111K pharmacophore	71
4.3.1. \square M-R111K pharmacophore is not organized around a dyad motif	71
4.3.2. \square M-R111K <i>pharmacophore</i> is a planar ring of four residues	73
4.4. Mutant cycle analysis	75
4.4.1. <i>TSha1</i> mutant channels	76
4.4.2. Determinin IC_{50} and $\square\square$ G of the mutant cycle analysis	77
4.4.3. The lid docking model of \square M-R111K- <i>TSha1</i>	77
CHAPTER FIVE: SUMMARY	82
CHAPTER SIX: REFERENCES	84
ACKNOWLEDGEMENTS	93
Curriculum Vitae et studiorum	94

LIST OF TABLES AND FIGURES

LIST OF TABLES

Table 2.1. Primer sequences of <i>TShal</i> point mutation.	31
Table 2.2. The transcription mixture	32
Table 3.1. The effect of \square M-RIIK interaction with <i>TShal</i> K ⁺ channels under different extracellular K ⁺ concentrations	38
Table 3.2. Summary of K _D , k _{on} and k _{off} values for open and close states of human Kv1.2 and <i>TShal</i> K ⁺ channels	42
Table 3.3. IC ₅₀ Values for <i>TShal</i> K ⁺ block of \square M-RIIK and Analogs	44
Table 3.4. Mutations of Leu1 affect the affinity of \square M-RIIK for the <i>TShal</i> K ⁺ Channel	48
Table 3.5. Summary of Association and dissociation rate constants of \square M-RIIK analogs	50
Table 3.6. Summary of Association and dissociation rate constants of \square M-RIIK Hyp15 mutants	52
Table 3.7. IC ₅₀ Values for <i>TShal</i> mutant K ⁺ block of \square M-RIIK WT	57
Table 3.8. IC ₅₀ Values for <i>TShal</i> mutant K ⁺ block of \square M-RIIK WT and analogs	59
Table 3.9. Summary of IC ₅₀ , \square and \square \square G values to identify the toxin binding orientation	63

LIST OF FIGURES

Figure 1.1. Schematic representation of the proposed transmembrane topology of voltage gated ion channels.	2
Figure 1.2. Inactivation mechanisms	3
Figure 1.3. The three-dimensional structures of potassium channels.	5
Figure 1.4. Cone snails.	9
Figure 1.5. Organizational diagram for <i>Conus</i> peptides.	10
Figure 1.6. Sequence alignment of \square M-RIIK with other M-superfamily peptides.	14
Figure 2.1. The artificial expression of ion channels on the membrane of <i>Xenopus laevis</i> oocytes	19
Figure 2.2. Schematic diagram of the main components of the two-electrode voltage clamp (TEVC).	21

Figure 2.3. Single pulse (IV) protocol.	24
Figure 2.4. Double pulse protocol.	24
Figure 2.5. Schematic representation of the site-directed mutagenesis to produce cRNA of <i>TShal</i> channel with selected mutation.	25
Figure 2.6. Schematic representation of the pSGEM vector and <i>TShal</i> ORF DNA	26
Figure 3.1. \square M-R111K reversibly blocks <i>TShal</i> -mediated currents	37
Figure 3.2. The effect of external potassium concentration ($[K]_0$) on the binding affinity of \square M-R111K to <i>TShal</i> -channels	38
Figure 3.3. \square M-R111K reversibly blocks <i>TShal</i> -mediated currents	39
Figure 3.4. Dose–response curve of the block of Kv1.2 mediated steadystate currents by \square M-R111K	40
Figure 3.5. The block of \square M-R111K of Kv1.2 is state dependent	41
Figure 3.6. Relaxation of \square M-R111K binding to closed Kv1.2 channels measured by a double pulse stimulation	43
Figure 3.7. The summary of the alanine mutagenesis assay	45
Figure 3.8. Mutation of residues L1, R10, K18, and R19 results in isoforms of \square M-R111K with low affinity for <i>TShal</i> channels	46
Figure 3.9. Changes in the affinity of the mutants of \square M-R111K at Leu1 position	49
Figure 3.10. \square M-R111K mutants do <i>not</i> block Nav1.4 mediated currents	53
Figure 3.11. The amino acid alignment of the pore region of the <i>Shaker</i> K ⁺ channel (S5-S6 linker) and the corresponding region of <i>TShal</i> K ⁺ channel	56
Figure 3.12. Influence of single point mutations in the pore region of <i>TShal</i> on \square M-R111K binding	58
Figure 3.13. Effect of point mutations of pore region of <i>TShal</i> channels on \square M-R111K binding. Whole-cell	58
Figure 3.14. Examples for mutant cycles of <i>TShal</i> E354 with \square M-R111K-Arg10	60
Figure 3.15. Summary of mutant cycle analysis	62
Figure 4.1. Superimposition of the 13 lowest-energy structures of \square M-R111K	69
Figure 4.2. The three-dimensional NMR structures of M superfamily representatives	70
Figure 4.3. Electrostatic surface potential for \square M-R111K	74
Figure 4.4. Close view of \square M-R111K- <i>TShal</i> docking model obtained from mutant cycle analysis	78
Figure 4.5. Orientation of \square M-R111K- <i>TShal</i> (lid) docking model obtained from mutant cycle analysis	80

ABBREVIATIONS

A	adenine	EDTA	Ethylenediamine tetracetic acid
A, Ala	Alanine	EGTA	Ethylenglycol-bis(β-aminoethylether) N,N,N',N'-Tetraacetic acid
A	Ampere	<i>et al.</i>	<i>et alii</i>
Å	Angstrom (10 ⁻¹⁰)	F, phe	phenylalanine
aa	amino acid	Fig, fig.	Figure
bp	base pair	g	gram
°C	degree Celsius	G	guanine
C	cytosine	G, Gly	glycine
C-, COOH-	carboxy terminus of terminus protein	H, His	Histidine
C, Cys	cysteine	h, hrs	hour(s)
Ca²⁺	calcium ion	H₂O	water
cDNA	complementary desoxyribonucleic acid	Hepes	N-2- Hydroxyethylpiperazine-N'-2-ethanesulfonic acid
Cl⁻	chloride ion	Hyp	hydroxyproline
CNS	central nervous system	Hz	hertz
cRNA	complementary RNA (ribonucleic acid)	I	current
CTX	Charybdotoxin (β-KTx)	I, Ile	Isoleucine
D, asp	aspartic acid	IC₅₀	half maximal inhibitory dose
d.(d).H₂O	Distilled (double distilled) water.	IV	current voltage relationship
DEPC	diethylpyrocarbonate	K	Kalven degree
DNA	desoxyribonucleic acid	K	Kilo (10 ³)
DNase	desoxyribo nuclease	K, lys	Lysine
dNTPs	desoxynucleoside triphosphate	K⁺	potassium ion
E, glu	glutamic acid, glutamate	kb	kilo base pair
e.g.	(<i>exempli gratia</i>); for example, for instance.	KcsA	K ⁺ channel from <i>Streptomyces levidans</i>

K_D	dissociation constant	P, Pro	Proline
kDa	kilo dalton	PCR	polymerase chain reaction
K^(O), K^(c)	dissociation constant for the open or close channel	Pfu	<i>Pyrococcus furiosus</i>
k_{off}^O, k_{off}^C	dissociation rate for the open or closed channel	pH	negative of the logarithm of the proton ion concentration
k_{on}^O, k_{on}^C	2 nd order association rate for the open or closed channel	pI	Isoelectric point
K_v	voltage gated potassium channel	Q, Gln	Glutamine
[K⁺]_o	extracellular K ⁺ concentration	R, Arg	arginine
L, Leu	Leucine	RNase	ribonuclease
L, l	liter	rpm	revolutions per minute
LB	Luria Broth	S, Ser	serine
m	milli (10 ⁻³)	s, sec	seconds
M, Met	Methionine	S.D.	standard deviation
M	molarity	SDS	sodium dodecyl sulfate
MES	(2-(4-morpholino)-ethane sulfonic acid)	S.E.(M.)	Standard error (of the mean)
min	minute(s)	Shaker-wt,	<i>Shaker</i> wild type,
N, Asn	Asparagine	T, Thr	Threonine
n , N	number of independent experiments	Tyr	Tyrosine
n	nano (10 ⁻⁹)	[T]	toxin concentration
N-, NH₂- terminus	amino terminus of a protein	Taq	<i>Thermus aquaticus</i>
Na⁺	sodium ion	TBE	Tris Boric acid EDTA buffer
Na_v	voltage gated sodium channel	TEA	Tetraethylammonium
NFR	normal frog Ringer	TEVC	two-electrode voltage clamp
O	4-hydroxyproline	T, Thr	Threonine
ORF	open reading frame	Ti	interpulse interval
Osmo	Osmolarity	Tricaine	3-aminobenzoic acid ethyl- ester
		Tris ,	Tris (hydroxymethyl)- aminomethane
		Tris-Base	
		TShal	Trout <i>Shaker</i> related K ⁺ channel.

U_o, U_c	unblock probability for open and closed channel	W, Trp	Tryptophane
V, val.	valine	WT, wt	wild type
V	potential in volts	Y, Tyr	Tyrosine
v/v	volume to volume.	ΔΔG	Gibbs free energy
V_{comm}	voltage command	μ-PVIIA	μ-conotoxin PVIIA
V_H	holding potential	μ	micro (10 ⁻⁶)
VGIC	voltage-gated ion channel(s)	μ-conotoxin	mu-conotoxin family

CHAPTER ONE: Introduction

1.1. Voltage-gated ion channels

Ion channels are membrane embedded proteins that mediate fast and selective ion transport across biological membranes and thereby have diverse physiological functions in a given cell. Throughout the biological world, these proteins form small, water-filled pores that allow selective flux of ions along their electrochemical gradient (Terlau and Stühmer, 1998; Hille, 2001).

Ion-selective pores were originally proposed in the classic experiments of Hodgkin and Huxley to explain separate components of Na^+ , K^+ and leak currents (Hodgkin and Huxley, 1952). Each channel is selective to conduct a particular class of ions (Na^+ , K^+ , Ca^{2+} and Cl^-) as a response to different stimuli that induce the opening and closing of the pore in a mechanism called gating. The gating mechanism can be activated by chemicals (ligands), mechanical deformation of the membrane or by changing the membrane potential voltage. Thus, ion channels can be grouped according to their ion selectivity and mode of gating into families. For example, voltage-gated K^+ channels are activated by depolarization of the membrane potential resulting in conformational changes that allow K^+ ions to permeate (Hille, 2001; Armstrong and Hill, 1998). Channels that are activated by voltage and selective for potassium ions are called Kv channels, likewise, those selective to sodium and calcium channels are Nav and Cav, respectively (Catterall *et al.*, 2003).

Based on the cloning of genes encoding voltage-gated ion channels, it became clear that the primary structures of these channels share several structural similarities. The main pore-forming α -subunit of voltage-gated ion channels (Fig. 1.1) consists functionally of either a single α -subunit containing four homologous domains (Na^+ and Ca^{2+} channels) or four distinct α -subunits (K^+ channels). The latter may be either a homomeric or heteromeric tetramer (MacKinnon, 1991). The α -subunit is composed of six highly hydrophobic transmembrane segments S1-S6. The S5-S6 segments are connected through the extracellular side of the membrane by a loop that forms the pore, called the P-loop. This loop is directly involved in the conductance pathway and formation of the selectivity filter. The α -subunits interact with auxiliary subunits for modulatory effects (Rettig *et al.*, 1994).

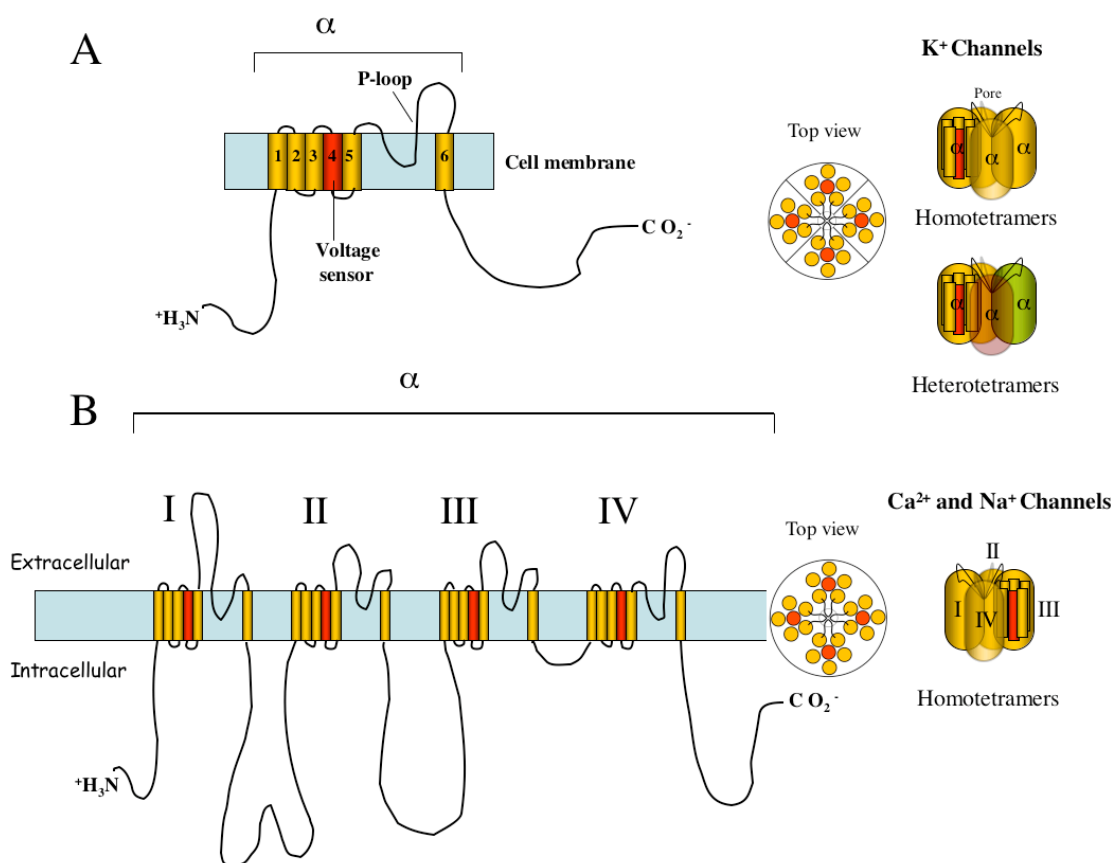


FIGURE 1.1. Schematic representation of the proposed transmembrane topology of voltage gated ion channels. **(A)** The α -subunit of K^+ channels showing the transmembrane segments (1-6) spanning the cell membrane. The segment 4 (red color) represents the voltage sensor. In the extracellular region appears the S5-S6 P-loop link that directly involved in the ion conduction pathway. In the intracellular region appears the N and C termini ends of the polypeptide. The right panel shows top and side views of homo- or heterotetramers of encircled four-fold α -subunits to form the central ion conduction pathway of a K^+ channel. **(B)** A single α -subunit polypeptide of 4 homologous domains (I-IV) forming functional pore of Ca^{2+} and Na^+ channels.

To regulate the gating of ion permeation, the structure of voltage-gated ion channels must be equipped with a charged transmembrane domain suitable to detect membrane potential changes. This voltage sensor has been identified as a series of highly conserved positively charged amino acids in the 4th transmembrane segment (S4). Upon depolarization, the sensor reacts by displacement of these charged residues resulting in a set of conformational changes in the protein. Finally, this (gating) process leads to opening of the pore resulting in ion conduction through the channel (Armstrong and Hill, 1998).

When the membrane is depolarized, some voltage-gated ion channels first open and then enter a non-conducting, ‘inactivated’ state. This inactivation process influences some key signaling properties of excitable cells, such as action potential duration, shape and firing

frequency. Inactivation may occur by at least two distinct mechanisms: fast N-type or slow C-type inactivation (Fig. 1.2). In K^+ channels, the N-type inactivation involves a region near the amino terminus, which forms a tethered inactivation particle that can block the internal mouth of the channel once it has opened (Hoshi *et al.*, 1990; Zagotta *et al.*, 1990). This “ball and chain” model mechanism was previously proposed for the fast inactivation of Na^+ channels (Armstrong and Bezanilla, 1977). In Na^+ channels, a hydrophobic motif of triplet residues (IFM) in the III-IV linker is crucial to fast inactivation (West *et al.*, 1992). The IFM motif has been suggested to function as a “latch” that holds the fast inactivation gate shut as a hinged lid model (Vassilev *et al.*, 1988). In contrast to N-type inactivation, in the C-type inactivation, rearrangement of the pore rather than motion of a cytoplasmic region of a channel is likely to play central role.

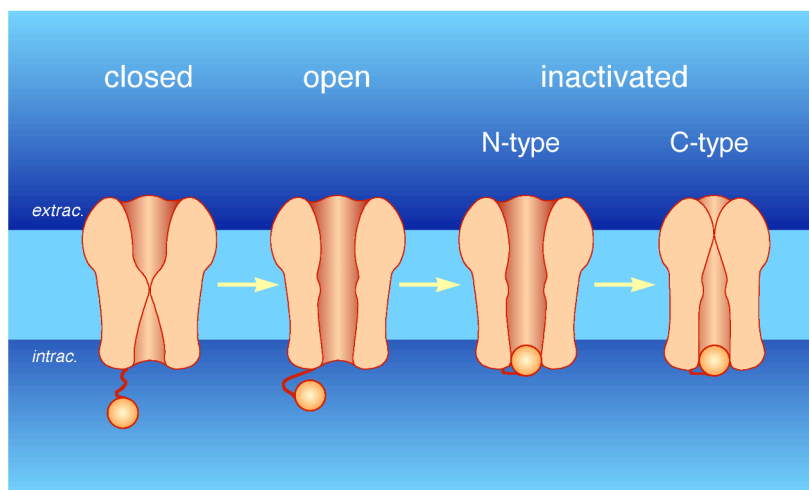


FIGURE 1.2. Inactivation mechanisms. Ion channels may can be inactivate from the open state by additional conformational changes leading to non conducting state. For K^+ channel, two inactivation mechanisms have been identified: a fast N-type and slow C-type of inactivation. (Adapted from Terlau and Stühmer, 1998).

1.1.1. Voltage-gated K^+ channels (VGKCs)

Potassium channels are ubiquitously expressed in excitable and nonexcitable tissues of organisms from bacteria to humans (Rudy, 1988). In excitable tissues, K^+ channels are involved in diverse physiological functions, such as setting the membrane resting potential and controlling shape and frequency of action potentials (Rudy, 1988; Hille, 2001). Furthermore, they take part in muscle contraction, cardiac pacemaking and hormone secretion (Hille, 2001). In nonexcitable cells, K^+ channels play an important role in cell proliferation, cell volume regulation and lymphocyte differentiation (Lewis and Cahalan,

1995). As K⁺ channels play fundamental roles in the regulation of membrane excitability, it is to be expected that both genetic and acquired diseases involving altered functioning of neurons, smooth muscle, and cardiac cells could arise subsequent to abnormalities in K⁺ channel proteins. Genetically linked diseases of the cardiac, neuronal, renal, and metabolic systems involving members of voltage-gated K⁺ channels "VGKCs" (see Char-Chang *et al.*, 2000)

Potassium channels conduct K⁺ ions across the cell membrane along the electrochemical gradient at a rate approaching the diffusion limit (up to 100 million ions per second). To approach this rate, the structure of K⁺ channels provides excellent solution of temporal control over the permeation selectivity. Like any ion channel, the amphiphilic character and the large size of these proteins made them relatively difficult to be solved as three-dimensional structures by X-ray crystallography or nuclear magnetic resonance (NMR). Recently, structural data of the pore region of a K⁺ channel from *Streptomyces lividans* (KcsA) have been obtained by X-ray crystallography (Doyle *et al.*, 1998; Fig. 1.3A). Followed by three-dimensional structures of two potassium channels were elucidated, the *Shaker* K⁺ channel from fruit fly *Drosophila melanogaster* (Sokolova *et al.*, 2001; Fig. 1.3B) and calcium-gated potassium channel from the archeon *Methanobacterium thermoautotrophicum* (MthK channel; Fig. 1.3C). The first was solved using electron microscopy (Jiang *et al.*, 2002). Most recently, X-ray crystal structure of the full-length voltage-gated K⁺ channel at a resolution of 3.2 Å from thermophilic archaeobacteria *Aeropyrum pernix* (KvAP) was determined (Jiang *et al.*, 2003; Fig. 1.3D and E). These structures have answered many questions concerning basic mechanisms of K⁺ channel function such as ion conduction selectivity, gating and voltage sensing (for review; MacKinnon, 2003).

Potassium channels represent a diverse group of ion channels that coded from around 80 genes. Mutations within a potassium channel gene inducing behavioural and electrical abnormalities led to the first cloning of a K⁺ channel from the *Drosophila* mutant *Shaker* (Tempel *et al.*, 1987; Pongs *et al.*, 1988).

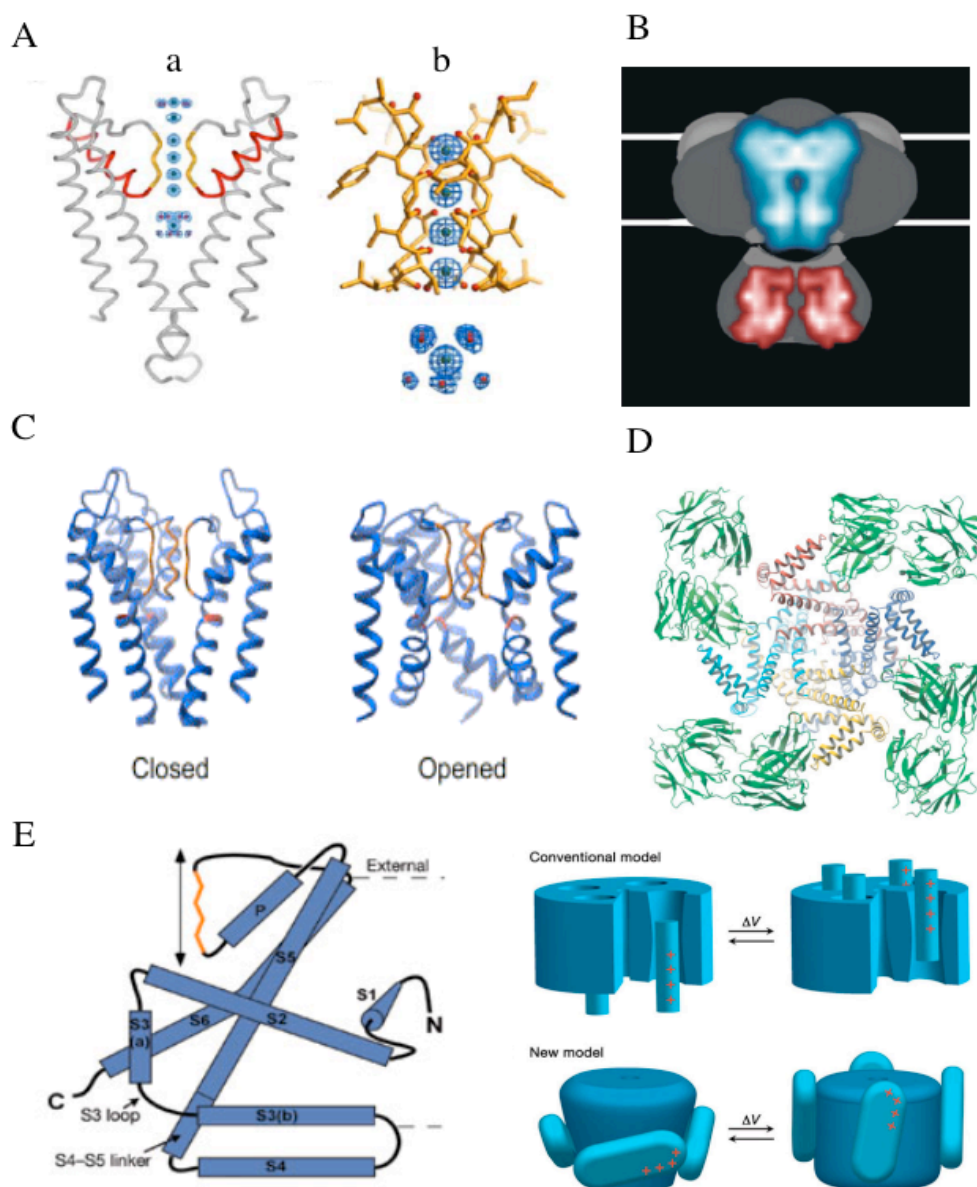


FIGURE 1.3. The three-dimensional structures of potassium channels. **A.** The KcsA K⁺ channel: **a)** Two of the four subunits from the KcsA pore are shown in the extracellular side on top. Each subunit contains an outer helix close to the membrane, an inner helix close to the pore, a pore helix (red) and a selectivity filter (gold). Blue mesh shows electron density for K⁺ ions and water along the pore. **b)** Close up view of the selectivity filter with dehydrated K⁺ ions. **B.** The three-D structure of Shaker potassium channel (KcsA; \square -subunit in blue) and the T1 domain (red) taken from electron microscopy. **C.** The open and close gating states of MthK potassium channel **D.** A schematic diagram of the KvAP subunit topology is shown with an orange selectivity filter and an arrow to indicate the ion pathway. The demarcation between the S4–S5 linker and S5 is indicated by a black line. **E.** On the left panel, the structure of the KvAP channel (blue, yellow, cyan and red helical structures) bound to four Fab fragments (green), viewed down the four-fold axis from the intracellular side. On the right panel hypothesis for gating charge movements. The conventional model of voltage-dependent gating by rotations of S4 helices. In the new model, gating charges (red plus signs) could be carried by movements of the voltage-sensor paddles against the lipid membrane, which in turn could open the pore. (Adapted from Doyle *et al.*, 1998; Sokolova *et al.*, 2001; Jiang *et al.*, 2002; Jiang *et al.*, 2003).

Based on their similarity with related genes from *Drosophila* (Covarrubias *et al.*, 1991), mammalian voltage-gated potassium channels have been originally grouped into four major subfamilies termed *Shaker* (Kv1), *Shab* (Kv2), *Shaw* (Kv3), and *Shal* (Kv4). By the heteromultimeric assembly of different subtypes derived from the same channel subfamily, neurons may generate an enormous diversity of potassium channel properties (Shen *et al.*, 1995). In addition to this, in recent years, an increasing number of pore-forming α -subunits were identified that do not form functionally active channels themselves (Kv5–Kv6, Kv8–Kv11), but act to modulate the electrical properties of potassium channel complexes (for review, see Trimmer and Rhodes). Therefore, it has been a challenge for basic research to identify and characterize the numerous molecular isoforms of VGKCs, as well as, to uncover their basic mechanistic properties.

1.1.2. Structural and functional studies on VGKCs

A number of techniques have become available during the last few years for studying ion channel structure and function. These techniques overcome the scarcity and technical difficulties of crystal structure studies. These studies give only a snapshot in time of a dynamic series of molecular motions. The combination of molecular biology and electrophysiological techniques has been widely used as experimental strategy to study the correlation between the structure and function of ion channels. Electrophysiology identifies the biophysical parameters that are inherent to each individual ion channel. On its part, most information regarding the molecular mechanisms underlying ion channel structure and function has been derived from site-directed mutagenesis studies (Ishii *et al.*, 1998). Cloned ion channels, in part genetically modified, are expressed in host cells and characterized by electro-physiological techniques. By analyzing changes in the currents, induced by certain mutations of the ion channel protein, conclusions regarding the importance of a given part of the protein for a certain function can be drawn (Terlau and Stühmer, 1998).

Many expression systems have been developed for this purpose, using oocytes from *Xenopus laevis* (Fig. 2.1) have been used as a reliable expression system for several proteins including ion channels (Gurdon *et al.*, 1971). The large size of *Xenopus* oocytes allows easy manipulations like cRNA injections and electrode penetration. In addition, low-noise recording from macropatches containing a large number of membrane proteins and few endogeneous channels are clear advantages of using oocytes as an expression system

(Stühmer, 1992). Nevertheless, the large size of oocytes introduces complications if rapid changes in membrane potential are required.

Conventional two electrode voltage clamp methods (TEVC) are easily applied to *Xenopus* oocytes. Specifically, one intracellular electrode is used to record the actual intracellular potential (the voltage electrode), and the second electrode (current electrode) is used to pass current so as to maintain the desired potential. This is achieved using a feedback circuit, which is the main component of the voltage clamp (Fig. 2.2, Stühmer, 1998).

One approach to study the structural and functional properties of TEVC is using small peptide toxins with well-defined structures (Miller, 1995; Ranganathan, *et al.*, 1996). These toxins naturally occur in the venoms of different organisms, such as scorpions, snakes, bees, spiders and many marine animals. There has also been considerable interest in these toxins as structural probes, due to the knowledge of their three-dimensional structure. They may be used to map the functional surface of their respective receptor (Miller, 1995). Alanine scanning mutagenesis is a reliable technique to identify important residues for toxin binding (Jacobsen *et al.*, 2000). In this technique, each residue would be substituted into Alanine once a time and tested against the interacting channel. The binding affinity of the reaction can be measured by electrophysiological recordings. Changes in the binding affinity correspond to the neutralized residue.

Complementary mutagenesis targeting residues in the channel pore has allowed derivation of models describing shape and dimensions of the receptor in the vestibule of the channel. This can be achieved using mutant cycle analysis. In its simplest form, exclusive interaction between two residues can be equally disrupted by mutations of either of the pair. If one is mutated, then mutation of the other should be without effect. On the other hand, if the two mutations produce independent effects, then the two mutations should have a simple additive effect. The mutant cycle analysis was first applied to the toxin interaction with a channel by Hildago and MacKinnon (1995). A coupling coefficient Δ is calculated, which is the energy of interaction between the two residues. The coupling energy ($\Delta\Delta G$) can be calculated from Δ -value and converted into distance between interacting residue pair (Hildago and MacKinnon, 1995; Schreiber and Fersht, 1995). It was suggested that a pair of residues showing a change in $\Delta\Delta G > 2.1$ KJ/mol may be expected to lie within 5 Å of each other

(Schreiber and Fersht, 1995). Therefore, a model of interaction between toxin-channel pair can be obtained from mutant cycle analysis combined with the NMR structures of the both interacting surfaces. From these reliable toxins used intensively to study the structure and function of VGICs, the toxin peptides from marine cone snails; the conopeptides

1.2. Conopeptides

1.2.1. Cone snails: source of conopeptides

Coral reef ecosystems house an extraordinary diversity of invertebrate species, many of which use bioactive compounds as a part of defensive or prey capture strategies. In these diverse habitats, the group of cone snails (genus *Conus*; Fig. 1.1.A) comprises of around 500 predatory species (Röckel *et al.*, 1995). Their venoms are the tools used by these carnivorous molluscs to capture prey, defense against predators, deter competitors and for other biological purposes (Olivera, 1997; Olivera *et al.*, 1990; Olivera *et al.*, 1985).

The spectrum of animals that the genus as a whole can envenomate is abroad, at least 5 phyla, and a wide variety of hunting strategies is used. The cone snail is harpooned with a disposable hollow tooth, which serves as a hypodermic needle for injecting the venom. This chitin-harpoon tooth is part of an efficient delivery system consisting of a venom duct, where venom is synthesized, and a venom bulb (Kohn *et al.*, 1960; Fig. 1.1.B and C). Depending on the envenomed prey, cone snails are generally divided into three groups. The largest class are the vermivorous (worm-hunting) species, most of these feed on polychaetes, hemichordate and echiuroid worms. The second major group is the molluscivorous (snail-hunting) species that hunt other gastropods. The final and most remarkable group are the piscivorous (fish-hunting) cone snails, which have venoms that very rapidly immobilize fish (Olivera *et al.*, 1985; Olivera, 1997; Terlau *et al.*, 1996).

Fish-hunting cone snails can generally be divided into two broad classes: "hook-and-line" fishing snails, which use their long proboscis to harpoon prey with a disposable harpoon-like tooth. The other group is the "net-fishing" cone snails, which engulf prey with a large distensible mouth before stinging (Fig. 1.1.B; Fig. 1.1.D). Among the latter is the geography cone, *Conus geographus*, the species most lethal to man (Cruz and White, 1995).

Rapid evolution of novel venom components has apparently occurred during the radiation of these molluscs in the last ~50 million years. As a result, every species in this successful group of molluscs has evolved a distinct complex of venom components corresponding to interactions with other organisms. In their peptide-rich venom, cone snails use the equivalent of a combinatorial-library strategy to generate novel pharmacologically active components in

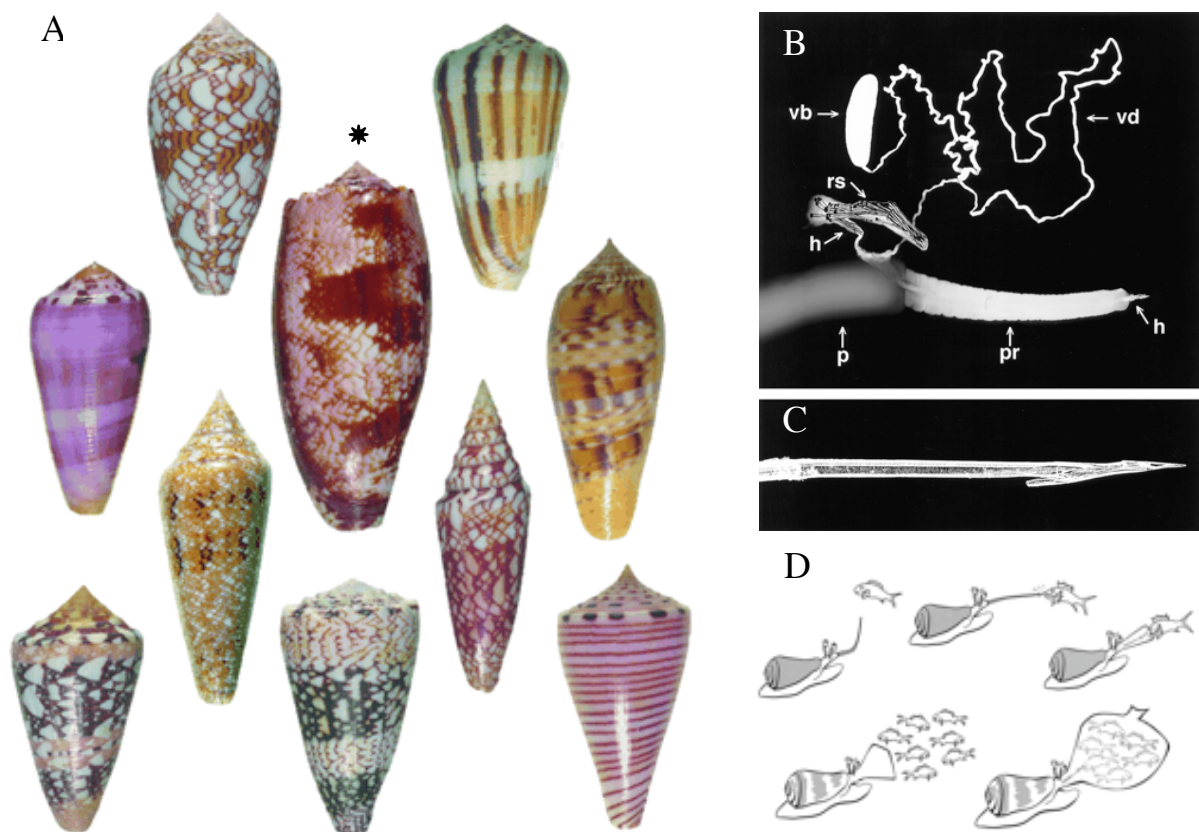


FIGURE 1.4. Cone snails. **A.** Cone snail shells, each represent a species. In the middle, the biggest shell for the most fetal *Conus geographus* (*). **B.** The venom delivery system. The venom apparatus in all cone snails comprises: vb, a venom bulb which pushes the venom out; vd, the venom duct where the venom is actually made and stored; rs, a radula sac where the harpoon-like teeth are stored; h, harpoon-like teeth; p, pharynx; pr, proboscis, which is used to deliver the harpoon and venom to the prey. The radula sac (rs) has been shown in cross-section, to make the harpoons (h) visible. Each harpoon, **C,** is used only once; in the radula sac they are found in various stages of assembly. **D.** A cartoon representing the hook-and-line (top panel) and the net strategy (bottom panel) of fish-hunting cone snails. *Conus magus* () is an example of hook-and-line piscivores. Species such as *Conus geographus* (*) use a net strategy (Adapted from Olivera, 1997).

their venom (Olivera *et al.*, 1985). During this strategy, many peptide sequences are explored through hypermutation in the evolution of each *Conus* species. There are an average of 100 different venom components per species, anticipate total of 50,000 different pharmacologically active components present in venoms of all living cone snails (Olivera *et*

al., 1990). Hence, *Conus* venom composes a very substantial neuropharmacological resource for novel compounds.

1.2.2. Conopeptide and conotoxins

The cone snail venom is a highly complex cocktail of peptide components known as conopeptides. According to their Cys composition, conopeptides can be divided into two main groups: peptides that lack or have only one disulfide cross-link and disulfide-rich conopeptides. The latter are referred to as conotoxins; the most characteristic and predominant venom components. In conotoxins, Cys residues may be found at high frequency with specific patterns in the primary sequence. Each pattern corresponds to specific disulfide connectivity, which is diagnostic of the gene superfamily that encodes the peptide. In many cases, such framework pattern can be indicative of the pharmacological target of the conopeptide (McIntosh *et al.*, 1999, Terlau and Olivera, 2004, see Fig. 1.2).

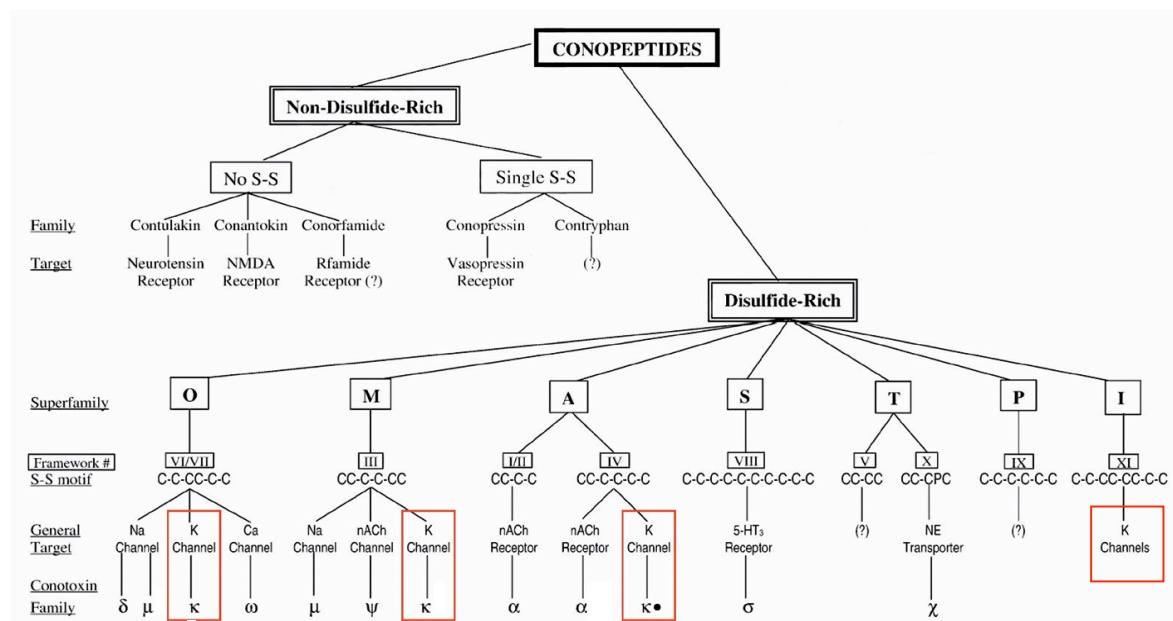


FIGURE 1.5. Organizational diagram for *Conus* peptides. Indicating gene superfamilies, disulfide patterns, and known pharmacological targets. *Conus* peptides can be divided into two broad classes: the disulfide-rich conotoxins and nondisulfide-rich peptides. Only the gene superfamilies for the disulfide-rich peptides are shown. The characteristic patterns of cysteine residues in peptides of each superfamily are shown; the nomenclature used is based on that proposed by McIntosh *et al.* (1999) and Olivera *et al.* (2002). The red lines surrounded □-conotoxins from different families. (Adapted from Terlau and Olivera, 2004).

Conotoxins are small disulfide-rich conopeptides, usually on the average of 12-30 amino acids. In contrast, the size range of toxin polypeptides from other venoms is typically 40-80 amino acids. Despite their small size, there is a remarkable interspecific sequence

divergence, even between homologous conopeptides from closely related *Conus* species (Woodward *et al.*, 1990; Olivera *et al.*, 2002). Adding to their variety, conopeptides contain posttranslationally modified amino acids found at a high frequency in some conopeptide families (Craig *et al.*, 1999). These include some that are well known and widely distributed such as hydroxylated proline and β -glycosylated Serine or Threonine, as well as others that are unusual; 6-Brominated Tryptophan, β -carboxylated glutamate, D-amino acids, and sulfated Tyrosine (for review, see Craig, 2000).

All conopeptides are initially made as larger precursor, usually 60-90 amino acid residues in length (Olivera *et al.*, 1990; Woodward *et al.*, 1990). The mature peptide, which is located at the C-terminus is excised by proteolytic cleavage. Those peptides with similar arrangements of Cys residues in the primary sequence of the mature toxin share a highly conserved signal sequence in the N-terminus. These features define members of a conopeptide gene superfamily. A relatively small number of gene superfamilies have undergone extensive proliferation and diversification in the genus *Conus* to generate the majority of the 50,000 different conopeptides found in the venoms of living *Conus* today (Olivera, 1997; Fig. 1.2).

Although conotoxins are remarkably diverse in terms of structure and function, these conopeptides fall into distinct categories. The analysis of mRNA and genes coding *Conus* peptides revealed an organization of superfamilies based on conserved sequence elements. There are probably only 5-10 major conotoxin gene superfamilies that encode over 80% of all conopeptides (Olivera and Cruz, 2001). Over the genus, superfamilies have differentiated functionally and structurally into discrete families, each with a defined pharmacological targeting specificity (Fig. 1.2). For instance, a family of *Conus* peptides, β -conotoxins, targets the nicotinic acetylcholine receptor (Hopkins *et al.*, 1995). β -Conotoxins inhibit Na^+ channels of muscle membranes leaving Na^+ channels of nerve membranes unaffected (Cruz *et al.*, 1985). β -Conotoxins exhibit high affinity to certain subtypes of Ca^{2+} channels such as conotoxin (GVIA) from *Conus geographus*, which specifically blocks N-type Ca^{2+} channels (Olivera *et al.*, 1984). β -conotoxins inhibit K^+ channels such as β -PVIIA from *Conus purpurascens* (Terlau *et al.*, 1996). Among the ligand-gated ion channels that conopeptides are known to inhibit are nicotinic acetylcholine receptors (McIntosh *et al.*, 1999), N-methyl-D-aspartate receptors (Olivera *et al.*, 1990) and 5HT3 receptors (England *et al.*, 1998). In order to achieve a desired physiological end point on injected prey, predator, or competitor,

an assemblage of conopeptides (from different conotoxin families) act together in a synergistic fashion to reach this effect (Olivera *et al.*, 1990; Terlau *et al.*, 1996). This ("toxin cocktail") is the equivalent to a combinatorial library strategy for drug delivery in modern medicine.

Due to diverse venom components, cone snails became specialists in evolving ligands targeted to both voltage- and ligand-gated ion channel superfamilies with impressive molecular specificity. In particular, their ability to discriminate between closely related members of a given ion channel family (McIntosh *et al.*, 1999). *Conus* peptides have been used to define specific molecular forms within a large ion channel family and to investigate the functional biology of a particular ion channel subtype. This specificity displayed by conopeptides is what makes them of exceptional interest and has led to their widespread use as research tools in neurobiology. Several pharmacological studies revealed therapeutic potentials of some conopeptides. An example is ω -MVIIA (generic name ziconotide) from *Conus magus*, which is highly specific for N-type calcium channels and has been through clinical trials as a drug for intractable pain (for review, Terlau and Olivera, 2004).

1.2.3. Conotoxins targeting VGKCs and dyad hypothesis

Despite the great variability of the *Conus* peptides characterized until now only relatively few have been identified that interact with K⁺ channels. The kappa conotoxins (in red squares; Fig. 1.5), which have been shown to inhibit voltage-activated K⁺ channels, are 27-34 amino acid residues long and contain 3 or 4 disulfide bonds (Craig *et al.*, 1998; Shon *et al.*, 1998; Fan *et al.*, 2003; Kaufenstein *et al.*, 2004). These ω -conotoxins belong to O, M, A and I superfamilies.

From I-superfamily, a peptide called ω -BtX was characterized from the venom of *Conus betulinus* (Fan *et al.*, 2003). This peptide was shown to upmodulate the Ca²⁺ and voltage-activated BK currents measured from rat adrenal chromaffin cells and did not affect other voltage-gated channels. Another member of the I-superfamily designated ViTx from *Conus virgo*, was shown to inhibit Kv1.1 and Kv1.3 subtypes, but not Kv1.2 (Kaufenstein *et al.*, 2003). In A-superfamily, the peptide, ω A-conotoxin SIVA was identified from the venom of the fish-hunting cone snail *Conus striatus* (Craig *et al.*, 1998). Recordings from frog cutaneous pectoris muscle and principal neurons from frog sympathetic ganglion reveal that

this peptide induces repetitive activity in these cells. Furthermore, *Shaker* channels expressed in *Xenopus* oocytes are blocked by micromolar concentrations of \square A-SIVA. However, the molecular identity of the vertebrate high-affinity K^+ channel target of this peptide has not yet been identified. The \square -conotoxin PVIIA (\square -PVIIA) from the venom of *Conus purpurascens* was the first conotoxin to be found to interact with a voltage-gated K^+ channel (Terlau *et al.*, 1996). \square -PVIIA is a 27-residue, belonging to O-superfamily with three disulfide bonds, which blocks the K^+ -conductance in oocytes expressing the *Shaker* K^+ channel encoded from *Drosophila*. No affinity to other K^+ channel subtypes, particularly to those of vertebrate origin has been found (Shon *et al.*, 1998; Terlau *et al.*, 1999). In addition to conotoxins, Sudaralal and co-workers (2004), isolated 13 amino acid non-disulfide conopeptide from the venom of *Conus monile*, designated Mo1659. Electrophysiological studies on the effect of Mo1659 on measured currents in dorsal root ganglion neurons suggest that the peptide targets non-inactivating voltage-dependent potassium channels.

Despite the structural divergence of unrelated K^+ channel-targeted toxins, a convergent functional feature has been identified for a variety of toxins, including charybdotoxin from a scorpion, BgK from a sea anemone, and dendrotoxin from snakes. Although for the different toxins more than one site has been identified as being important for binding (for scorpion toxins, see Miller, 1995; Eriksson, *et al.*, 2002; Gao *et al.*, 2003), all these peptides share a dyad motif of a lysine and a hydrophobic, usually aromatic residue, which plays a key role in the interaction with the target K^+ channel (Stampe *et al.*, 1994; Dauplais *et al.*, 1997; Savarin *et al.*, 1998; Gilquin *et al.*, 2002; Srinivasan *et al.*, 2002). In particular, there is evidence that the lysine residue of this functional dyad occludes the K^+ channel pore (Miller, 1995; Eriksson, *et al.*, 2002; Gao *et al.*, 2003). In accordance with this observation, the diverse peptides which interact with the voltage-gated Kv1 subfamily of K^+ channels (such as the *Shaker* channel from *Drosophila*) all seem to contain a functional dyad (Dauplais *et al.*, 1997; Savarin *et al.*, 1998; Rauer *et al.*, 1999 and Jacobsen *et al.*, 2000; Gilquin *et al.*, 2002; Srinivasan *et al.*, 2002), which therefore was proposed to be a minimal functional core for the binding of the toxins to Kv1 channels.

Although structurally unrelated to other known K^+ channel blockers, \square -PVIIA shares the common feature of a functional lysine-hydrophobic residue dyad (Jacobsen *et al.*, 2000). The three dimensional structure of \square -PVIIA was elucidated by NMR spectroscopy (Scanlon *et*

al., 1997; Savarin *et al.*, 1998). It was predicted that the determinant by which \square -conotoxin PVIIA occludes the pore should include a binding dyad, composed of Lys 7 and Phe 9 or Phe 23 (Savarin *et al.*, 1998). This prediction was based on the observation that a similar critical dyad is present in the determinant by which other toxins, even structurally unrelated, block voltage-gated K^+ channels (Dauplais *et al.*, 1997). An alanine walk along the polypeptide chain of the toxin (Jacobsen *et al.*, 2000) experimentally confirmed this prediction.

\square M-conotoxin RIIIK (\square M-RIIIK) is a 24 amino acid peptide from *Conus radiatus*, which is structurally similar to \square -conotoxin GIIIA, a peptide known to block specifically skeletal muscle Na^+ channels (Fig. 1.6). Ferber and co-workers (2003), showed that \square M-RIIIK does not interact with Na^+ channels but inhibits *Shaker* potassium channels expressed in *Xenopus* oocytes. It was demonstrated that \square M-RIIIK binds to the pore region of *Shaker* channels and the interaction was state-dependent. Furthermore, an introduction of a negative charge at residue 427 of *Shaker* channels (K427D) greatly enhanced the affinity of \square MRIIK binding.

\square M-RIIIK	LOS CC SLNLR L COVOA CK RNO CC T#
μ -GIIIA	RD CC TOOK K - CK DRQ CK OQR CC A#
μ -GIIIB	RD CC TOOR K - CK DRR CK OM KCC A#
ψ -PIIIE	HO CC LYG K CRRYOG CS SAS CC QR#
ψ -PIIIF	GO CC LYG S CROFOG C YNAL CC RK#

FIGURE 1.6. Sequence alignment of \square M-RIIIK with other M-superfamily peptides. O represents 4-hydroxyproline and # an amidated C-terminal amino acid.

The teleost homolog of *Shaker*, the trout *TShal* K^+ channel, from CNS of *Oncorhynchus mykiss*, was recently cloned and identified to be the equivalent of mammalian Kv1.2 channels (Nguyen and Jeserich, 1998). In its outer vestibule, *TShal* is equipped with a Glu residue in an equivalent position to Lys427 of *Shaker* channel. Functionally, \square M-RIIIK was described to block the *TShal* K^+ channel in a state-dependent with an IC_{50} of 20 nM for the

closed state and 60 nM at 0 mV for the open state of *TSha1* channels. Therefore, *TSha1* K⁺ channels was found to be the highest-affinity target of \square M-R111K yet identified (Ferber *et al.*, 2003). Interestingly, the 24-amino acid sequence of \square M-R111K contains three positively charged residues but no aromatic side chain (Fig. 1.6). This lack of an important component of dyad motif raised the question of whether the pharmacophore of \square M-R111K is organized around a dyad motif. If not, then what are the structural and functional parameters required for \square M-R111K binding to *Shaker*-type K⁺ channels?

1.3. Objectives

In this study, we investigated the structural and functional properties of \square M-R111K interacting with *TSha1* K⁺ channel in order to identify the pharmacophore of this peptide. The *Xenopus* expression system was used to functionally express wild type and mutated *TSha1* K⁺ channels and to investigate the properties of \square M-R111K wild type and mutated forms. Both alanine scanning mutagenesis and mutant cycle analysis were performed to identify the pharmacophore model of \square M-R111K binding to the pore region of *TSha1* channel. To investigate how \square M-R111K binds to K⁺ channels, the following questions will be addressed:

- What are the key interacting residues (pharmacophore) of \square M-R111K to block K⁺ channels?
- Does the difference in affinity of \square M-R111K mutants affect their kinetics of binding?
- Does the pharmacophore of \square M-R111K possess the dyad motif?
- Does the \square M-R111K interact with Kv1.2, the mammalian K⁺ channel equivalent to *TSha1*?
- Is there a novel docking behavior of \square M-R111K?

CHAPTER TWO: Materials and Methods

2.1. Electrophysiological methods

Different electrophysiological techniques can be used according to experiment requirements. We used the two-electrode voltage clamp technique (TEVC) in combination with the *Xenopus* oocyte heterologous expression system. This technique is useful for stable conditions during long experiments and controlled extracellular composition.

2.1.1. *Xenopus* oocyte preparations

The *Xenopus* oocytes, from the South African clawed frog (Fig. 2.1A), are well established as a reliable heterologous expression system to study ion channels and membrane-bound proteins (Gurdon *et al.*, 1971). The *Xenopus* oocytes are relatively large in size (~1 mm diameter) and contain very few endogenous channels making them a very useful model system to study heterologously expressed ion channels (Methfessel *et al.*, 1986; Stühmer, 1992; Stühmer and Parekh, 1995). The rapid advance in molecular biology allows successful heterologous expression of mutated ion channels on the surface of *Xenopus* oocytes (Ishii *et al.*, 1998).

2.1.1.1. *Xenopus* oocyte solution

To obtain a batch of *Xenopus* oocytes for electrophysiological recording, solutions were used in two steps of preparation:

1) Oocyte handling solutions

Skinning solution pH 7.4 (adjusted by NaOH)	200 mM	K-aspartate
	20 mM	KCl
	1 mM	MgCl ₂
	10 mM	EGTA
	10 mM	HEPES

Antibiotics solution	4 mg/l	Cefuxorixim / Zinacef 750
	100U/ml	Penicillin / Streptomycin
Barth Medium pH 7.4 (adjusted by NaOH)	84 mM	NaCl
	10 mM	KCl
	2.5 mM	NaHCO ₃
	6.5 mM	Ca(NO ₃) ₂
	0.6 mM	CaCl ₂
	7.5 mM	Tris-HCl
	2% (v/v)	Antibiotics solution
Ca²⁺ free Barth Medium pH 7.4 (adjusted by NaOH)	84 mM	NaCl
	10 mM	KCl
	2.5 mM	NaHCO ₃
	7.5 mM	Tris-HCl
Collagenase solution	1 mg/ml	Collagenase Type 2
	200 ml	Ca ²⁺ -free Barth

Collagenase Type 2 was purchased from Worthington Biochemical Corporation (Lakewood, NJ, USA), Cefuxorixim/Zinacef 750 by Aventis (Strasbourg, France), and Penicillin/Streptomycin by Gibco (Invitrogen, NY, USA). All other chemicals used in this study were purchased from Sigma (MO, USA) and Merck (Darmstadt, Germany) or otherwise mentioned.

2) Extracellular recording solutions

Normal Frog Ringer's solution (NFR) pH 7.2 (adjusted by NaOH)	115 mM	NaCl
	2.5 mM	KCl
	1.8 mM	CaCl ₂
	10 mM	HEPES

NFR-[K⁺] (mM)	NaCl	KCl	CaCl₂	HEPES: pH 7.2 (adjusted by NaOH)
0	117.5 mM	0 mM	1.8 mM	10 mM
5	112.5 mM	5 mM	1.8 mM	10 mM
10	107.5 mM	10 mM	1.8 mM	10 mM
50	67.5 mM	50 mM	1.8 mM	10 mM

Normal Frog Ringer (NFR pH 5 and 9)	
NaCl	115 mM
KCl	2.5 mM
CaCl ₂	1.8 mM
MES (for NFR pH 5)	10 mM (adjusted by HCl)
Tris-Base (for NFR pH 9)	10 mM (adjusted by NaOH)

2.1.1.2. *Xenopus* oocyte handling

Ovarian tissue containing oocytes at different stages of maturation was surgically removed from female *Xenopus laevis* specimens under anesthesia (20-30 min in a Tricaine solution at 0 °C, 2.5 g/l, Fig. 2.1B). The oocytes were extracted from the tissue by partial enzymatic digestion of the follicular cell layer. The digestion was done under 2-3 hours incubation in collagenase solution at 17 °C in shaking incubator (GFL 1083, Burgwedel, Germany). To inhibit the enzymatic reaction, oocytes were extensively washed in Barth Medium. Oocytes between stage IV and VI were selected and incubated at 17 °C in Barth medium in a standing incubator (Mettler ICP 400, Schwabach, Germany).

Selected oocytes were microinjected with ~50 nl (Drummond Nanoinject, Gauting, Germany) of solution containing 0.25 µg/µl of cRNA. The original DNA clone of the *Shaker*-related K⁺ channel (*TSha1*), from CNS of rainbow trout (*Oncorhynchus mykiss*), was kindly provided by Prof. Dr. G. Jeserich (Osnabrück University, Osnabrück, Germany). The original DNA clone of Kv1.1, Kv1.5 and Kv1.6 K⁺ channels were generous gifts of Dr. Martin Stocker (UCL, London, UK). The Kv1.2 and Kv1.3 were obtained from Prof. S. Grissmer (University of Ulm, Ulm, Germany). The sodium channel of rat skeletal muscle (Nav1.4) was a gift from Prof. Gail Mandel (University of Stony Brook, NY, USA). Injected

oocytes were then incubated at 17 °C in Barth solution containing penicillin-streptomycin and cefuroxime for 1-4 days to allow the expression of the ion channels. Attention was paid to alternate antibiotics in order to avoid the development of resistance.

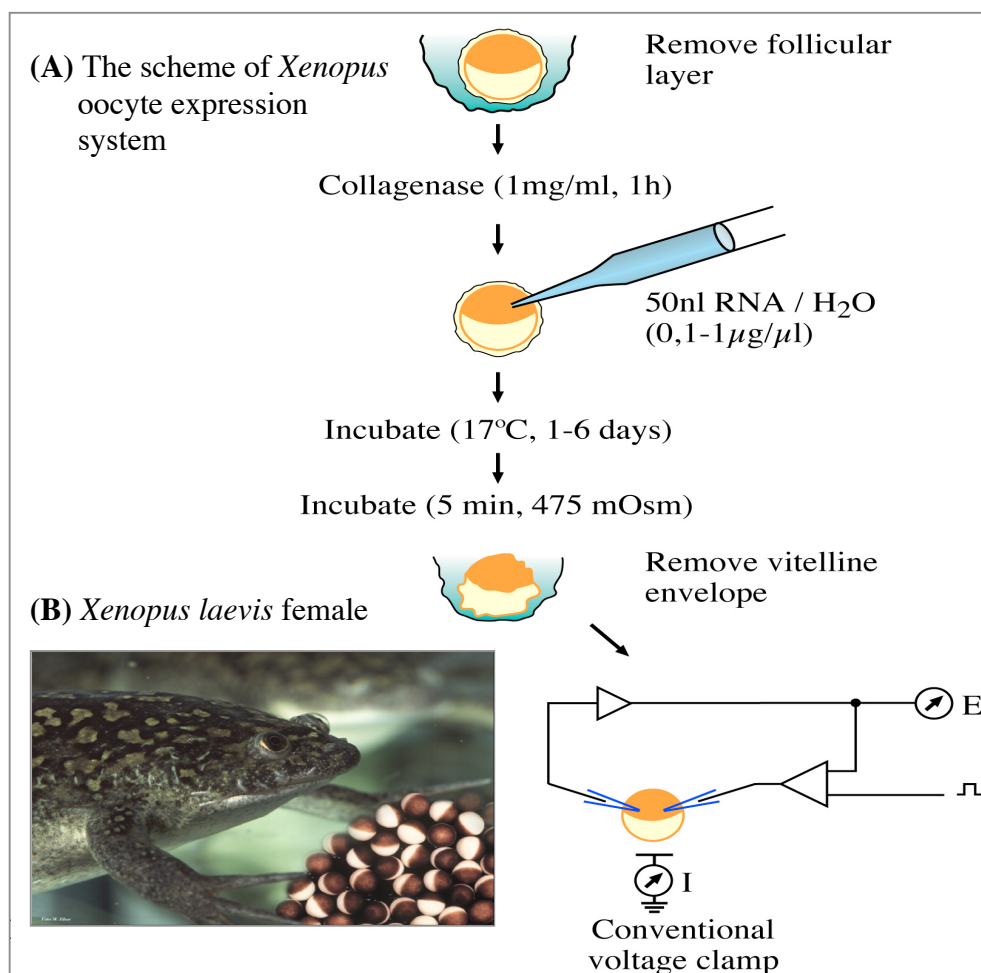


FIGURE 2.1. The artificial expression of ion channels on the membrane of *Xenopus laevis* oocytes (A) Summary of oocyte preparation for electrophysiological recordings with two electrode voltage clamp technique. (B) The source of oocytes, the *Xenopus laevis* female with some oocytes. [Modified from Terlau and Stühmer (1998)].

Prior to the electrophysiological measurements, the removal of vitelline membrane that surrounds the cytoplasmic membrane of the oocyte is an important step for optimal exchange of solutions. Control experiments had shown that IC_{50} of $\square M-R111K$ in the presence of the vitelline membrane was about 3-4 times higher compared to experiments where this membrane had been removed. The vitelline membrane was mechanically removed by fine forceps (No.5, Dumont and Fils, Montignez, Switzerland) after incubating in a hypertonic skinning solution that allows easy detachment from oocyte (Fig. 2.1A). Finally, the oocyte was placed in the measuring chamber containing normal frog Ringer's (NFR) for

electrophysiological experiment (Fig. 2.1A). Experiments were performed at room temperature 19-22 °C.

The conotoxin in this study, ω M-conotoxin RIIIK (ω M-RIIIK), WT and mutant analogs were synthesized at the peptide synthesis facility of the University of Utah by the group of Prof. Jean Rivier (Salk Institute, San Diego, USA) as described previously (Shon *et al.*, 1998). These conotoxins were properly folded, tested and aliquoted by the group of Prof. Baldomero Olivera (Salt Lake, Utah, USA).

2.1.2. Two-electrode voltage clamp (TEVC)

The *Xenopus laevis* oocytes are extensively used for two-electrode voltage clamp recordings to investigate the electrophysiological properties of heterologous expressed voltage-gated ion channels (Methfessel *et al.*, 1986; Goldin, 1992; Stühmer and Parekh, 1995; Stühmer, 1998). In TEVC, the whole cell currents of the oocyte were recorded by two inserted electrodes. During the experiments, one intracellular electrode measures the membrane potential (voltage electrode), and the second (current electrode) injects sufficient current to maintain the voltage clamped to the desired value (command potential) using feed back amplifier circuit (Fig. 2.2). The amount of current that passes through the current electrode is the measured parameter and it is determined by the discrepancy between the membrane potential and the command potential.

To limit possible voltage clamp artifacts, the electrodes should be as close as possible to the center of the oocyte without damaging the cell. In any case, the oocyte membrane cannot be considered isopotential on time scale of ≈ 300 μ s, or when the total current is >20 μ A (Baumgartner *et al.*, 1999).

In addition, there is a resistance in series with the membrane (series resistance, R_s) that is due to the nature of elements that the injected current has to traverse such as the bath, cytoplasm and the electrodes (Fig. 2.2). When a current flows across the membrane, the R_s leads to a discrepancy between the measured membrane potential (controlled by the amplifier) and the "real" potential difference across the membrane. Therefore, the R_s was manually compensated.

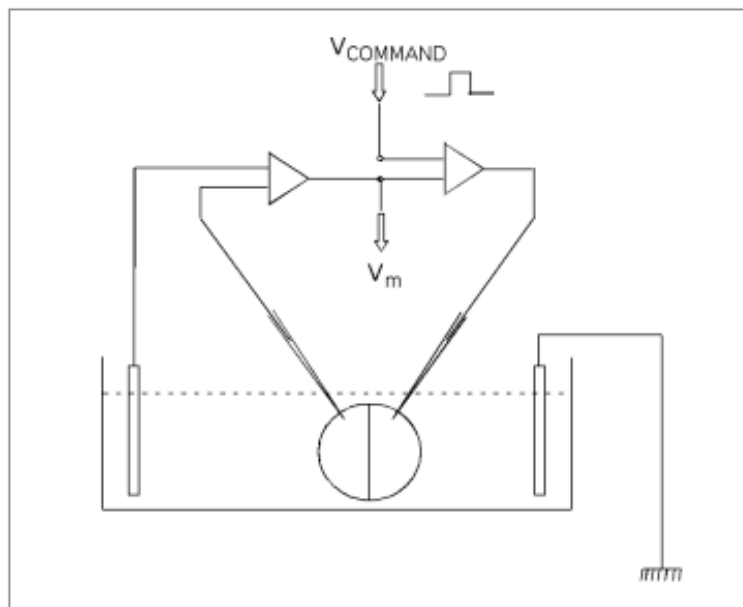


FIGURE 2.2. Schematic diagram of the main components of the two-electrode voltage clamp (TEVC). The difference in potential between the bath and the potential electrode (left), V_m , is compared to the command potential, V_{comm} and determines the amount of current injected into the oocyte through the current electrode (right). [Modified from Stühmer (1998)].

2.1.2.1. Instrumentation

Mechanical stability and electrical shielding are crucial for voltage clamp setup. The support system of the cell, the micromanipulators and the microscope (inverted microscope Zeiss Axiovert S100, magnification objectives 5X and 10X) were located on an antivibration table. The complete section of the setup is mechanically separated from the Faraday cage by a second table. Each individual component was grounded individually in order to obtain optimal shielding and at the same time avoiding current (ground) loops between the instruments.

The amplifier used for the voltage clamp recordings was a Turbo TEC-10CX (NPI Electronic, Tamm, Germany) with electronic built-in series resistance compensation (Rs-comp). The electrical stimulation of the current was performed through the EPC9 built-in ITC-16 AD/DA converter, controlled by a Macintosh G4 computer (Apple computer, Cupertino, CA, USA). The acquisition of data was made using Pulse software (HEKA, Lambrecht/Pfalz, Germany).

Extracellular solutions were exchanged through a gravity perfusion system by using a mechanical valve (Hamilton Deutschland, Darmstadt, Germany), which allows the change of up to 6 different solutions. The solution level of the recording chamber was maintained constant through a pressure driven level sensor system (Lorenz, Lindau, Germany). Lyophilized α M-RIIK was dissolved in NFR to required final concentration, and applied by using a Pasteur pipette directly to the bath chamber. These chambers (vol. \sim 650 μ l) were specially designed to allow 3 times wash in of 2 ml toxin volume to minimize toxin waste and to overcome the perfusion system limitation. The toxin wash in was repeated to insure the total exchange of the NFR solution with required toxin concentration.

2.1.2.2. Micropipettes and electrodes

Microelectrodes for TEVC recordings were made from borosilicate filament glass capillaries (Hilgenberg, Malsfeld, Germany). The edges of the glass capillary were cut into appropriate length and fire rounded in order to improve the junction between the pipette holder in the head-stage. This procedure also helps to protect the Ag/AgCl coated electrode wire from scratches produced by the rim of the glass. Capillaries for TEVC microelectrodes were pulled in two steps to the appropriate length and size in a vertical temperature controlled pipette puller PIP5 (HEKA, Lambrecht/Pfalz, Germany).

To reduce noise characteristics and potential changes in the capacity of the pipette tips during solution exchanges, pipettes were coated with the polymer RTV (GE Bayer Silicones, Bergen, The Netherlands), which is highly hydrophobic and has a low dielectric characteristic. The fluid silicone layer was applied about 1 mm from the tip of the TEVC microelectrodes to avoid contact with the oocyte. The polymer was hardened under a hot air stream avoiding any contact of the polymer with the cell membrane since it can lead to increases in the holding current during the experiments.

The TEVC pipettes were made from capillary glass containing a thin filament, which ensures that the electrode filling solution reaches the tip. The back end of the pipette was waxed to prevent creeping of the filling solution from the pipette to the electrode holder. TEVC pipettes were filled with 2 M KCl and stored in a closer container under moist environment. Before use, the tip was broken, under a microscope (Microforge, Narishige, Japan), to decrease the resistance into the range of 0.5 to 1 M Ω , which corresponded to a tip diameter

2-10 μm . The prepared electrodes can be reused for several oocytes as long as they maintain their low resistance.

The microinjection needles (Drummond 3-000-203-G/X, Broomal, USA, see Fig. 2.1.B) were pulled using a standard pipette puller (Heka, Lambrecht, Germany). The tips of the pipettes were broken under a microscope (microfuge, Marishige, Japan) and heat-polished to avoid oocyte damage. The injection needles were back-filled with mineral oil to allow precise hydraulic control of the cRNA flow. The cRNA was taken from sterile eppendorf tube via sterile standard capillary tube to fill the injection needle.

2.1.2.3. TEVC stimulation protocols

The membrane was kept at a holding potential of -100 mV , where the probability of the ion channels under investigation to be in the closed conformation is almost 1. The pulse interval between two stimulations was always kept long enough to ensure reequilibration of the channel states and toxin binding. Current signals were sampled at 250-100 μs (sampling rate of 4-10 kHz). The signal was low pass filtered with a Bessel filter at a frequency of 1 kHz (for K^+ channels) and 3 kHz (for Nav1.4 Na^+ channel). To obtain different parameters for the characterization of the channel protein and the toxin binding, several stimulation protocols were generated.

2.1.2.3.1. Single pulse (I-V) protocol

For K^+ channels, series pulses ranging from -60 mV to $+60\text{ mV}$ in increments of 20 mV were applied (Fig. 2.3A). The interpulse interval was 10 sec. The steady state of whole cell K^+ currents at a test pulse of 0 mV were sampled (Fig. 2.3B). For Nav1.4 Na^+ channel, series pulses ranging from -60 to $+40\text{ mV}$ in increments of 10 mV were applied with 3 s interpulse intervals. During experiments, several control I-V pulses were taken under NFR washing to insure steady state current and avoid run up or run down states (in/decrease in current). However, small run up or run down (less than 10%) were corrected by offline analysis using Igor pro software (version 4.07 Carbon, Oregon, USA) with special program designed by Dr. Michael Ferber in our group by using Igor WaveMetrics Software (Lake Oswego, OR, USA).

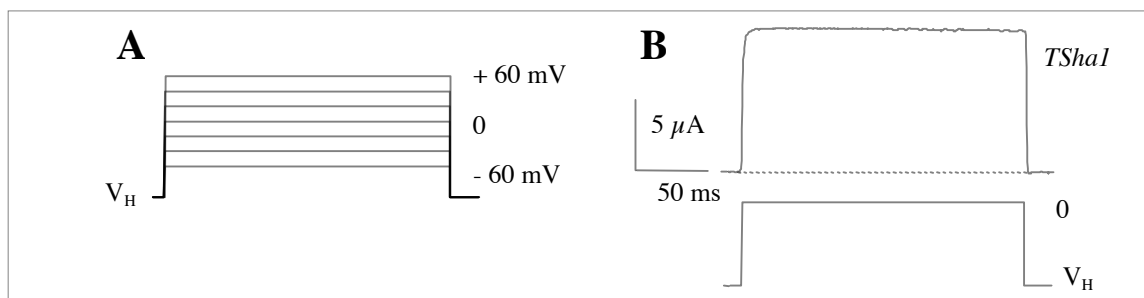


FIGURE 2.3. Single pulse (IV) protocol. **A)** Starting from holding potential (V_H) depolarization pulses with a duration of 200 ms are applied. **B)** Current responses of *TShal* K^+ channel to the protocol of panel A at 0 mV test pulse.

2.1.2.3.2. Double pulse (DP) protocol

To measure the kinetics of \square M-RIIIK binding to closed channels, we used double pulse protocol. Two identical voltage steps from the holding potential to 0 mV, separated by an increase of time intervals (T_i : 0.25-7 s) were used to test of -100 mV the re-equilibration of binding to closed channels (Fig. 2.4).

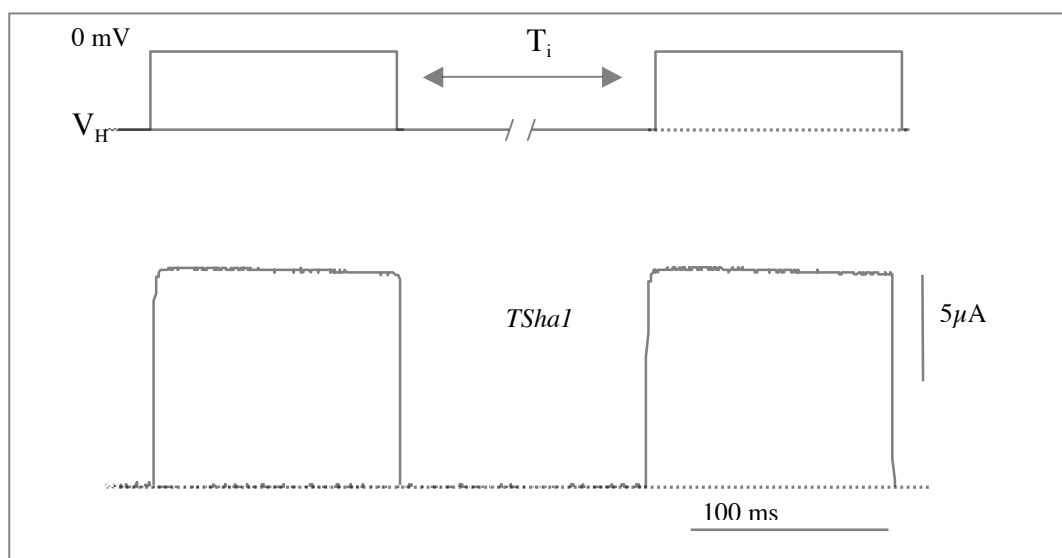


FIGURE 2.4. Double pulse protocol. Two identical voltage steps are separated by a variable interpulse at V_H (top). The bottom panel shows the current responses elicited by the double pulse protocol for 0 mV and $T_i = 250$ ms.

2.1.2.3.3. Leakage and capacitive current correction

The currents measured during TEVC experiments were subtracted online with a standard P/n protocol (Heinemann *et al.*, 1995). In a voltage range where voltage dependent channels are

considered not active, a scaled down version of the pulse protocol was applied n times and the resulting current was averaged, scaled and subtracted from that elicited by the main test pulse. A scaling factor of 0.25 was used and 4 to 8 leak responses were averaged to decrease the noise.

2.2. Molecular Biology

In vitro site-directed mutagenesis is an invaluable technique for studying protein structure-function relationships. This technique was used to obtain selected point mutations within the pore region of *TShal* channel for mutant cycle analysis experiments. All methods were performed following standard procedures (Sambrook *et al.*, 1989; Ishii *et al.*, 1998, Fig. 2.5) and according to manufacturer protocols when commercial kits were used.

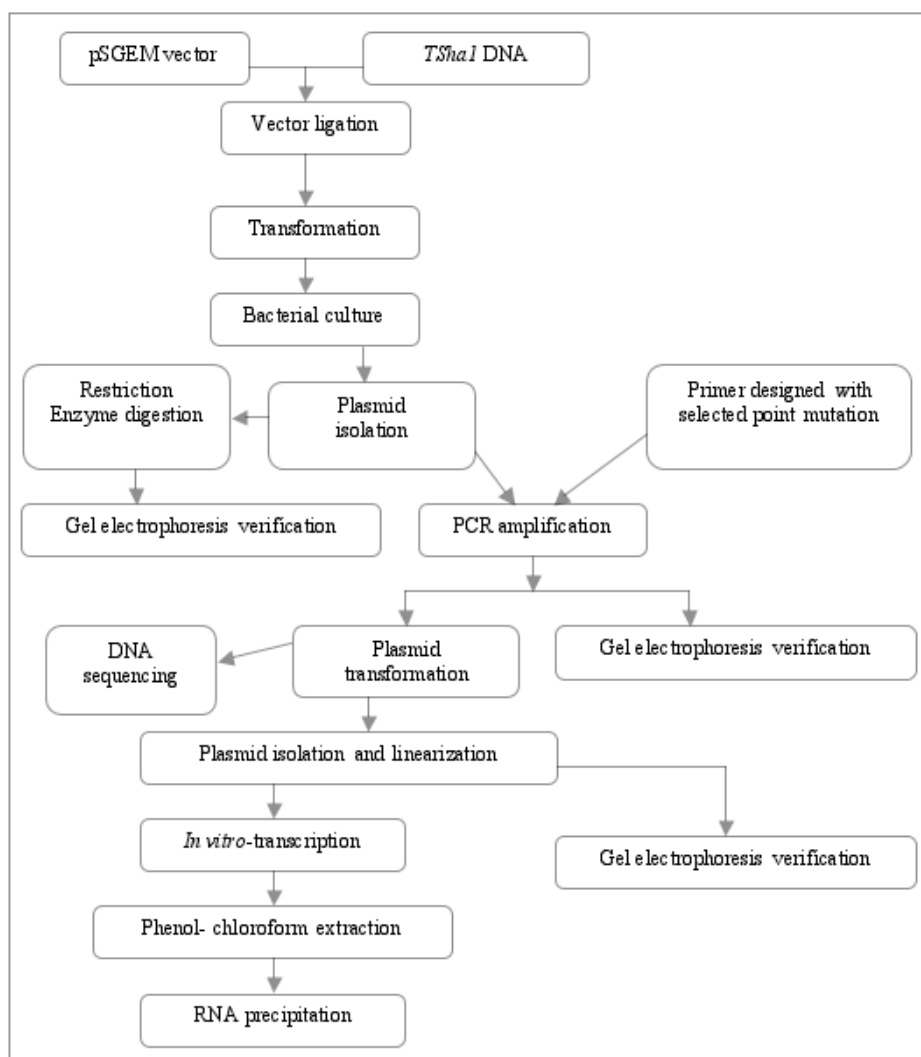


FIGURE 2.5. Schematic representation of the site-directed mutagenesis to produce cRNA of *TShal* channel with selected mutations.

2.2.1. Vector ligation

The *Shaker*-related K⁺ channel (*TShal*), from CNS of rainbow trout *Oncorhynchus mykiss*, has an open reading frame (ORF) of 1892bp DNA (Nguyen and Jeserich, 1998 and Nguyen *et al*, 2000, see Fig. 2.6).

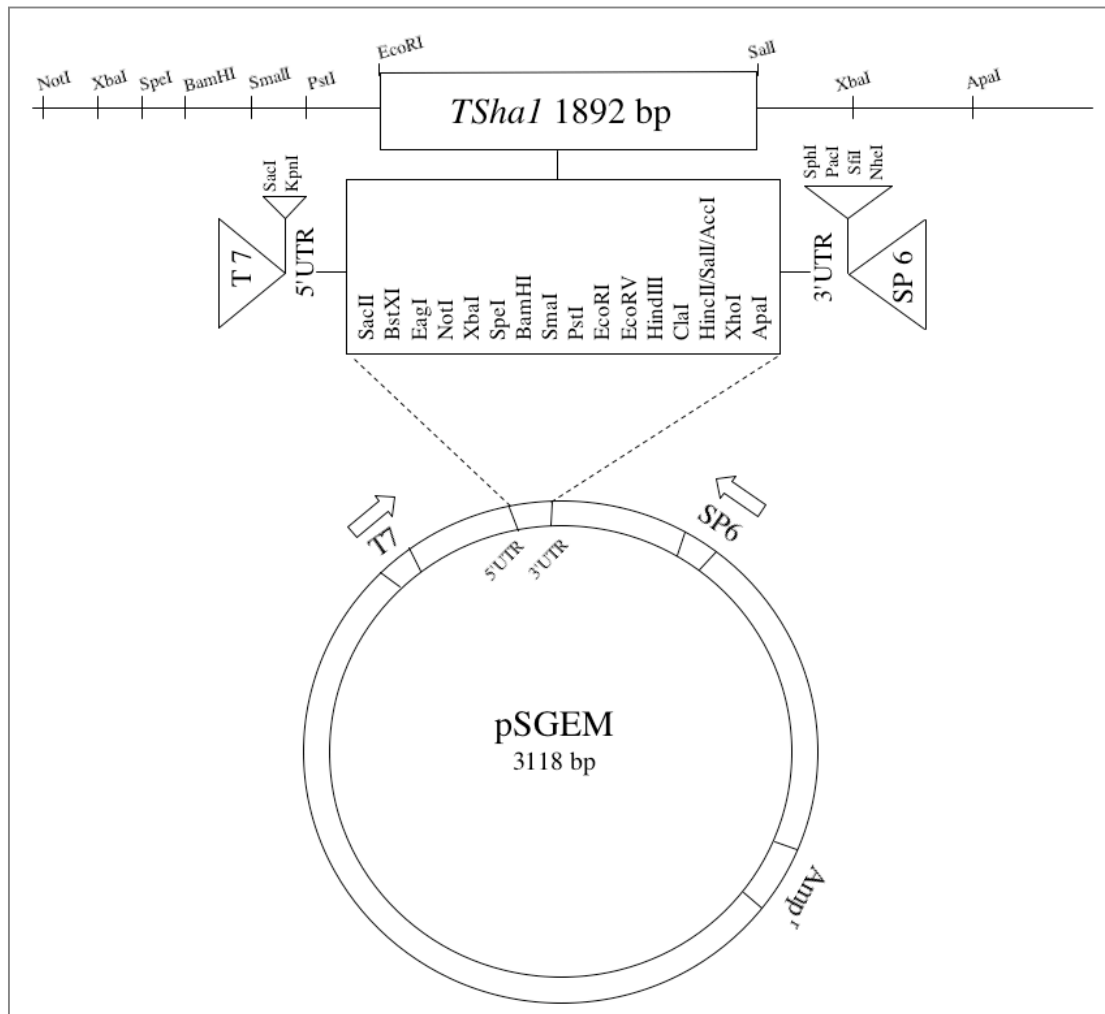


FIGURE 2.6. Schematic representation of the pSGEM vector and *TShal* ORF DNA with restriction sites, Amp^r gene T7 and SP6 polymerase promoters. [Modified from Liman *et al.* (1992)].

The vector used throughout this study was pSGEM (3118 bp), a modified version of pGEMHE, which was a generous gift of Prof. Dr. Michael Hollmann (Bochum University, Bochum, Germany). To increase the expression in *Xenopus* oocytes, pSGEM plasmid is provided with 3' and 5' untranslated regions (UTRs) of a *Xenopus* β -globin gene (Krieg and

Melton, 1987). The vector contains a cassette of four restriction sites, including *NheI*, upstream the SP6 polymerase promoter that can be used for sense template linearization (Liman *et al*, 1992 and Villmann *et al*, 1997, Fig. 2.6). In pSGEM vector, the T7 polymerase promoter which is used for *in vitro* transcription. The plasmid also contains *Amp^r* gene for selective culturing of successful transformed vectors.

Both *TShal* DNA and pSGEM vector were fragmented by *EcoRI* and *SalI* digestion (Fig. 2.6) and cleaned with a QIAEX II gel extraction kit (Qiagen, Hilden, Germany). In a sterile tube, 1.5 μ l 10 x T4 DNA ligase (New England BioLabs, Beverly, MA, USA) and the DNA solutions containing the fragments to be ligated were added to a final volume of 15 μ l. The ligation reaction was incubated at 16 °C overnight.

2.2.2. *TShal* DNA Transformation

The DH5 α and XL1-Blue competent bacterial cells were used for transformation. The DH5 α cells (0.2 ml; Gibco, Invitrogen, Karlsruhe, Germany) were defrosted on ice, mixed with 0.5 μ l pSGEM-*TShal* (4983 bp) ligation mixture and incubated on ice. The mixture tube was incubated 1 min at 42 °C for heat shock and re-incubated on ice for 3 min. Next, 800 μ l of LB medium [see the bacterial culture section] was added to the mixture and incubated 35-45 min with shaking at 37 °C (Eppendorf Thermomixer, Hamburg, Germany). Before plating, tube was centrifuged for 5 min at 9000 rpm to precipitate bacterial cells. These cells were spread on Ampicillin-LB agar plates [see the bacterial culture section] and incubated overnight at 37 °C. The XL1-Blue competent cells were used for site-directed mutagenesis experiment according to the standard procedure from the manufacturer (Stratagene, Heidelberg, Germany).

2.2.3. Bacterial culture

Once grown in LB agar plates, 10-12 individual colonies were sub-cultured in 4ml (100 μ g/ml) Ampicillin-LB broth and incubated overnight at 37 °C with 220 rpm shaker incubator (GFL, Burgwebel, Germany). The LB agar plates can be supplemented with 100 mg/ml Ampicillin (100 μ g/ml end concentration; Roche, IN, USA) at 50 °C after autoclaving the following components:

LB Medium	LB Agar plates
10 g Bacto-Trypton	10 g Bacto-Trypton (Difco Labs, MI. USA)
5 g Bacto-Yeast Extract	5 g Bacto-Yeast Extract
5 g NaCl	5 g NaCl
1000 ml H ₂ O	14 g Bacto-agarose
	1000 ml H ₂ O

2.2.4. Plasmid isolation

From 3 ml LB cultures, the *TShal*-pSGEM plasmid constructs were isolated in mini-scaled preparation using NucleoSpin[®] mini-preparation kit (Macherey-Nagel GmbH, Düren, Germany). The isolated plasmid was tested through restriction digestion and visualized by agarose gel electrophoresis as described below.

2.2.5. Restriction enzyme digestion

In principle, a restriction enzyme that cleaves the construct plasmid to give predicted fragments is selected. The HindIII enzyme was used to give two predicted fragments, 1176 kb and 3807 kb. Total volume of 15 μ l mixture of 1 μ l plasmid DNA, 1.5 μ l HindIII buffer, 0.1 μ l HindIII enzyme (New England BioLabs, Beverly, MA, USA) and d.d.H₂O was incubated for 2 to 6 hrs at 37 °C for digestion. The digested DNA was verified in agarose gel electrophoresis as described below.

2.2.6. Agarose gel electrophoresis

Nucleic acids were separated by size and electrical charge on slab agarose gel via submarine gel electrophoresis. The mesh framework of agarose gel obstacles large electrical charged particles and allows smaller ones to pass through the gel. Intercalating dye [ethidium bromide, 1% (v/v)] was used to visualize DNA samples under UV radiation. Molecular size markers 100bp and 1Kb DNA Ladders (MBI Fermentas, Vilnius, Lithuania) were run simultaneously in marker lane to estimate the size of the DNA samples. The electrophoresis tank was filled with 1x TBE buffer and DNA samples were run in 1% agarose gel (SeaKem LE agarose, BMA, BioWhittaker, Denmark). The DNA samples of 10-15 μ l were mixed with 5 μ l loading buffer and loaded into separated lanes. The gel was run for 35 min at (80-120) mV using standard power supply (Pack P25, Biometra, Göttingen, Germany). Finally, DNA

bands were visualized and the gel was developed by image Master machine (Amersham, Pharmacia, Freiburg, Germany). The electrophoresis buffer contents were:

5 X TBE pH 8 (adjusted by NaOH)	Tris-Base	54 g
	Boric acid	27.5 g
	0.5 M EDTA	20 ml
Loading Buffer	Glycerin	40 % (v/v)
	Bromophenol Blue in H ₂ O	0.25 % (v/v)

2.2.7. Mutagenic primer design and PCR amplification

The mutagenic oligonucleotide primers to be used in the QuickChange[®] site-directed mutagenesis kit must be designed individually according to the desired mutation. The manufacturers (Stratagene, Heidelberg, Germany) suggestions for designing mutagenic primers were taken into consideration. Briefly, both sense and antisense mutagenic primers, between 25 and 45 bases in length, must contain the desired mutation and anneal to the same sequence on opposite strands of the plasmid. The melting temperature (T_m) of the primers should be ≥ 78 °C and the desired mutation should be in the middle of the primer with ~10–15 bases of correct sequence on both sides. Also, the primers optimally should have a minimum guanine/cytosine (GC) content of 40% and should terminate in one or more C or G bases. Optimal mutagenic primers were designed using Lasergene Navigator software (Navigator 1.66, DNASTAR, London, UK). All designed primers were purchased from Metabion GmbH (Planegg-Martinsried, Munich, Germany). Summary of selected *TShal* mutation and their corresponded sense and antisense primers are shown in Table 2.1.

Polymerase chain reaction (PCR) amplification for the *TShal*-pSGEM plasmid as DNA template was done according to QuickChange[®] site-directed mutagenesis protocol. In a sterile PCR tube, 0.5 μ l (10 ng DNA sample), 1.25 μ l (10mM) sense primer, 1.25 μ l (10mM) antisense primer, 1 μ l (25 mM) dNTPs (Stratagene, Heidelberg, Germany), and 5 μ l 10 x PCR buffer (Stratagene, Heidelberg, Germany) were added to a final volume of 50 μ l d.d.H₂O. The mixture was aliquot into sterile PCR tubes and kept on ice. A 1 μ l (2.5 U/ μ l) *PfuTurbo*[®] polymerase (Stratagene, Heidelberg, Germany) was added to each reaction tube. In the same time, negative control sample was run in same PCR using the same components without the DNA sample. The PCR conditions were initial step at 95 °C for 30 s followed by

16 reaction cycles of denaturation at 95 °C for 30 s, annealing at 55 °C for 1 min, and a final 10 min extension at 68 °C. The PCR was run using Thermocycler machine (T3, Biometra, Göttingen, Germany). After the amplification, an aliquot of the PCR products were verified on 1% agarose gel.

2.2.8. Plasmid transformation

Following temperature cycling, the product was treated with 1 μ l *DpnI* endonuclease (10 U/ μ l, Stratagene, Heidelberg, Germany) to digest the parental methylated DNA template and to select for mutation-containing synthesized DNA. The *DpnI*-treated plasmid DNA was then transformed into XL1-Blue supercompetent cells. Briefly, XL1-Blue cells were defrosted on ice, mixed with 1 μ l *DpnI*-treated plasmid and incubated for 30 min on ice. The mixture tube was incubated 45 s at 42 °C for heat shock and re-incubated on ice for 2 min. Next, 500 μ l of preheated NZY⁺ medium (Stratagene, Heidelberg, Germany), was added to the mixture and incubated for 1 h at 37 °C with shaking (Eppendorf Thermomixer, Hamburg, Germany). Following transformation, cells were spread on Ampicillin-LB agar plates (see cell culture section).

2.2.9. Plasmid isolation and linearization

The mutated plasmid construct was isolated using the same mini-scaled preparation mentioned in the plasmid isolation section. The concentration and purity of isolated DNA plasmid was measured using a Biophotometer (Eppendorf, Hamburg, Germany). All constructs were sequenced using dideoxy chain termination method with dye terminators on an applied Biosystems 373 DNA sequencer (Applied Biosystems, Weiterstadt, Germany). Sequencing was performed within the house of Max-Planck Institute for Experimental Medicine (Göttingen, Germany) by Mr. Fritz Benseler. After sequencing, plasmids with required mutations were linearized for *in vitro* transcription. Briefly, 4 μ g of DNA were linearized with 2 μ l *NheI* (New England BioLabs, Beverly, MA, USA), and incubated for 3 hs at 37 °C. The linearized plasmids were verified in 1% agarose gel electrophoresis as mentioned above.

TABLE 2.1. Primer sequences of *TShal* point mutation. The upper primer is the sense and the lower one is the anti sense of each corresponded mutant.

<i>TShal</i> mutation	5'-Primer sequence-3'
E348K	ACTTTGCGGAAGCTGATAAGCCCGAATCGCAATTTG CAAATTGCGATTTCGGGCTTATCAGCTTCCGCAAAGT
E348S	CTACTTTGCGGAAGCTGATTCGCCCGAATCGCAATTTG CAAATTGCGATTTCGGGCGAATCAGCTTCCGCAAAGTAG
P349K	CTTTTCGGAAGCTGATGAGAAGGAATCGCAATTTGAAAGCATCC GGATGCTTTCAAATTGCGATTCTTCTCATCAGCTTCCGCAAAG
S351K	GAAGCTGATGAGCCCGAAAAGCAATTTGAAAGCATCCAG CTGGGATGCTTTCAAATTGCTTTTCGGGCTCATCAGCTTC
E354K	GCCCGAATCGCAATTTAAAAGCATCCCAGACGC GCGTCTGGGATGCTTTTAAATTGCGATTTCGGGC
E354Q	GCCCGAATCGCAATTTCAAAGCATCCCAGACGC GCGTCTGGGATGCTTTGAAATTGCGATTTCGGGC
S366T	TGGTGGGCTGTTGTCACTATGACGACAGTAGG CCTACTGTCGTCATAGTGACAACAGCCCACCA
M375K	CCAATGGTGGTTCGGCTTCATGTCACCATACCC GGGTATGGTGACATGAAGCCGACCACCATTGG
M375L	AGTAGGGTATGGTGACTTGGTCCCGACCAC GTGGTCGGGACCAAGTCACCATACCCTACT
M375I	AGTAGGGTATGGTGACATTGTCCCGACCACC GGTGGTCGGGACAATGTCACCATACCCTACT
V376K	AGTAGGGTATGGTGACAAGGTCCCGACCAC GTGGTCGGGACCTTGTCCACCATACCCTACT
V376H	GGGTATGGTGACATGCACCCGACCACCATTGG CCAATGGTGGTTCGGGTGCATGTCACCATACCC
V376S	GGGTATGGTGACATGAGCCCGACCACCATTGG CCAATGGTGGTTCGGGCTCATGTCACCATACCC
V376T	AGGGTATGGTGACATGACCCCGACCACCATTGG CCAATGGTGGTTCGGGGTTCATGTCACCATACCCT
V376E	GGGTATGGTGACATGGAGCCGACCACCATTGG CCAATGGTGGTTCGGCTCCATGTCACCATACCC

2.2.10. *In vitro* transcription

The transcription was performed with the T7 polymerase (Stratagene, Heidelberg, Germany) to obtain cRNA as described in standard procedure (Krieg and Melton, 1987). Briefly, the linearized plasmid solution up to 100 μ l with DEPC water was mixed with equal volumes of phenol and chloro-isoamylalcohol. After centrifugation for 3 min at 13200 rpm (Centrifuge 5415D, Eppendorf, Köln, Germany), the upper phase was separated to a second tube and the lower phase of the first tube was mixed with 100 μ l DEPC water and recentrifuged. Next, the upper phase collected again from the first tube, added to the second tube and the second tube containing the upper phases was rewashed with equal volume of chloroform-isoamylalcohol to be purified for precipitation.

The extracted DNA was precipitated for 12 hs at -20°C with 0.1 vol. of sodium acetate and 3 vol. of absolute ethanol. Then, the DNA sample was centrifuged for 30 min at 13200 rpm (Centrifuge 5804R, Eppendorf, Köln, Germany). The precipitated sample was washed with 0.5 ml 70% cold ethanol and recentrifuged for 3 min at 13200 rpm. Finally, the pellet was dried at room temperature.

The transcription mixture (Table 2.2) was incubated for 1h at 37°C . After treatment by 5 μ l DNase for 15 min at 37°C , the mixture tube was re-extracted by phenol and chloroform and precipitated. The concentration and purity of isolated cRNA was measured using a Biophotometer (Eppendorf, Hamburg, Germany) and stored at -80°C to be used.

TABLE 2.2. The transcription mixture was followed:

Vol. μ l	Material	Source
13	Linearized DNA resuspended in DEPC water	
5	ATP (10 mM)	Amersham Biosciences, Uppsala, Sweden
5	CTP (10 mM)	Amersham Biosciences, Uppsala, Sweden
5	UTP (10 mM)	Amersham Biosciences, Uppsala, Sweden
2,5	GTP (10 mM)	Amersham Biosciences, Uppsala, Sweden
5	CAP (5 mM)	Amersham Biosciences, Uppsala, Sweden
10	5 x Transfer buffer	Amersham Biosciences, Uppsala, Sweden
2,5	RNasin (100 U)	Promega, Madison, WI, USA
2	T7 RNA polymerase (0,4 μ l + 1,6 μ l dilution buffer)	Stratagene, Heidelberg, Germany
50	Total volume	

2.3. Data analysis

Data were expressed statistically as [mean \pm standard error (S.E.)] using Excel software (Microsoft, USA) and Igor pro (version 4.07 Carbon, Oregon, USA). Offline analysis was performed with a Macintosh G4 computer (Apple, Cupertino, CA, USA), with modified Igor software programs that were written by our group. Curve fittings and corrections also were done by Igor pro software. Mutagenic primers design was done utilizing Lasergene Navigator software (Navigator 1.66, DNASTAR, London, UK). The acquisition of data from the amplifier was made using Pulse software (HEKA, Lambrecht/Pfalz, Germany). The student *t*- test for unpaired-comparison was used to compare two means. The difference is considered significant when $P < 0.05$.

The IC_{50} values for the block characteristics of toxin block during the electrophysiological experiments were calculated from the steady state of whole cell currents at a test potential of 0 mV obtained from oocyte expressing *Shaker* channels.

$$IC_{50} = fc / (1-fc) * [T]$$

Where *fc* is the fractional current ($fc = \text{sample current} / \text{control current}$) and $[T]$ is the toxin concentration.

For dose response curves, curves are fitted according to:

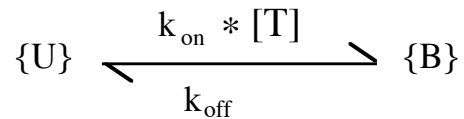
$$\square = 100 / \{1 + ([T] / IC_{50})^n\}$$

where \square is the relative response, and *n* represent the Hill coefficient, which represents cooperativity for the block of the channel by the toxin.

The kinetic parameters of toxin binding to open channels can be obtained by investigating binding relaxations during partial block conditions (Terlau *et al.*, 1999). The ratio of the currents under control conditions and in the presence of toxin shows a single exponential relaxation of the block, a single exponential relaxation of the block was calculated as:

$$y = y_0 + A \exp(-t/\tau)$$

where τ is the time constant of activation or recovery from inactivation, y indicate the state probability of the channel from which the current fraction collected. In principle, the toxin binding to channel pore can be interpreted by a simple bimolecular reaction scheme:



where $\{U\}$ represents the toxin-free channels and $\{B\}$ the channels bound to a toxin molecule. The transition rates are the product of the second order dissociation constant and the toxin concentration, ($k_{\text{on}} * [T]$) and the dissociation constant k_{off} . From the experimental parameters τ and U , it is possible to evaluate $K^{(O)}$, $k_{\text{off}}^{(O)}$, $k_{\text{on}}^{(O)}$ according to the inverse relationships:

$$K^{(O)} = \frac{[T] * U^{(O)}}{1 - U^{(O)}} \quad ; \quad k_{\text{off}}^{(O)} = \frac{U^{(O)}}{\tau^{(O)}} \quad ; \quad k_{\text{on}}^{(O)} = \frac{1 - U^{(O)}}{[T] * \tau^{(O)}}$$

The parameters of toxin binding to the closed state were calculated by performing a similar analysis for the currents obtained from double pulse protocols, which are used to characterize the reequilibration of closed channel binding.

For both open and close channels, the resting unblock probabilities, U^o and U^c , depends on the toxin concentration, $[T]$, following a simple Langmuir isotherm, where the equilibrium dissociation parameter (K_D) is $K^{(O)}$ for open and $K^{(C)}$ for close channels with:

$$K_D = (k_{\text{off}} / k_{\text{on}}) * [T]$$

Also, the time constant (τ) depends on $[T]$ according to:

$$\tau = 1 / (k_{\text{off}} + k_{\text{on}} * [T])$$

The mutant cycle analysis was performed to reveal the interaction between given pairs of toxin and channel residues (Hildago and MacKinnon, 1995; Schreiber and Fersht, 1995). Values for the coupling coefficient α were obtained from cycle of channel and toxin interaction in WT and mutant forms (mut), by using the formula:

$$\alpha = [(IC_{50}^{WT_{channel}:WT_{toxin}} * IC_{50}^{mut_{channel}:mut_{toxin}}) / (IC_{50}^{WT_{channel}:mut_{toxin}} * IC_{50}^{mut_{channel}:WT_{toxin}})].$$

Unity reflects no interaction, whereas deviation from unity indicates progressively stronger interactions. The change in coupling energy $\Delta\Delta G$ for a given pair of toxin channel residues was calculated according to $\Delta\Delta G = RT \ln \alpha$ (with $R = 8.314 \text{ Jmol}^{-1} \cdot \text{K}^{-1}$ and $T = 295 \text{ K}$). It was suggested that a pair of residues showing a change in $\Delta\Delta G > 2.1 \text{ KJ.mol}^{-1}$ may be expected to lie within 5 Å of each other (Schreiber and Fersht, 1995; Rauer *et al.*, 1999).

CHAPTER THREE: Results

3.1. κ M-RIIK interacting with *Shaker*-type K^+ channels

κ M-conotoxin RIIK blocks *Shaker*-related potassium channels from the trout *Oncorhynchus mykiss* (*TShal*) with high affinity. We identified the interacting residues of κ M-RIIK pharmacophore by using the alanine substitution assay. To investigate which part of the toxin is interacting with which residues at the pore region of the *TShal* channel, a mutant cycle analysis was performed.

3.1.1. κ M-RIIK specificity interacts with *TShal* channels

3.1.1.1. Determining IC_{50} of open state block

The affinity of κ M-RIIK isoforms was functionally assayed by two-electrode voltage clamp measurements using *Xenopus* oocytes expressing the trout *TShal* K^+ channel. κ M-RIIK blocks *TShal* mediated K^+ currents with an IC_{50} of 76 ± 10 nM ($n = 9$), obtained from measuring steady state currents. The inhibition of *TShal* K^+ conductance is readily reversible when the recorded chamber was washed with toxin free-NFR as shown in the *bottom panel* of Fig. 3.1A. The affinity was confirmed by dose response measurement with an $IC_{50} = 70 \pm 11$ nM (Fig. 3.1B). This value is almost identical to the value from the measurements of the fractional currents. The Hill coefficient was close to 1, suggesting that the binding of a single toxin molecule is sufficient to inhibit the *TShal* channel.

3.1.1.2. Interaction at different extracellular K^+ concentrations

Because κ M-RIIK carries a net positive charge at neutral pH (Ferber *et al.*, 2003), we expected a substantial electrostatic component in the interaction between the toxin and pore region of the channel. To examine this possibility, we studied the RIIK block under different extracellular potassium concentrations, ($[K^+]_o = 0, 2.5, 5, 10$ and 50 mM). The affinity of the peptide to *TShal* channels was calculated from the steady state ratio measurement of control current to current under toxin condition (see Materials and Methods; Terlau *et al.*, 1999).

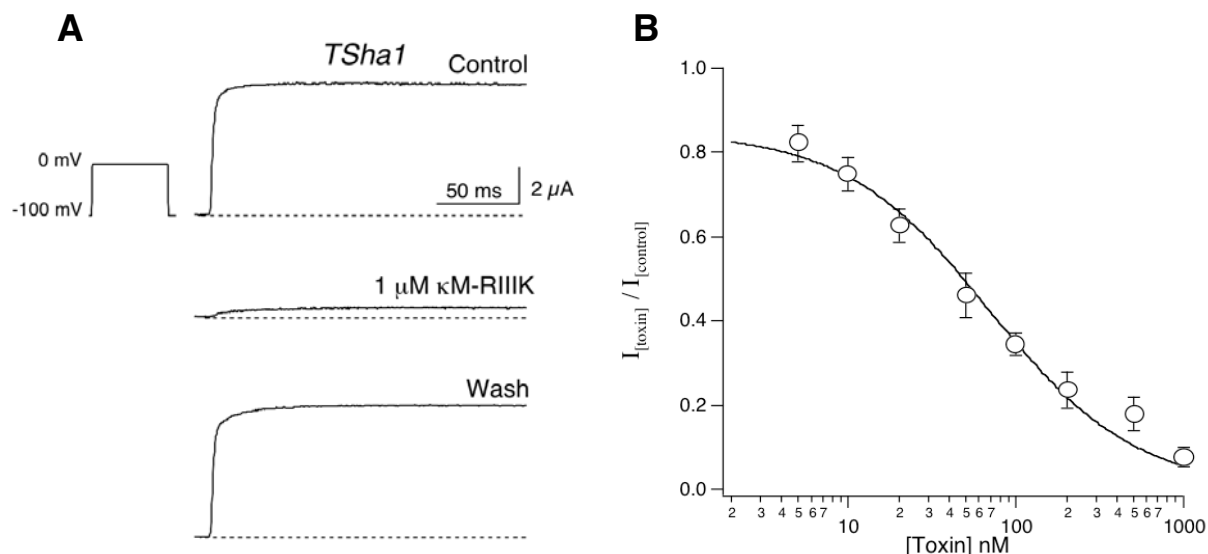
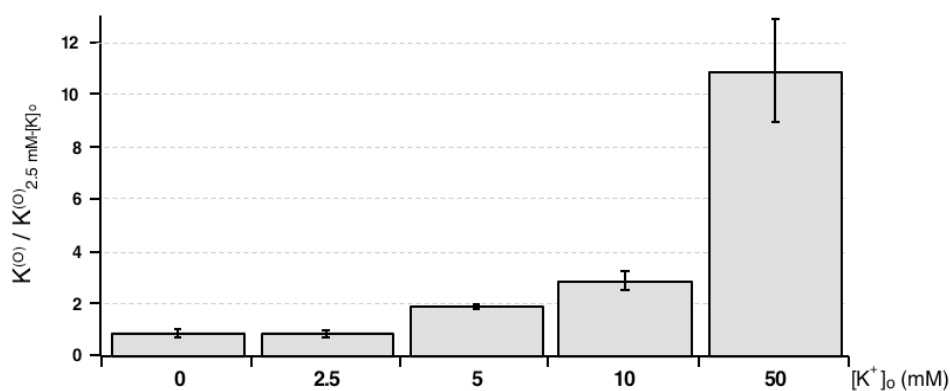


FIGURE 3.1. κ M-RIIIK reversibly blocks *TSha1*-mediated currents. **(A)** Whole-cell currents recorded from oocytes expressing *TSha1* K^+ channels upon depolarization to 0 mV are shown before (control), after addition of 1 μ M κ M-RIIIK, and after subsequent wash with NFR, indicating the reversibility of the block of the toxin. The holding potential was -100 mV. The *dashed lines* correspond to zero current. **(B)** Dose-response curve for the block of *TSha1* current by κ M-RIIIK at a test potential of 0 mV (total number of experiments = 12 with n between 4 and 11 for the different indicated toxin concentrations).

From these ratios, it was possible to calculate the dissociation constant for open state ($K^{(O)}$) but also the "on" and "off" rate values. From Table 3.1 and Fig. 3.2, it becomes clear that the affinity of the toxin weakened exponentially as $[K^+]_o$ increases, with $K^{(O)}$ increases from 75 nM at 0 and 2.5 mM and approaching 870 nM at 50 mM. Examining the effect of different $[K^+]_o$ on the kinetics of the κ M-RIIIK blockade to *TSha1*, revealed that the observed change in $K^{(O)}$ is mainly due to changes in $k_{off}^{(O)}$. Overall, the dissociation rate varies strongly with the $[K^+]_o$, with an about 5-fold increase at 50 mM. The variation in association rate is small in comparison, leading to 2.5-fold decrease at 50 mM $[K^+]_o$. During the experiments, it was noticed that increasing the $[K^+]_o$ to 115 mM by substituting the Na^+ ions was not tolerated by the *TSha1* channels. This was reflected by tonic increase in leakage current. Therefore, higher concentrations than 50 mM $[K^+]_o$ could not be investigated. The fact that the affinity of κ M-RIIIK associated with an increase in the $k_{off}^{(O)}$ rates indicates a competition between κ M-RIIIK molecules and $[K^+]_o$ on available carboxylate groups close to the outer surface of the channel pore. Hence, the binding interaction is partly due to electrostatic forces between toxin and channel pore residues.

TABLE 3.1. The effect of κ M-RIIK interaction with *TShal* K⁺ channels under different extracellular K⁺ concentrations

[K] ₀ mM	K ⁽⁰⁾ (0mV) nM	k _{on} ⁽⁰⁾ μM ⁻¹ *S ⁻¹	k _{off} ⁽⁰⁾ S ⁻¹	k _{on} ⁽⁰⁾ ratio ([K] ₀ / 2.5-mM [K] ₀)	k _{off} ⁽⁰⁾ ratio ([K] ₀ / 2.5-mM [K] ₀)	n
0	75 ± 16	56 ± 11	4 ± 1	0.6	0.7	4
2.5	76 ± 13	89 ± 11	6 ± 1	1	1	5
5	162 ± 10	90 ± 11	14 ± 3	1	2.3	4
10	219 ± 32	75 ± 9	16 ± 2	0.8	2.7	5
50	871 ± 150	35 ± 13	28 ± 9	0.4	4.7	3

**FIGURE 3.2.** The effect of external potassium concentration ([K]₀) on the binding affinity of κ M-RIIK to *TShal*-channels. The affinity of the interaction is decreasing (shown here as increasing of relative currents) by increasing the [K]₀ indicating that toxin molecules are blocking the pore region of the channel with dominant electrostatic interactions.

3.1.2. κ M-RIIK interacts with mammalian Kv1.2

In order to investigate the specificity of the binding of κ M-RIIK to a given voltage-gated K⁺ channel, the affinity of κ M-RIIK for different mammalian potassium channels of the Kv1 family was performed. It is shown that κ M-RIIK blocks the human Kv1.2 potassium channel, whereas the other members of the Kv1 family tested are not affected by the peptide. The block of Kv1.2 currents is state dependent with different steady state affinities and binding kinetics for the closed and open channel conformation. This section was a contribution by a collaborative work with Dr. Michael Ferber in the group.

3.1.2.1. Determining IC_{50} of open state block of Kv1.2

Ten potassium channel subunits from different families (Kv1.1, Kv1.3, Kv1.4, Kv2.1, Kv3.4, Kv4.2, Kv10.1 (reag), and Kv11.1 (herg)) were expressed in *Xenopus* oocytes. None of the expressed channels showed any sensitivity for κ M-RIIK applied in a concentration of up to 10 μ M. However, as already described in Ferber *et al.* (2003). *Shaker* K^+ channels are blocked by κ M-RIIK with an IC_{50} of about 1 μ M. In order to establish the pharmacological profile of κ M-RIIK on mammalian Kv1 channels, the activity of this peptide was tested on human Kv1.2, rat Kv1.2, rat Kv1.5 and rat Kv1.6 expressed in *Xenopus* oocytes. The results are shown in Fig. 3.3. κ M-RIIK at a concentration of 5 μ M has no effects on Kv1.5 mediated currents. For Kv1.6 mediated currents, a small reduction (< 10%) is observed which would correspond to an IC_{50} above 50 μ M. In contrast to the low affinity of κ M-RIIK to these channels the same concentration of κ M-RIIK leads to an almost complete block of human Kv1.2 or rat Kv1.2 mediated currents.

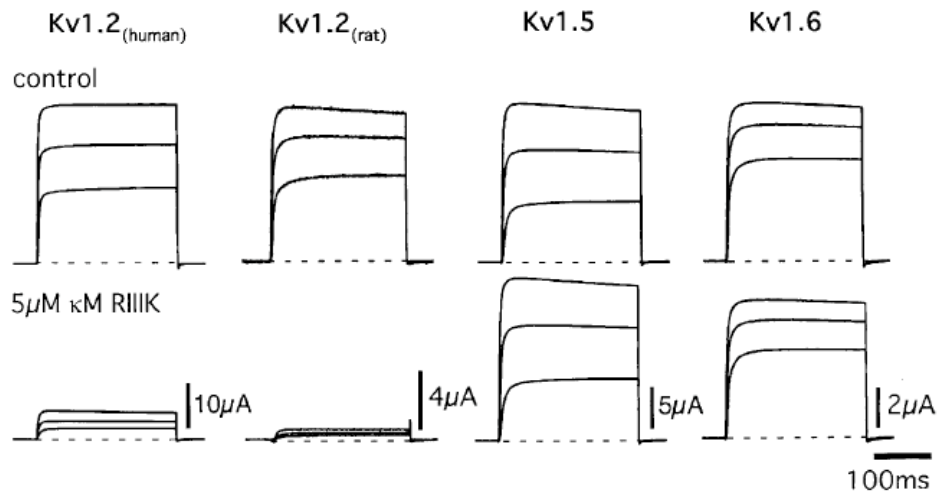
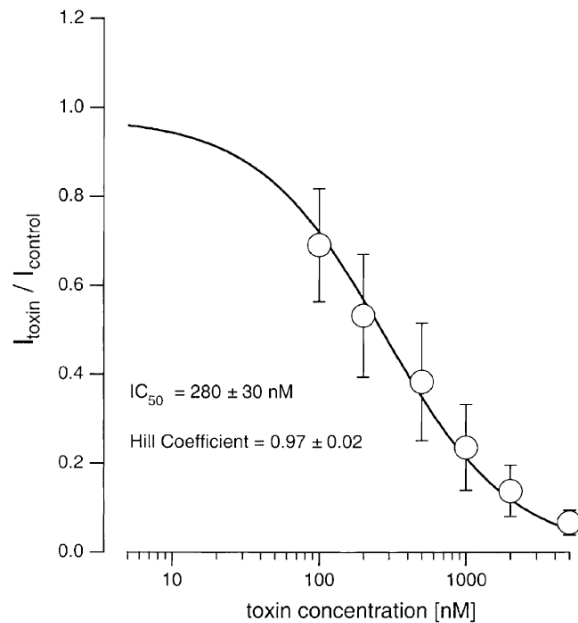


FIGURE 3.3. κ M-RIIK specifically blocks Kv1.2 mediated currents. Whole cell currents recorded from oocytes expressing Kv1.2, Kv1.5 or Kv1.6 K^+ channels evoked by test potentials to 0, +20 and +40 mV from a holding potential of -100 mV under control conditions (*upper panel*) and after addition of 5 μ M κ M-RIIK (*lower panel*). Whereas Kv1.5 and Kv1.6 mediated currents are almost unaffected by the toxin, Kv1.2 mediated currents are almost completely blocked.

This inhibition is readily reversible (*not shown*). The IC_{50} for human Kv1.2 channels obtained by measuring the steady state currents at 0 mV during dose response experiments is about 300 nM (Fig.3.4). The Hill coefficient is about 1 indicating no cooperativity for the block of Kv1.2

channels by the peptide. The IC_{50} for rat Kv1.2 channels calculated from fractional currents is 335 ± 78 nM ($n = 5$). These results establish Kv1.2 as a specific mammalian target of \square M-RIIIK.

FIGURE 3.4. Dose–response curve of the block of Kv1.2 mediated steady-state currents by \square M-RIIIK. The mean steady-state current at 0 mV in the presence of the toxin is normalized to the control and plotted as a function of toxin concentration (circles). Values are shown as mean \pm S.D. ($n = 6$).



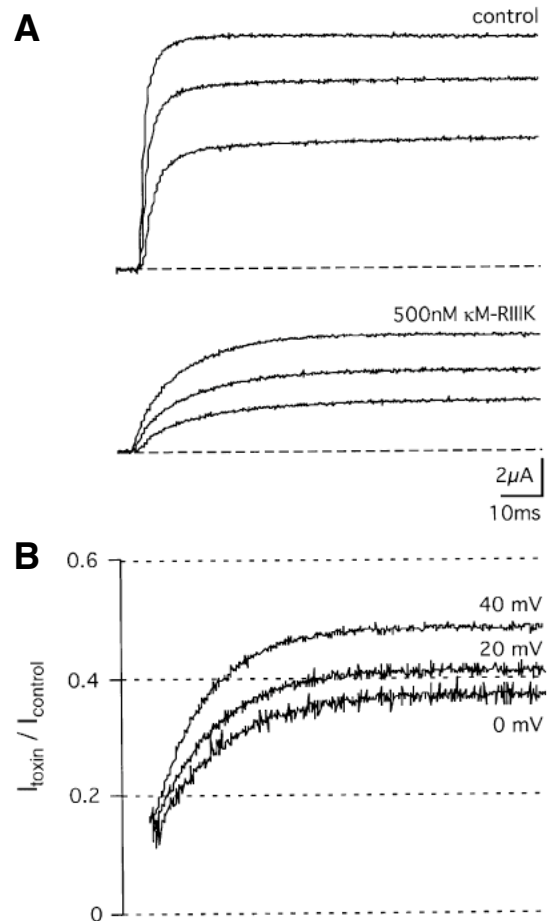
3.1.2.2. Inhibition of Kv1.2 mediated currents is state dependent

It had been shown that the block of *Shaker* and *TShal* mediated currents by \square M-RIIIK is state dependent (Ferber *et al.*, 2003) as seen by different steady-state affinities. The binding kinetics also differ for the open and closed state of the channels. To test whether the block of Kv1.2 mediated currents by \square M-RIIIK is also state dependent, Kv1.2 currents were evoked by depolarizing pulses to 0, +20 and +40 mV in the absence (Fig. 3.5A, *upper traces*) and presence (Fig. 3.5A, *lower traces*) of 500 nM \square M-RIIIK. In the presence of the toxin an apparent slowing of the activation of the evoked currents is observed. As has been shown earlier (Terlau *et al.*, 1999; Ferber *et al.*, 2003) this slowing reflects a reequilibration of toxin binding to the open channels. The ratio of partially blocked Kv1.2 current to unblocked control traces ($I_{\text{toxin}} / I_{\text{control}}$) represents the unblock probability (Fig. 3.5B).

The unblock probability increases exponentially from a starting value at the beginning of the pulse which corresponds to the unblock probability for the closed state of the channels to a new steady-state value in a voltage dependent manner. This behavior is similar to what had been originally described for the block of *Shaker* channels by \square -conotoxin PVIIA (Terlau *et al.*, 1999)

and shows that the properties of α M-RIIIK binding kinetics to open channels can indeed be investigated by the relaxation of partial block during depolarizing voltage steps. Assuming a bimolecular reaction the relaxation kinetics and the steady state unblock probability can also be used to calculate the kinetic parameters of the binding to the open state of the channel (see Terlau *et al.*, 1999).

FIGURE 3.5. The block of α M-RIIIK of Kv1.2 is state dependent. **(A)** Whole cell currents recorded from oocytes expressing Kv1.2 channels evoked by test potentials to 0, +20 and +40 mV from a holding potential of -100 mV under control conditions (*upper panel*) and after addition of 500 nM α M-RIIIK (*lower panel*). The *dashed lines* correspond to zero current. **(B)** Current ratios obtained from the currents in **(A)** for the three test potentials showing a single exponential relaxation of the probability of the channels to be unblocked.



The relaxation time constant and the steady-state unblock probability were obtained from single exponential fits of the ratio $I_{\text{toxin}} / I_{\text{control}}$ and used to calculate the affinity to the open state as well as the on- and off-rate. The results from such calculations are shown in Table 3.2. The mean steady-state affinity calculated from the ratio measurements is 420 nM which is in good agreement with the results obtained from the dose-response experiments (see above). The slight difference for the IC_{50} values obtained with both methods is not significant and within the scatter of the ratio analysis (Table 3. 2).

TABLE 3.2. Summary of K_D , k_{on} and k_{off} values for open and close states of human Kv1.2 and *TShal* K⁺ channels

	Open state				Close state			
	$K^{(O)}$ (0 mV) (nM)	$k_{on}^{(O)}$ ($\mu\text{M}^{-1}\text{s}^{-1}$)	$k_{off}^{(O)}$ (s^{-1})	n	$K^{(C)}$ (0 mV) (nM)	$k_{on}^{(C)}$ ($\mu\text{M}^{-1}\text{s}^{-1}$)	$k_{off}^{(C)}$ (s^{-1})	n
Kv1.2	420 ± 77	43 ± 4	17 ± 2	10	227 ± 68	5.7 ± 1.5	1.07 ± 0.23	5
<i>TShal</i> *	65 ± 16	88 ± 13	5.2 ± 0.9	4	18 ± 7	16.9 ± 4.0	0.25 ± 0.02	3

* The data for *TShal* are taken from Ferber *et al* (2003).

A comparison of the open channel binding of μM -RIIHK to *TShal* and Kv1.2 show that the 8-fold difference in the affinity is due to changes in the on- as well as in the off-rate of toxin binding. The $k_{on}^{(O)}$ for the binding of μM -RIIHK to open Kv1.2 channels is reduced 2-fold and the $k_{off}^{(O)}$ is increased about 3-fold.

Figure 3.6. shows an example of double pulse stimulations, which were used to characterize the reequilibration of toxin binding to the closed channel. The evoked currents resulting from depolarizing pulses to 0 mV show that the activation of the currents under control conditions is almost identical and independent of the different interpulse intervals (8 ms to 2 s; Fig. 3.6A). In contrast, the currents evoked by the first pulse in the presence of 500 nM μM -RIIHK activated slow as shown already in Fig. 3.5, whereas the currents elicited by the second pulse after short interpulse interval exhibited a faster activation comparable to the one observed under control conditions. This indicates that the first pulse caused an unblock of the toxin bound to the closed channel and indicates that within the short time between the two pulses μM -RIIHK did not have enough time to rebind to the closed channels.

With longer interpulse intervals the activation of the currents measured during the second pulse became slower indicating rebinding of the toxin to the closed states. From the development of the apparent slowing of the activation the steady-state affinity to the closed state ($K^{(C)}$) as well as the rate constants ($k_{on}^{(C)}$; $k_{off}^{(C)}$) for the binding of μM -RIIHK to the closed state of Kv1.2 channels can be calculated. The steady-state value (U_C) of the unblock probability obtained for long interpulse intervals is 0.2 (Fig. 3.6B) which corresponds to an IC_{50} for the closed state of 125 nM. The IC_{50} obtained for $n = 5$ are given in Table 3.2. The mean IC_{50} of μM -RIIHK binding to closed channels is about 200 nM demonstrating the affinity of the peptide to the closed state is 2-fold higher than

to the open state at 0 mV. This change in affinity is mainly due to a 17-fold reduction of $k_{\text{off}}^{(C)}$; whereas the $k_{\text{on}}^{(C)}$ is only reduced about 7-fold. These data show that the binding of $\square\text{M-R111K}$ to the open and closed channel is very different, but also indicate that the interaction of $\square\text{M-R111K}$ with Kv1.2, *Shaker* and *TShal* K channels is similar (Ferber *et al.*, 2003; see also Table 3.2). Compared to the binding of $\square\text{M-R111K}$ to the closed state of *TShal* channels the observed 10-fold reduction in affinity for Kv1.2 $K^{(C)}$ is due to an about 3-fold reduction in $k_{\text{on}}^{(C)}$ and a 4-fold increase in $k_{\text{off}}^{(C)}$.

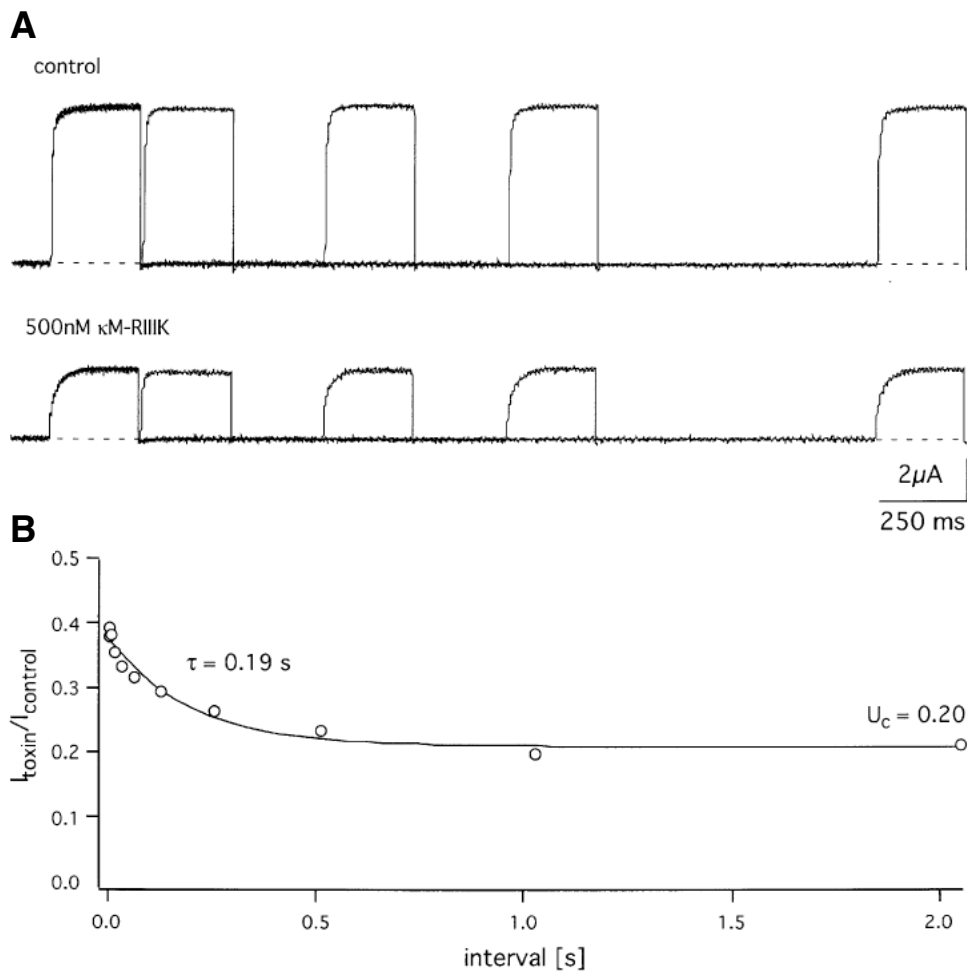


FIGURE 3.6. Relaxation of $\square\text{M-R111K}$ binding to closed Kv1.2 channels measured by a double pulse stimulation. **(A)** Superimposed records of responses to double pulse stimulations before (*upper panel*) and after the application of 500 nM $\square\text{M-R111K}$ (*lower panel*). Each stimulation consisted of a 250 ms conditioning pulse to 0 mV followed by a test pulse of the same amplitude and duration. The interval between the two pulses ranged from 2 to 8192 ms. Successive stimulations were separated by 45 s at the holding potential of -100 mV. For clarity reasons not all pulses are shown. The *dashed lines* correspond to zero current. **(B)** The amplitude of the second response at the half maximal activation time of the control normalized to the first response is plotted versus the pulse interval (circles). The solid line represents a single exponential fit decaying with a time constant (τ) of 190 ms to an unblock probability U_c of 0.20.

3.2. Alanine scanning mutagenesis

3.2.1. Identification of the residues important for \square M-R111K

To investigate which amino acids of \square M-R111K are important for the binding, all amino acids besides the cysteines have been mutated into an alanine. The affinity of the toxin mutants was functionally assayed by two-electrode voltage clamp measurements using *Xenopus* oocytes expressing the trout *TShal* K⁺ channel. The results of these assays are shown in Table 3.3.

TABLE 3.3. IC₅₀ Values for *TShal* K⁺ block of \square M-R111K and Analogs. The IC₅₀ values (in nM) of the \square M-R111K WT and mutants interactions are given by Mean values \pm SE

\square M-R111K	IC ₅₀	n	IC ₅₀ mutant / IC ₅₀ WT
WT	76 \pm 10	9	1
L1A	3180 \pm 120	6	42
O2A	200 \pm 20	4	3
S3A	750 \pm 110	6	10
S6A	240 \pm 30	4	3
L7A	310 \pm 40	6	4
N8A	420 \pm 80	3	6
L9A	90 \pm 10	3	1
R10A	4220 \pm 330	7	56
L11A	970 \pm 120	6	13
O13A	510 \pm 70	6	7
V14A	1130 \pm 170	5	15
O15A	850 \pm 110	3	11
O15R	2700 \pm 370	4	36
O15K	450 \pm 30	4	6
K18A	3900 \pm 530	6	52
R19A	1530 \pm 240	9	20
K18R/R19K	180 \pm 40	7	2
N20A	430 \pm 40	3	6
O21A	130 \pm 20	3	2
T24A	120 \pm 30	3	1

Parallel to our alanine scanning analysis, the structure of \square M-R111K was solved by Carlomagno and coworkers at the Max-Planck-Institute for Biophysical Chemistry (Göttingen, Germany) using nuclear magnetic resonance (NMR) technique (see also Discussion). Figure 3.7 shows the relative changes in the affinity of \square M-R111K mutants and the structure of the peptide. Alanine scanning mutagenesis revealed three groups of \square M-R111K residues summarized in Fig. 3.7. For six amino acids (O2, S6, L7, L9, O21, and T24; green labeled in Fig. 3.7A and B), the alanine substitution resulted in an IC₅₀ value that was within 5-fold of that of wild-type \square M-R111K. To

this relative small change in affinity introduced by the alanine mutation, we assume that this group is not directly involved in the binding of the toxin. We note that some substitutions (O2A, S6A, and L7A) cause a larger change in the IC_{50} value than others (L9A, O21A, and T24), indicating that although these residues are not dominant determinants for binding they may slightly contribute to the interaction with the *TShal* channel.

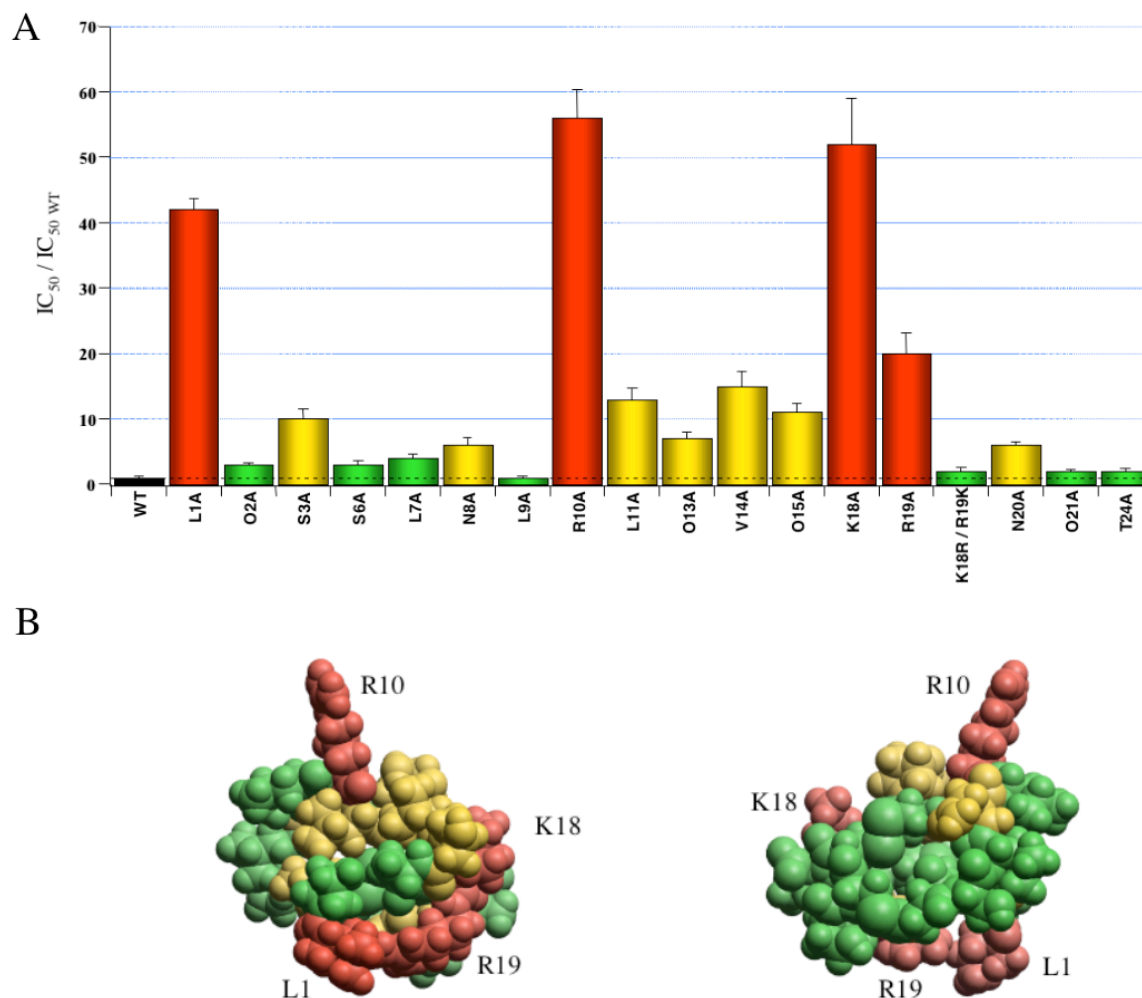


FIGURE 3.7. The summary of the alanine mutagenesis assay. **(A)** Bar-diagram shows the affinity of all alanine mutants and a double mutant analogs of \square M-RIIK compared to the IC_{50} value of the \square M-RIIK wild-type. **(B)** The space-filled model showing the map of the functionally important residues of \square M-RIIK with the three-dimensional structure. To visualize the different changes in the affinity observed for the corresponding alanine mutants, the residues are color-coded: red for an alanine substitution that increased the IC_{50} of \square M-RIIK by ≥ 20 -fold (L1, R10, K18, and R19), yellow for an alanine substitution that affected the affinity by more than 5-fold but by less than 16-fold (S3, N8, L11, O13, V14, O15, and N20), and green for the rest. The right figure shows the opposite view of the toxin. The *dashed line* corresponds to wild-type level.

A second group, where alanine mutations of seven (S3, N8, L11, O13, V14, O15, and N20; yellow labeled in Fig 3.7A and B) residues exhibited an intermediate behavior, with IC_{50} values

more than 5-fold greater but less than 16-fold less than that of wild-type IC_{50} . Interestingly, S3, L11, O13, V14, O15, and N20 are located on the same side of the molecule (Fig. 3.7B).

Figure 3.8 shows that mutations of four other residues (L1, R10, K18, and R19; red labeled in Fig. 3.7A and B) resulted in a major reduction of the affinity for *TSha1* K^+ channels (Table 3.3). The IC_{50} values of these analogs are increased by ≥ 20 -fold, indicating an important role of these amino acids in receptor binding. Interestingly, the affinity of the double mutant K18R/R19K for the *TSha1* K^+ channel is close to that of the wild type, indicating that the positive charge is important at both positions, but the specific nature of the side chain is not critical for the interaction with the *TSha1* K^+ channel.

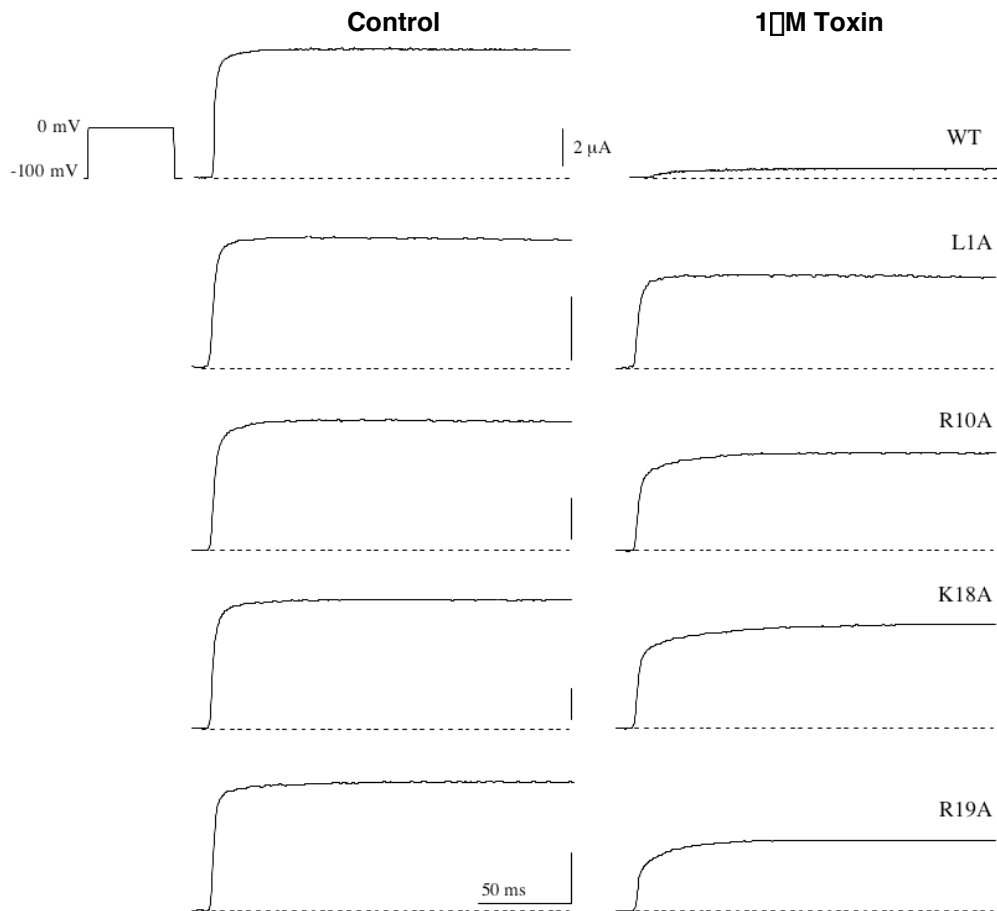


FIGURE 3.8. Mutation of residues L1, R10, K18, and R19 results in isoforms of μ M-R11IK with low affinity for *TSha1* channels. Whole-cell currents recorded from oocytes expressing *TSha1* K^+ channels before and after addition of the μ M-R11IK isoform are shown. Notice the apparent slowing of activation of the currents in the presence of R10A, K18A, and R19A illustrating the re-equilibrium of toxin binding to the open state (Terlau *et al.*, 1999). The pulse protocol was like that described in the legend of Figure 3.1. The vertical bars represent 2μ A. The dashed lines correspond to zero current.

Somewhat surprisingly for a peptide blocking K⁺ channels, these four critical residues are distributed at various sites in the molecule (Fig. 3.7B). Furthermore, the structure of \square M-RIIIK does not provide any evidence of the existence of a hydrophobic-positively charged amino acid dyad, as Leu1, the most important hydrophobic residue for binding, is more than 6 Å from any positive charge.

3.2.2. Evaluation of additional substitutions for Leu1.

The alanine walk identified Leu1 as the only hydrophobic residue that substantively affects binding of \square M-conotoxin RIIIK to the *TShal* channel. The solution structure determined by NMR indicates that Leu1 is too far from any positively charged residue to serve as the hydrophobic component of a dyad (Fig. 3.7B), a conserved motif in otherwise divergent K⁺ channel-targeted toxins. However, the fact that the N-terminal region (amino acids 1-11) is flexible leads to some reservations regarding this conclusion. In other toxins, the hydrophobic component of the dyad is most commonly an aromatic residue, while a lysine plays the role of the positively charged component; this lysine occludes the extracellular opening of the ion channel pore. Thus, if Leu1 is part of a functional dyad that forms following a conformational change upon binding of the receptor, it is reasonable to predict that the substitution of the leucine with an aromatic amino acid can be well-tolerated and perhaps even leads to an increase in binding affinity. To test this hypothesis, we evaluated the effect of various substitutions of Leu1 on the interaction of \square M-RIIIK with the *TShal* channel (Table 3.4) by investigating the affinity of different Leu1 mutants on *TShal* channels, again using two electrode voltage clamp measurements within the *Xenopus* expression system.

In contrast to what was predicted on the basis of the dyad hypothesis, both a phenylalanine (the most common amino acid as the hydrophobic half of the dyad) and a tyrosine substitution for Leu1 caused a greater apparent decrease in affinity (>100-fold) than the L1A substitution (about 40-fold).

TABLE 3.4. Mutations of Leu1 affect the affinity of \square M-RIIIK for the *TShal* K⁺ Channel. The IC₅₀ values (in nM) of the \square M-RIIIK WT and mutants interactions are given by Mean values \pm SE

\square M-RIIIK	IC ₅₀ \pm SEM	n	IC ₅₀ mutant/IC ₅₀ WT
WT	76 \pm 10	9	1
L1A	3180 \pm 120	6	42
Ac-L1	7620 \pm 380	5	100
L1E	56500 \pm 12350	5	745
L1H	5430 \pm 400	4	72
L1I	1380 \pm 450	5	18
L1M	340 \pm 50	5	4
L1K	950 \pm 140	4	13
L1R	190 \pm 5	4	3
L1F	5260 \pm 710	4	69
L1Y	12290 \pm 1110	3	162

Unexpectedly, the replacement of Leu with a positively charged amino acid (e.g., the L1R and L1K mutations) had a weaker effect on the affinity for the *TShal* channel (2- and 12-fold, respectively) than the L1A mutant. Introducing a negative charge (L1E) or blocking the positive charge (N-acetylated \square M-RIIIK) causes a drastic decrease in affinity (>500- and >100-fold, respectively).

To test the tolerance of Leu1 position for charge changes, we introduced L1H mutant. The net charge of the amidazol group of L1H mutant can be switched from negative to positive, by changing the pH of the NFR from acidic (pH 5) to basic (pH 9) values (pI of His is at pH 7.65). As seen in Fig. 3.9, L1H mutant at pH 5 (positively charged) caused a decrease in affinity (~ 4-fold, 360 \pm 30, n = 3). While at pH 9, L1H mutant (negatively charged) caused a dramatic decrease in affinity (~ 440-fold, 33490 \pm 770, n = 3). These L1H experiments show that for the affinity of \square M-RIIIK to *TShal* channel, substitution of the Leu1 position to positive is more tolerated than negative charged side chains.

The data in Tables 3.3 and 3.4, and Fig. 3.9, do not support the involvement of Leu1 in a dyad. These results, together with the structural data that indicate that Leu1 is not close to any positively charged side chain, allows us to conclude that this leucine does not serve as the hydrophobic component of a dyad.

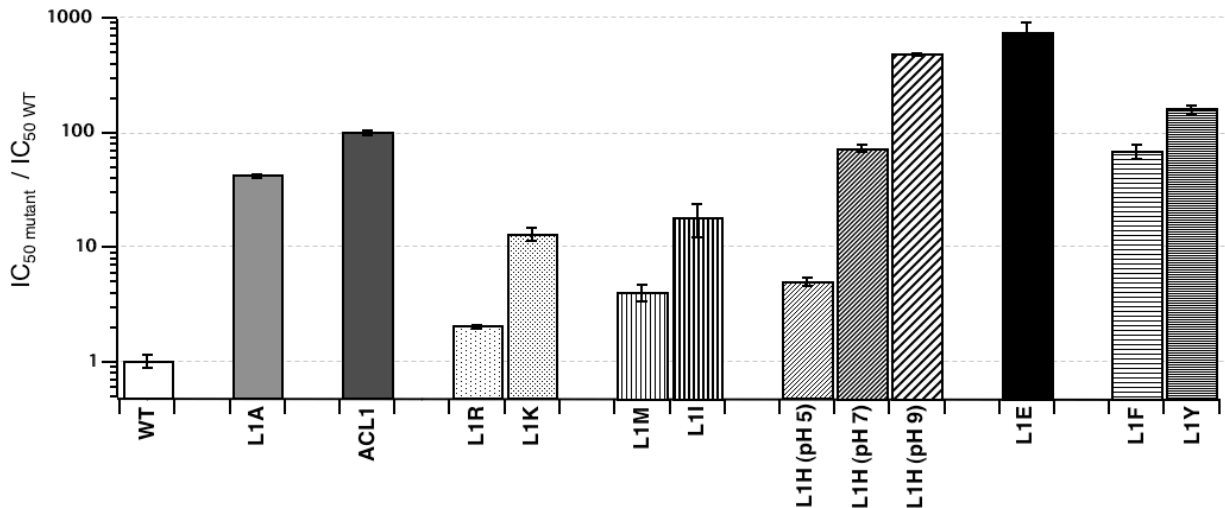


FIGURE 3.9. Changes in the affinity of the mutants of $[M-R111K$ at Leu1 position investigated in comparison to the IC_{50} value of the $[M-R111K$ wild-type. For L1A (gray bar) the IC_{50} is increased around 40-fold, while capping the positively charged N-terminus by acetyl group (ACL1; dark gray bar) leads to an increase of the IC_{50} more than 100-fold. Substituting Leu1 by the positively charged amino acid (L1R and L1K; dotted bars) resulted in a minor increase of the IC_{50} values of 3 and 13, respectively. Also, a minor increase in IC_{50} values is observed when hydrophobic residues are introduced (L1M and L1I; vertical-stripped bars). Affecting the charge of the amidazol group of L1H mutant (diagonal- stripped bars) from negative to positive, by changing the pH of the NFR from acidic to basic values, leads to increase in the IC_{50} . The most pronounced increase in IC_{50} value (> 700 folds) is seen by replacement of L1 with negative charged residue (L1E; black bar). Introducing aromatic residues (Y or F, horizontal-stripped bars) into L1 caused a increase of IC_{50} values, around 70 and 160-folds, respectively.

3.2.3. $[M-R111K$ mutants affect the binding kinetics

We examined the functional effect of $[M-R111K$ mutants on the blocking activity by measuring the association ($k_{on}^{(0)}$) and dissociation ($k_{off}^{(0)}$) rates of toxin with *TShal* channels expressed in *Xenopus* oocytes, using two electrode voltage clamp. The rate constants were determined from the time-course of the transition from unblocked to steady state-blocked current ratios on open state channels at 0 mV potential (see Materials and Methods; Terlau *et al.*, 1999).

Table 3.5 summarizes the kinetic parameters of the binding of 27 mutants of $[M-R111K$ investigated. In nearly all cases, we observed that the major reason for the lower affinities of $[M-R111K$ mutants is mainly due to an increase in dissociation rates (up to 80-fold in L1Y) and a decrease in the association rates (down to 50-fold in AcL1). In surveying the mutants in Table 3.5, we classified residues into three groups according to “on-” and “off”-rate effects, which reflect primarily intimate interactions with the channel.

The first group is composed of the important positively charged residues (R10, K18 and R19). Except for L1A, members of this group showed the biggest reduction in binding affinity comparing to other alanine mutants; with $K^{(0)}$ reduced 20- to 55- fold to that of the \square M-R11IK wild-type. This change in affinity is mainly due to 5- to 10- fold reduction in $k_{on}^{(0)}$, whereas the $k_{off}^{(0)}$ is only increased about 3- to 5- fold (see current traces in Fig. 3.8 for comparison). As expected, the mutant K18R/R19K has a $K^{(0)}$ value close to that of the wild-type, but the double mutation introduce a 2-fold reduction in $k_{on}^{(0)}$ rate, while $k_{off}^{(0)}$ rate is almost not affected. Although the charge was conserved, it seems that the relative bulky side chain of Arg hindered the association rate.

TABLE 3.5. Summary of Association and dissociation rate constants of \square M-R11IK, $k_{on}^{(0)}$ and $k_{off}^{(0)}$, and the dissociation constant ($K^{(0)}$) measured at 0 mV on *TShal* K^+ channels. Each value represents the mean \pm SE of the number of measurements reported (n).

\square M-R11IK	$K^{(0)}$ (0mV) nM	$k_{on}^{(0)}$ \square M ⁻¹ *S ⁻¹	$k_{off}^{(0)}$ S ⁻¹	$K^{(0)}$ ratio (mut/wt)	$k_{on}^{(0)}$ ratio (mut/wt)	$k_{off}^{(0)}$ ratio (mut/wt)	n
WT	76 \pm 13	89 \pm 11	6 \pm 1	1	1	1	5
L1A	2980 \pm 30	81 \pm 7	243 \pm 23	39	1	40.5	5
O2A	170 \pm 20	120 \pm 10	20 \pm 3	2	1.3	3.3	3
S3A	490 \pm 130	47 \pm 10	21 \pm 5	6	0.5	3.5	3
S6A	240 \pm 30	28 \pm 6	7 \pm 1	3	0.3	1.2	3
L7A	300 \pm 40	91 \pm 6	27 \pm 3	4	1	4.5	6
N8A	320 \pm 30	32 \pm 1	10 \pm 1	4	0.4	1.6	3
L9A	90 \pm 10	247 \pm 17	22 \pm 1	1	2.8	3.7	3
R10A	4200 \pm 410	15 \pm 3	53 \pm 13	55	0.2	3.7	5
L11A	850 \pm 120	79 \pm 8	64 \pm 7	11	0.9	10.7	6
O13A	470 \pm 40	119 \pm 7	56 \pm 6	6	1.3	9.3	5
V14A	830 \pm 40	51 \pm 3	42 \pm 1	11	0.6	7	4
O15A	930 \pm 160	91 \pm 9	81 \pm 7	12	1	13.5	3
K18A	3600 \pm 1080	7 \pm 1	20 \pm 2	47	0.08	3.3	5
R19A	1600 \pm 240	20 \pm 3	29 \pm 5	21	0.2	4.8	7
K18R/R19K	90 \pm 10	42 \pm 4	4 \pm 0.4	1	0.5	0.7	3
N20A	390 \pm 20	23 \pm 2	9 \pm 1	5	0.3	1.5	3
O21A	120 \pm 10	56 \pm 3	7 \pm 0.2	2	0.6	1.2	3
T24A	90 \pm 20	56 \pm 21	5 \pm 1	1	0.6	0.8	3
Ac-L1	7020 \pm 1300	2 \pm 0.4	10 \pm 1	92	0.02	1.7	3
L1F	6000 \pm 1230	52 \pm 8	322 \pm 85	79	0.6	53.7	4
L1Y	10800 \pm 460	45 \pm 8	480 \pm 69	142	0.5	80	3
L1I	890 \pm 290	8 \pm 1	8 \pm 3	12	0.09	1.3	5
L1M	360 \pm 40	35 \pm 3	12 \pm 1	5	0.4	2	3
L1R	160 \pm 10	70 \pm 12	11 \pm 2	2	0.8	1.8	4
L1K	890 \pm 50	27 \pm 7	24 \pm 6	12	0.3	4	4
L1H	5550 \pm 700	4 \pm 1	21 \pm 6	73	0.04	3.5	3
L1E	30480 \pm 4230	11 \pm 1	327 \pm 60	401	0.1	54.5	3

The second group comprise mainly from hydrophobic residues located on the middle region of the toxin (L7, L9, L11, O13, V14 and O15A). These mutants affected the equilibrium block by major increase in $k_{\text{off}}^{(0)}$ of about 4- to 14- fold, whereas the on-rates are hardly not affected. The L9A mutant is exceptional for being the only mutant that shows an increase on both rates resulting in an overall affinity close to wild-type. This might indicate an important role of Leu9 in the initial binding kinetics. Presumably, Leu9 has a key role on the flexibility of the N-terminus arm made of the first 11 residues to facilitate the docking of the $\square\text{M-RIIIK}$ to the pore region of the channel. This assumption is supported by the effects observed for the L11-O13-V14-O15 region of the toxin for which the binding affinity of the corresponding alanine mutants was mainly affected by an increase in $k_{\text{off}}^{(0)}$ rates 7- to 14-fold.

The third group is mainly composed of polar residues where the alanine substitution leads to less effects on both $k_{\text{off}}^{(0)}$ and $k_{\text{on}}^{(0)}$ values comparing to the first two groups. The small increase in $K^{(0)}$ values ranged from 1- to 6-fold, which is due to an about 1- to 3-fold decreased on rates and increased off rates. The amino acids belonging to this group are located bordering the first two groups and they may play indirect role in binding and performing structural support by polar binding in the toxin peptide.

Leu1 position shows tight structural requirements for maintenance of blocking activity. We tested 10 mutants on this position to understand the functional effect of Leu1 to binding kinetics of $\square\text{M-RIIIK}$ (see above). Neutralizing the side chain of Leu1 by Ala substitution decreased the affinity of the block 40-fold, which is due to an increase in the $k_{\text{off}}^{(0)}$ of around 40-fold. This profound effect is clearly seen in the current trace of L1A mutant when compared with that of the WT in Fig. 3.8. In contrast to the changed amino acids important for binding, the presence of 1 $\square\text{M}$ L1A did *not* result in an apparent slowing of the activation due to the state dependence of the binding. This indicates the importance of the Leu side chain as the first residue of $\square\text{M-RIIIK}$ for contributing in hydrophobic interaction(s) with hydrophobic residues in the pore region of *TShal* channel. Such property is never been represented *at least* among conotoxins targeting K^+ channels characterized up to date.

We tested the substitution of Leu1 with other hydrophobic amino acids (Met or Ile) on the functional effect of \square M-RIIIK binding kinetics. With little effect on the $k_{\text{off}}^{(0)}$, both L1M and L1I reduced their $K^{(0)}$ values, about 5- to 12- fold, mainly due to decreased on rates, which are about 3- and 10-fold, respectively. Similarly, the substitution of Leu1 with positively charged amino acids (Arg or Lys) resulted in about 2- to 12- fold reduction in their $K^{(0)}$ values, which is mainly due to about 2- and 4-fold decrease in off rates, respectively. It is worth to mention that Lys substitute at the same position (L1K), which can be grossly envisioned as a pseudo-methionine with a positively charged head resulted $k_{\text{off}}^{(0)}$ close to that of L1M binding but with increased $k_{\text{on}}^{(0)}$ that is about two times.

On the other hand, replacement of the Leu1 with His or Glu, containing acidic side chain, are not compatible with toxin binding. Negative charges carried by these substitutes and size differences largely affected the affinity of toxin binding. Both mutants had on rates that are decreased by more than 10 times and increased off rates, an effect which was more strikingly for the Glu substitution (about 55-fold).

The substitution of Leu1 with aromatic amino acids (Phe or Tyr) resulted in a little effect on $k_{\text{on}}^{(0)}$ of toxin binding. Both, L1F and L1Y have an about 80- to 140- fold reduction in their $K^{(0)}$ values, which is mainly due to decreased off rates, about 54- and 80-fold, respectively. This observation may be correlated with the bulky size of both Phe and Tyr residues.

The results obtained by this kinetic analysis again indicate the importance of the presence of a positive charge contributed by the free N-terminus to the potency of \square M-RIIIK to block K^+ channels (see Fig. 3.9). Therefore, we analyzed the functional effect of masking the N-terminus with Acetyl group. Using ACL1 analog, the equilibrium block was largely decreased, about 90-fold, mainly manifested by profound, about 50-fold decreased on rate to that of WT. Thus, this \square M-RIIIK analog results in an unusual barrier for binding, by masking the positively charged N-terminus, which must be overcome before the bound state can be reached.

On the basis of the kinetic analysis of the binding of different Leu substitution, we find that this position tolerates the existing of positively charged and hydrophobic side chains but the toxin binding is incompatible with aromatic and acidic side chains or capping the positively charged N-

terminus. The kinetic data analysis provides a kinetic explanation of different functional effects of studied α M-RIIIK mutants. The overall results support the importance of positively charged and hydrophobic residues, mainly Leu1 for the binding affinity of α M-RIIIK to *TShal* K⁺ channels.

3.2.4. α M-RIIIK mutants do *not* interact with Nav1.4 sodium channel

α M-conotoxin RIIIK and α -conotoxin GIIIA (α -GIIIA), which is known to selectively block Nav1.4 channels, have the same cysteine backbone of the class III framework which is different to the one of α -PVIIA belonging to the α -superfamily of conopeptides (see Fig. 1.5). Despite the structural similarities between α -GIIIA and α M-RIIIK, the sodium channels Nav1.2, Nav1.4 and Nav1.5 are not affected by α M-RIIIK (Ferber *et al.*, 2003). To identify if any of α M-RIIIK mutant inhibits Na⁺ currents, the activity of these peptides were tested individually on Nav1.4 channels expressed in *Xenopus* oocytes. The results are shown in Fig. 3.10. None of the α M-RIIIK analogs tested so far, which are all alanine mutants from L1A-L19A, at a concentration of 10 μ M has effects on Nav1.4 mediated currents.

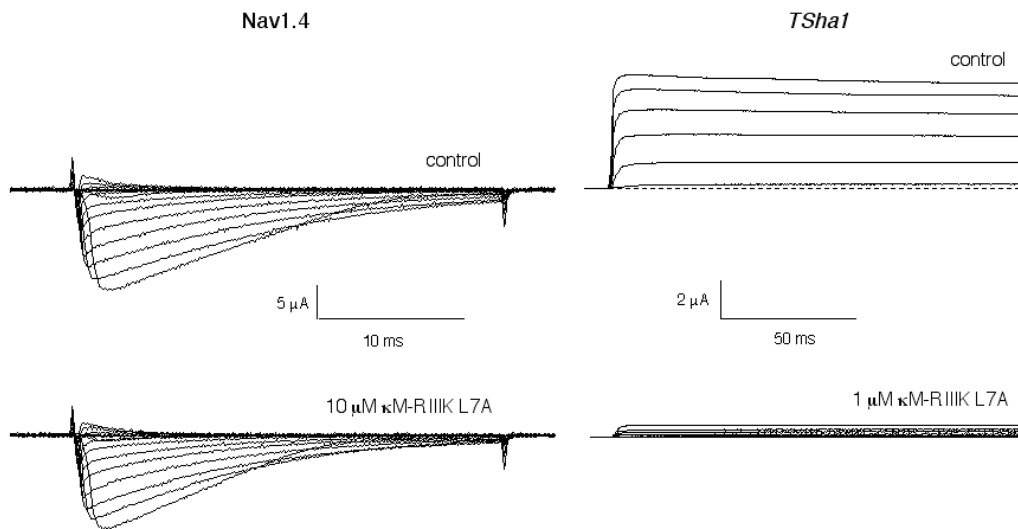


FIGURE 3.10. α M-RIIIK mutants do *not* block Nav1.4 mediated currents. Whole cell currents recorded from oocytes expressing Nav1.4 (*left panel*) and *TShal* K⁺ channels (*right panel*). Current traces of Nav1.4 evoked by depolarization from a holding potential at -100 mV and stepped for 30 ms to test potentials between -60 mV and $+40$ mV in 10 mV increments, under control conditions (*upper-left panel*) and after addition of 10 μ M α M-RIIIK L7A mutant (*lower-left panel*). Clearly, Nav1.4 mediated currents are almost unaffected by the toxin. Current traces of *TShal*, evoked by depolarization started from holding potential at -100 mV and stepped for 250 ms to test potentials between -60 mV and $+60$ mV in 20 mV increments (*upper-right panel*) and after addition of 1 μ M α M-RIIIK L7A mutant (*lower-right panel*). Almost all *TShal*-mediated K⁺ currents were blocked by the toxin. The *dashed lines* correspond to zero current.

Structure-function studies on the α -conotoxins have established that the arginine residue (Arg13 in α -GIIIA) is a critical residue for blocking voltage-gated sodium channels, because the charged guanidino group of the arginine residue is believed to functionally block the pore (Becker *et al.*, 1992; French, *et al.*, 1996; Hui *et al.*, 2002). In contrast, α M-RIIIK lack this critical arginine residue and, instead, contains a hydroxylated proline at the homologous position 15 (Hyp15, see Fig. 1.6 in introduction) when both toxin sequences aligned according to their Cys arrangement.

In order to investigate the functional importance of Hyp15 of α M-RIIIK on K^+ channel binding, the positively charged residue (O15K and O15R) were introduced and the blocking activity was measured. The association ($k_{on}^{(0)}$) and dissociation ($k_{off}^{(0)}$) rates of toxin with *TShal* channels expressed in *Xenopus* oocytes, was calculated as described before. In parallel experiments, we tested the ability of α M-RIIIK O15K and O15R mutants to block Nav1.4 mediated currents.

Both Hyp15 mutants resulted in a reduced affinity to *TShal* channels. The off rates of toxin binding for O15K and O15R increased about 8- and 20-fold, causing about 6- and 39-fold decrease in the steady state affinity of O15K and O15R. However, the on rate of O15R is only reduced about 2.5-fold, while that of O15K is mainly not affected. Interestingly, and in comparison to α M-RIIIK O15A mutant, the binding affinity was two times higher in favor of O15K, which is mainly due to almost two times reduction of the $k_{off}^{(0)}$ value. From their kinetic rates, the binding affinity favors the positive charge of Lys over neutral Ala substitution at position 15. Although the charge is conserved in Arg, the bulky size of Arg seems to hinder toxin association, which causes reduction in the on rate. This observation supports our view that Hyp15 residues may face the conducting pathway of the channel pore.

When tested on Na^+ channels, both α M-RIIIK O15K/R mutants at concentrations of 2, 5 and 10 μ M has no effects on Nav1.4 mediated currents (*data not shown*).

TABLE 3.6. Summary of Association and dissociation rate constants of \square M-RIIIK Hyp15 mutants, $k_{on}^{(0)}$ and $k_{off}^{(0)}$, and the dissociation constant ($K^{(0)}$) were measured at 0 mV on *TSha1* K⁺ channels. Each value represents the mean \pm SE of the number of measurements reported (n).

\square M-RIIIK	$K^{(0)}$ (0mV) nM	$k_{on}^{(0)}$ \square M ⁻¹ *S ⁻¹	$k_{off}^{(0)}$ S ⁻¹	$K^{(0)}$ ratio (mut/wt)	$k_{on}^{(0)}$ ratio (mut/wt)	$k_{off}^{(0)}$ ratio (mut/wt)	n
WT	76 \pm 13	89 \pm 11	6 \pm 1	1	1	1	5
O15A	930 \pm 160	91 \pm 9	81 \pm 7	12	1	13.5	3
O15K	430 \pm 20	103 \pm 10	45 \pm 5	6	1.2	7.5	4
O15R	2940 \pm 540	38 \pm 7	122 \pm 42	39	0.4	20.3	4

Taken together, these data indicate that for \square M-RIIIK binding to *TSha1* K⁺ channels, the substitution of Lys is more tolerated than incorporating a bulky Arg residue or neutralize the polarity on position 15 of the toxin. This indicates that Hyp15 may face the pore region of *TSha1* channel but is *not* involved in direct electrostatic interactions. Moreover, \square M-RIIIK and \square -GIIA are structurally very similar, but have a very different pharmacological profile. The data obtained by the Hyp15 mutants indicate that this functional diversity seems to be *not* bridged between those closed-related conotoxin families by only single amino acid substitution.

3.3. Mutant cycle analysis

After determining the critical residues important for \square M-RIIIK binding, we identified the counter interacting residues in the pore region of *TSha1* K⁺ channel by means of mutant cycle analysis (Hildago and MacKinnon, 1995; Schreiber and Fersht, 1995). On the bases of coupling energy calculations, we could characterize the structural bases and built the model of \square M-RIIIK docking to the *TSha1* K⁺ channel. Performing a mutant cycle analysis requires interaction of both mutant and wild-type forms of both toxin and channel. Therefore, we constructed selected point mutation within the pore region of *TSha1* channel and investigated the binding of \square M-RIIIK WT and mutants on these channel isoforms.

3.3.1. *TShal* mutant channels

Based on previous extensive site-directed studies on *Shaker* K⁺ channel and homologous sequences of mammalian Kv1 channel, 15 point-mutations were selected at seven positions within the P-loop of *TShal* channel (Fig. 3.11). The mutated amino acids, predicted to interact with the toxin pharmacophore residues, are located in three regions: the turret region, the pore helix and the bottom of the outer vestibule of the channel, close to the channel selectivity filter. In the turret region, we focused on the negatively charged residues Glu348 and Glu354, which are aligned with the important corresponding *Shaker* residues Ser421 and Lys427, respectively (MacKinnon and Miller, 1988; MacKinnon *et al.*, 1990; Ferber *et al.*, 2003). Also, the hydrophobic residue Pro349 (resembles *Shaker* residue Glu 422) and the polar Ser 351 residues, a conservative residue equivalent to Ser 424 in *Shaker* sequence (MacKinnon and Miller, 1989; MacKinnon *et al.*, 1990; Jacobsen *et al.*, 2000). In the pore helix, the *TShal* residue Ser366 (as Thr439 in *Shaker*) was selected. While in the bottom of the vestibule, both Met375 and Val376 were chosen as corresponded to the important equivalent residues M448 and T449 of *Shaker* channels, respectively (Shon *et al.*, 1998; Jacobsen *et al.*, 2000; Ferber *et al.*, 2003). *In vitro* site-directed mutagenesis was used to obtain selected point mutations within the pore region of *TShal* channel for mutant cycle experiments. All methods were performed following standard procedures (Sambrook *et al.*, 1989; Ishii *et al.*, 1998, see Fig. 2.5).

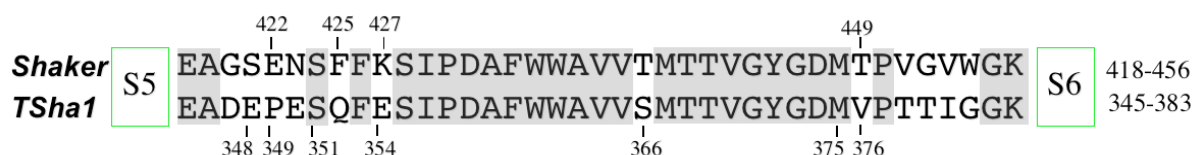


FIGURE 3.11. The amino acid alignment of the pore region of the *Shaker* K⁺ channel (S5-S6 linker) and the corresponding region of *TShal* K⁺ channel (Nguyen *et al.*, (2000)). The gray shading indicates conservative amino acid sequences.

A number of pore mutations of the *TShal* channel were generated and affinities of [M-R111K WT were measured by two-electrode voltage clamp measurements using *Xenopus* oocytes expressing *TShal* mutant channels. The effects of these single amino acid substitutions on the affinity of [M-R111K WT are shown in Table 3.7 and Fig. 3.12.

Four out of the 15 constructed mutations, in Ser366 and Val376 loci, failed to yield functional channels, and V376H had low expression and could therefore not be used for measurement. Some mutations (S351K, E354K, E354Q and M375I) resulted in a decreased affinity of \square M-R111K of about ≥ 2 -fold. Some other mutation (E348S, E348K, P349K, M375L and V376T) resulted in a decreased affinity of \square M-R111K of < 2 -fold. In particular, the affinity of three mutations (V376T, E348S and E348K) is not significantly different than the wild-type toxin ($P = 0.058$; 0.169 and 0.239 , t -test), respectively. One mutation, M375K, is not sensitive to \square M-R111K and therefore was not useful for the cycling analysis. The whole cell current traces for representative *TShal* K^+ currents recorded from oocytes expressing mutant channels in the absence and presence of \square M-R111K are shown in Fig. 3.13.

TABLE 3.7. IC_{50} Values for *TShal* mutant K^+ block of \square M-R111K WT. The IC_{50} values are given by mean values \pm SE. NF: not functional. LE: low expression.

\square M-R111K	IC_{50} (0 mV) nM	n
WT	76 ± 10	9
E348S	110 ± 30	4
E348K	50 ± 10	3
P349K	130 ± 20	3
S351K	160 ± 10	4
E354K	490 ± 110	3
E354Q	270 ± 30	4
S366T	NF	--
M375K	10730 ± 2460	3
M375L	140 ± 40	3
M375I	1360 ± 70	5
V376T	120 ± 20	3
V376H	LE	--
V376S	NF	--
V376E	NF	--
V376K	NF	--

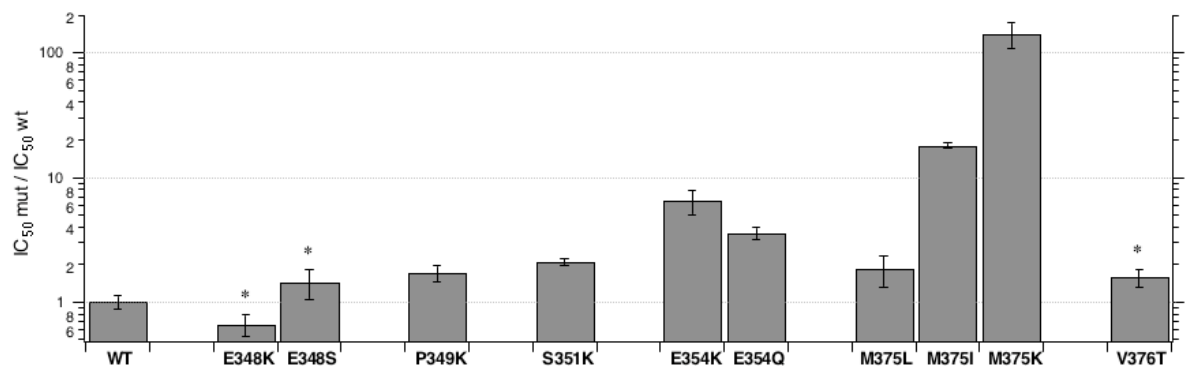


FIGURE 3.12. Influence of single point mutations in the pore region of *TSha1* on κ M-R11IK binding. The bar diagram shows the affinity of κ M-R11IK to the individual channel mutants normalized to wildtype IC₅₀. Astrisks represent a non-significant mean value compared to WT.

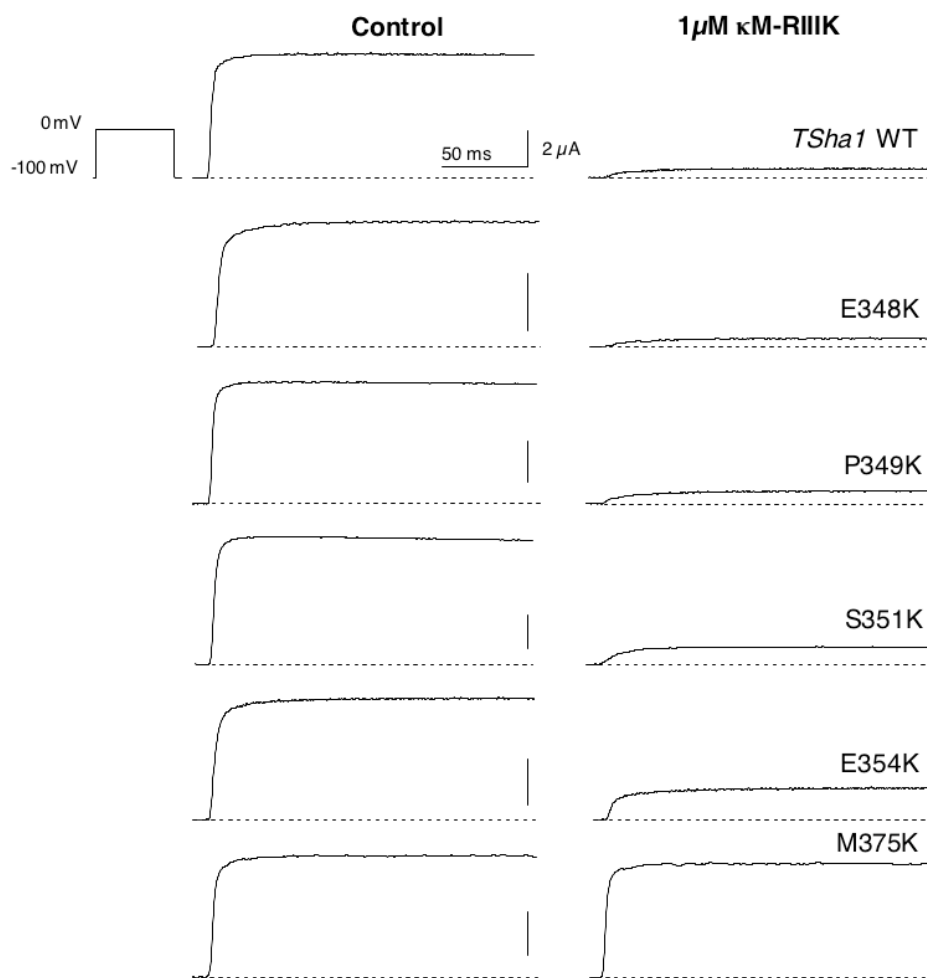


FIGURE 3.13. Effect of point mutations of pore region of *TSha1* channels on κ M-R11IK binding. Whole-cell currents recorded from oocytes expressing *TSha1* mutant channels before and after addition of the κ M-R11IK WT are shown. Notice the apparent slowing of activation of the currents in the presence of toxin illustrating the re-equilibrium of toxin binding to the open state (Terlau *et al.*, 1999). The pulse protocol was like that described in the legend of Fig.3.1. The vertical bars represent 2 μ A. The dashed lines correspond to zero current.

3.3.2. Determining IC₅₀ and $\Delta\Delta G$ values of the mutant cycle analysis

We performed mutant cycle analysis using the functional *TShal* mutants that showed sensitivity to \square M-RIIK from Table 3.7. From the toxin mutants available, we used the residues known to be critical for binding (Leu1, Arg10, Las18 and Arg19). Performing mutant cycle analysis requires determinations of blocking affinity of all of the following combinations: WT channel-WT toxin, mutant channel-WT toxin, WT channel-mutant toxin, and mutant channel-mutant toxin (see Materials and Methods and Schreiber and Fresht, 1995). Therefore, we obtained IC₅₀ values for block of WT *TShal* channels by \square M-RIIK mutant toxin derivatives L1A, L1I, R10A, K18A, R19A and K18R/R19K from the alanine scanning mutagenesis (Tables 3.3 and 3.4). The IC₅₀ values of the interacting toxin-channel pairs are summarized in Table 3.8.

TABLE 3.8. IC₅₀ Values for *TShal* mutant K⁺ block of \square M-RIIK WT and analogs. The IC₅₀ values (in nM) are given by Mean values \pm SE, n = number of independent experiments.

<i>TShal</i>	\square M-RIIK analogs IC ₅₀ [nM]						
	WT	L1A	L1I	R10A	K18A	R19A	K18R / R19K
WT	76 \pm 10 (9)	3180 \pm 120 (6)	1380 \pm 450 (5)	4220 \pm 330 (7)	3900 \pm 530 (6)	1530 \pm 240 (9)	180 \pm 40 (7)
E348S	110 \pm 30 (4)	1920 \pm 290 (4)	480 \pm 120 (3)	1220 \pm 280 (3)	600 \pm 100 (3)	820 \pm 210 (4)	100 \pm 10 (3)
E348K	50 \pm 10 (3)	440 \pm 110 (3)	540 \pm 100 (4)	770 \pm 100 (4)	720 \pm 50 (4)	460 \pm 60 (4)	150 \pm 10 (3)
P349K	130 \pm 20 (3)	1740 \pm 110 (3)	280 \pm 20 (5)	680 \pm 100 (3)	3390 \pm 100 (3)	200 \pm 30 (3)	140 \pm 10 (4)
S351K	160 \pm 10 (4)	2960 \pm 310 (4)	1700 \pm 390 (4)	810 \pm 40 (3)	1390 \pm 350 (3)	770 \pm 80 (4)	260 \pm 60 (3)
E354K	490 \pm 110 (3)	14070 \pm 4740 (3)	1310 \pm 100 (3)	1640 \pm 300 (3)	2070 \pm 220 (3)	740 \pm 140 (3)	620 \pm 80 (3)
E354Q	270 \pm 20 (6)	1660 \pm 80 (5)	1400 \pm 200 (5)	1700 \pm 340 (4)	1870 \pm 350 (4)	1550 \pm 110 (5)	490 \pm 30 (4)
M375I	1360 \pm 70 (5)	11400 \pm 1030 (3)	4740 \pm 580 (4)	37400 \pm 7260 (3)	35160 \pm 7330 (3)	5910 \pm 790 (4)	1420 \pm 150 (3)
V376T	120 \pm 20 (3)	3550 \pm 220 (3)	580 \pm 180 (3)	2490 \pm 520 (4)	4650 \pm 1800 (3)	3990 \pm 1070 (3)	310 \pm 50 (3)

The IC₅₀ values from Table 3.8. were used to calculate the Δ -values and obtain the coupling energies, $\Delta\Delta G$, between amino acid residues of the toxin and the amino acid residues within the pore region of *TShal*. An example of Δ and $\Delta\Delta G$ calculation is demonstrated in Fig. 3.14 (see Materials and Methods). The summary of $\Delta\Delta G$ values in KJ/mol are shown in Fig. 3.15. Residues of toxin-channel pairs that yield $\Delta\Delta G$ values exceeded 2.1 KJ/mol indicate an interaction within 5 Å distance of these amino acids. (for

review see Rauer *et al.*, 1999).

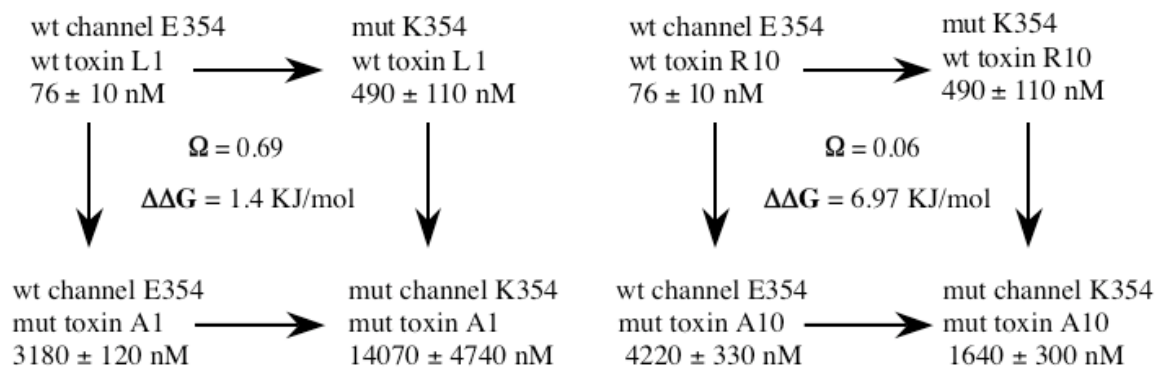


FIGURE 3.14. Examples for mutant cycles of *TShal* E354 with \square M-R11IK-Arg10 (indicating an interaction; $\square = 2.78$) and \square M-R11IK-Leu1 (indicating no interaction; $\square = 1.28$). IC₅₀ values are given as mean ± S.E.. Data are taken from Table 3.10.

In general, *TShal* mutant channels interact to \square M-R11IK analogs with different affinities. The channel mutant E348K was blocked with reduced potency with WT, L1A and R19A analogs of the toxin. When the same channel residue is substituted by a polar residue (E348S; less positive), the channel was preferentially blocked by L1I, R10A, K18A, R19A and K18R/R19K but less potent by the WT and L1A analogs of \square M-R11IK. This means that Glu348 sense the charge changes exposed by corresponded toxin residues, including the N-terminus. For Glu348, this mutant has a strong electrostatic interaction with Arg10, Lys 18 and N-terminus of Leu1 (Fig. 3.15) with \square \square G values between 3 and 5.6 KJ/mol.

The hydrophobic residue Pro349 when mutated into Lys (P349K), was blocked with high affinity by \square M-R11IK WT, R19A and K18R/R19K analogs and with less potency with L1I. In contrast, the affinity of L1A, R10A and K18A to Pro349 is very low. These results show that Pro249 could interacts with Leu1 residue of the toxin, however, Pro349 position is close enough to sense the presence of both Arg10 and Arg19 toxin residues. In fact, the coupling energy of P349K-L1A pair was 2.81 ± 0.16 KJ/mol and increased with preserved hydrophobicity by interacting with L1I yielding 5.24 ± 0.13 KJ/mol. P349K mutant showed a high coupling energy when interacted with R10A (5.83 ± 0.34 KJ/mol) and R19A (6.35 ± 0.39 KJ/mol).

The L1A and L1I mutants had a reduced affinity by the polar residue Ser351, when mutated into Lys, more than 10-fold. In contrast, the positively charged residues R10A, K18A and

R19A had a higher affinity for S351K, yielded coupling energies ranging from about 4 to 6 KJ/mol. This implies that Ser351 most likely interacts with the positively charged residues of the toxin pharmacophore.

Interestingly, the data for the negatively charged residue Glu354 (equivalent to Lys427 in *Shaker*) indicate that this residue seems to interact with all the critical residues of \square M-R111K. When mutated into Lys (E354K), the currents were blocked by L1I, R10A, K18A, R19A and K18R/R19K mutants with a 2- to 4-fold reduced potency compared to the WT toxin. When the same channel residue is substituted into a neutral residue (E354Q), the channel was less sensitive to all interacting toxin analogs except L1A. All together, Glu354 seem to sense the charge changes exposed by corresponding toxin residues, including the N-terminus (as seen with Glu348). Both channel mutants (E354K; E354Q) seem to sense the electrostatic interactions with Arg10, Lys18, Arg19 and Leu1 (Fig 3.15) with \square \square G values between 3 and 7 KJ/mol.

The other hydrophobic channel residues, Met375 and Val376, which both are located close to the selectivity filter only seem to be involved in hydrophobic interactions with Leu1, yielding coupling energy close to 4 KJ/mole with L1I. However, since Arg19 is located close to Leu1 in the folding structure of the toxin (see Fig. 3.7), Met375 could sense this residue of the toxin with corresponded \square \square G \sim 4 kJ/mol. Similarly, L1I-M375L pair (conserve the hydrophobic residues) was analysis and yielded \square \square G \sim 3 kJ/mol (*data not shown*). In summary, Leu1 may involved in a hydrophobic interaction with a hydrophobic pocket formed by Met375 and Val376, in addition to Pro349.

These changes in binding energies have been used as the basis for calculating a docking model of how \square M-R111K blocks *TShal* channels (see Discussion).

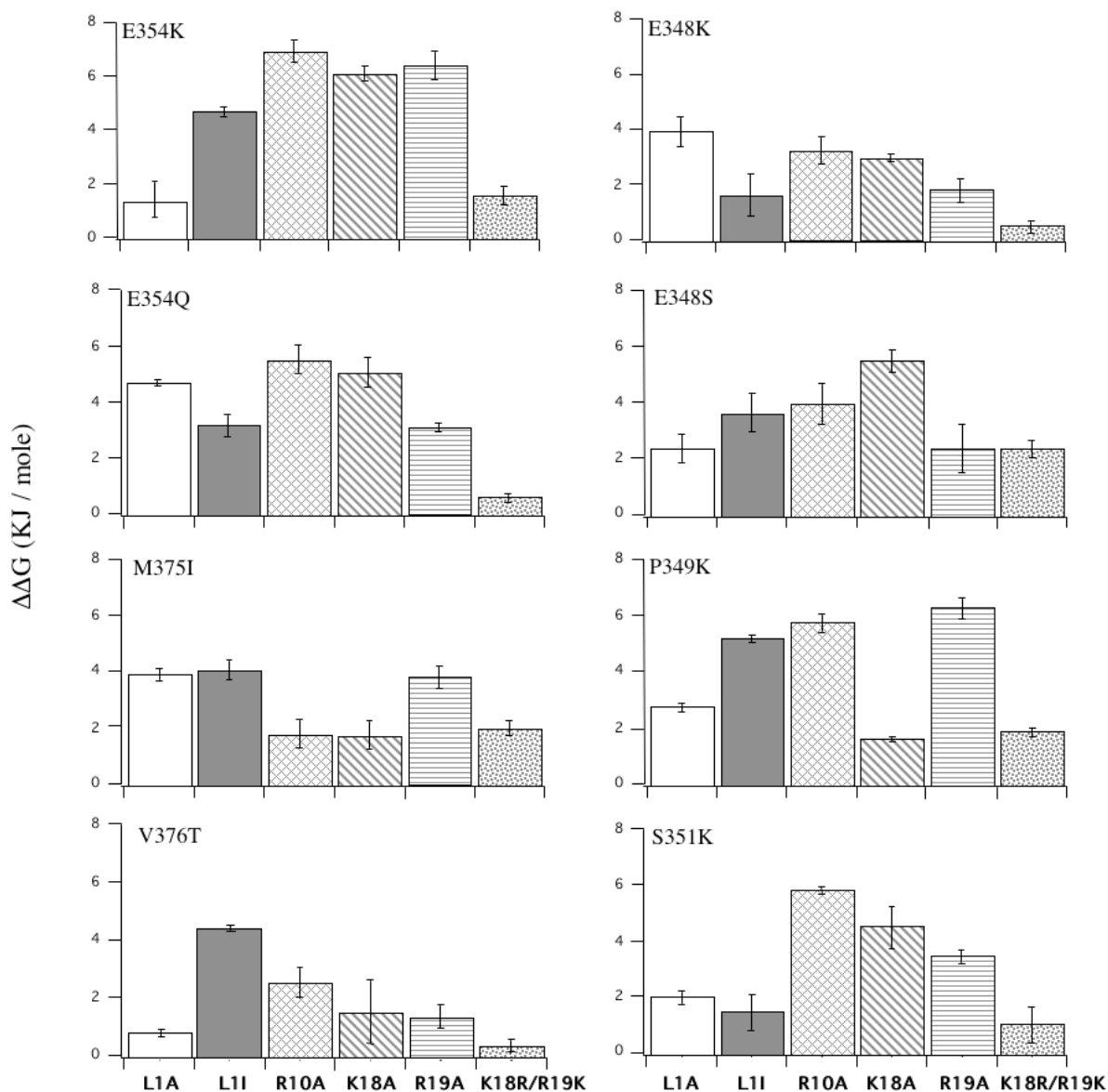


FIGURE 3.15. Summary of mutant cycle analysis. Coupling energy ($\Delta\Delta G \pm SE$) between *TShal* mutants and analogs of $\square M$ -RIIK representing important residues for binding (Leu1, Arg10, Lys18 and Arg 19). $\Delta\Delta G$ values exceeding 2.5 KJ/mol indicate coupling interaction within 5 Å distance (Rauer *et al.*, 1999). L1A mutant (empty bars), L1I (gray-filled bars), R10A (net-filled bars), K18A (diagonal-stripped bars), R19A (horizontal-stripped bars) and K18R/R19K (mosaic-filled bars). All numbers represent the means of 3-6 independent determinations. $\Delta\Delta G$ are taken as absolute values.

3.3.3. Docking orientation of \square M-RIIIK interaction with *TSha1*

According to the docking model, two potential orientations of the peptide within the ion channel pore are possible. Both models showed a lid which exposed Hyp15 or Hyp13 residues facing the vestibule, close to Val376 (see Fig. 4.4). To identify which one of the amino acid is facing the Val376 residue in the channel, we performed mutant cycle analysis using the *TSha1* V376T mutant. The IC_{50} values for these toxin-channel pairs are summarized in Table 3.9.

TABLE 3.9. Summary of IC_{50} , \square and $\square\square$ G values to identify the toxin binding orientation.

\square M-RIIIK	IC_{50} (nM)	\square	N	$\square\square$ G (KJ/mol)
WT	120 \pm 20	-	3	-
O13A	1030 \pm 210	1.28	6	0.69
O15A	3730 \pm 840	2.78	7	2.51

P-Value for comparison between IC_{50} means of both mutants is significant ($P=0.0146$).

In summary, data indicate that \square M-RIIIK docks in a position where Hyp15 shows interaction with V376T with $\square = 2.78$, and coupling energy $\square\square$ G = 2.5 KJ/mol, while V376T interaction with Hyp13A had an $\square = 1.28$, corresponding to a binding energy of 0.69 KJ/mol.

It is clear that \square M-RIIIK interacts mainly with the negatively charged and hydrophobic residues of the external pore region of *TSha1* K^+ channels. These findings are consistent with our view on the blocking behavior of \square M-RIIIK. The positive charged residues of the pharmacophore interact with negatively charged residues of the turret region of the ion channel pore. Furthermore, a hydrophobic pocket, made of Pro349, Met375 and Val376, is interacting with Leu1. The charged N-terminus is involved in stabilizing the association of block.

CHAPTER FOUR: DISCUSSION

In the present work, we described the structural and functional parameters important for the binding of \square M-RIIIK to the pore of *TShal* K⁺ channels. \square M-RIIIK reversibly blocks *TShal* channels in a bimolecular reaction. Both the structural and mutational analysis suggested that, uniquely among well-characterized K⁺ channel-targeted toxins, \square M-RIIIK blocks voltage-gated K⁺ channels with a pharmacophore that is *not* organized around a lysine-hydrophobic amino acid dyad motif.

4.1. \square M-RIIIK: a peptide blocking K⁺ channels

4.1.1. \square M-RIIIK specificity interacts with the pore *TShal* channels

The conotoxin \square M-RIIIK has been described to block the pore region of *Shaker*-type K⁺ channels. It was reported that \square M-RIIIK has a higher affinity for *Shaker* channels with a mutation in the pore region (K427D) than the wild-type channel (Ferber *et al.*, 2003). In the sequence of the *TShal* channel, the homologous position to Lys427 in *Shaker* has a Glu residue. Therefore, we assessed the binding affinity of \square M-RIIIK on *TShal* K⁺ channels expressed in oocytes using two-electrode voltage clamp technique. We found that \square M-RIIIK binds reversibly to *TShal* K⁺ channels and inhibits the flow of the ionic current. The binding of a single \square M-RIIIK molecule is sufficient to inhibit the *TShal* channel. The IC₅₀ value of the block was estimated to be around 70 nM.

4.1.2. \square M-RIIIK binding is altered by [K⁺]_o

\square M-RIIIK is a basic peptide carrying a net positive charge in aqueous solution of roughly +4 at a neutral pH. As a result, binding of \square M-RIIIK should be sensitive to through-space electrostatic forces, including external potassium concentration, [K⁺]_o. The kinetic analysis (Table 3.1) revealed that the observed decrease in binding affinity is mainly due to an increase in toxin dissociation rate. This result indicates that [K⁺]_o ions destabilize the \square M-RIIIK binding, suggesting that the toxin senses the occupancy of an external K⁺ binding site within the outer pore region of *TShal* channels. Blocking effects of some peptide toxins on K⁺ channels are known to depend on [K⁺]_o. For example, the effects of CTX, \square -PVIIA and Maurotoxin are diminished by greater external [K⁺]_o (Anderson *et al.*, 1988; Miller, 1995;

Terlau *et al.*, 1999; Avdonin *et al.*, 2000). This sensitivity to $[K^+]_o$ was mainly manifested by an increase in toxin dissociation rate. K^+ channels are thought to contain multiple K^+ binding sites, and the occupancy of K^+ in the outermost binding site is considered to accelerate the toxin dissociation rate (MacKinnon and Miller, 1988).

4.1.3. \square M-RIIIK: first conotoxin targeting mammalian Kv1.2

In this study we show that \square M-RIIIK blocks the human and rat Kv1.2 channels with an IC_{50} in the nanomolar range. The other mammalian members of the Kv1 family tested at a concentration of 5–10 \square M are almost not affected by this peptide. The state dependence of binding of \square M-RIIIK to Kv1.2 channels is similar to what has been reported for the interaction of this peptide with *Shaker* and *TShal* channels (Ferber *et al.*, 2003). *TShal* K^+ channels from the trout *Oncorhynchus mykiss* are known to be the fish homologue of mammalian Kv1.2 K^+ channel (Nguyen and Jeserich; 1998 and Nguyen *et al.*, 2000). Therefore, we expected that \square M-RIIIK interacts with Kv1.2 K^+ channels with a high affinity.

Interestingly, \square M-RIIIK has a higher affinity to *TShal* and Kv1.2 than \square -PVIIA (*unpublished data*). This indicates that different sets of amino-acid residues on the targeted channels and therefore different structural properties are important parameters for the binding of either \square M-RIIIK or \square -PVIIA. Furthermore, our observations suggest that \square M-RIIIK might have a broader spectrum of target channels than \square -PVIIA. A previous study had shown that a mutation in the pore region of *Shaker* channels (K427D) results in an about 10-fold increase in the affinity of \square M-RIIIK, but has only minor effects on the binding of \square -PVIIA (Jacobsen *et al.*, 2000; Ferber *et al.*, 2003). This indicates a functional importance of this residue for the binding of \square M-RIIIK. Accordingly, the affinity of \square M-RIIIK to *TShal*, which has a negative charge at this position (Glu354), is about 50 fold higher than its affinity to *Shaker*. \square M-RIIIK blocks *TShal* with an IC_{50} for the closed state of about 20 nM (Ferber *et al.*, 2003). At the homologous position Kv1.2 shows an uncharged amino acid (Pro359) and the affinity of \square M-RIIIK to Kv1.2 is about 200 nM for the closed state, which is about 5-fold higher than for *Shaker*, but about 10-fold less compared to *TShal*. This underscores the relevance of this position in \square M-RIIIK binding to its target. According to the structural data available (Doyle *et al.*, 1998), this residue is located in the outer vestibule of the ion channel pore.

Recently, a 35 amino acid conotoxin, designated ViTx, has been described that affects Kv1.1 and Kv1.3 but not Kv1.2 K⁺ channels (Kaufenstein *et al.*, 2003). ViTx is structurally not related to \square -PVIIA and \square M-RIIIK instead it belongs to the I-superfamily of conopeptides containing four disulfide bridges. A recently characterized conopeptide from *Conus monile*, Mo1659, that belongs to the non-disulfide conopeptide, has been described to block K⁺ currents from non-inactivating voltage-dependent K⁺ channels in neurons. Mo1659 has a unique sequence of 13 residues, which is completely devoid of the common hydrophobic, aliphatic amino acids, and disulfide bridges. Instead, it has one Arg residue placed in the center of a cluster of aromatic residues (Sudarslal *et al.*, 2004). Together with the data presented here, this shows that conopeptides with different structural frameworks target the same K⁺ channel family. Furthermore, it indicates that the knowledge about the structural framework is not enough to predict the molecular target of the channel. Hopefully, the information about additional toxin and channel properties like charge distribution or the three-dimensional structure of these molecules will help to predict their targets and will prosper out the understanding of toxin-channel interaction.

With respect to the binding to close and open states of the channel, \square M-RIIIK and \square -PVIIA which both block K⁺ channels, behave quite similar. Both exhibit a state dependence of the block (Terlau *et al.*, 1999; Ferber *et al.*, 2003). This indicates that independent of the different structural frameworks of neurotoxins that block Kv1 K⁺ channels similar blocking mechanisms might be employed. Together with similar data of peptide neurotoxins from other organisms (Avdonin *et al.*, 2000), our observations imply that a state dependence of the block caused by toxins that bind to the outer mouth of the pore may be a common phenomenon.

The data on conotoxins interacting with K⁺ channels available at the moment show that cone snails have evolved different conotoxin families targeting K⁺ channels. The structural heterogeneity might be a 'conopeptide counterpart' of the known diversity of K⁺ channels. A functional role within the predatory behavior of the snails has been so far assigned only to \square -PVIIA (Terlau *et al.*, 1996). \square -PVIIA is part of the venom components involved in the very fast effects induced by the venom, the so-called lightning strike cabal. In how far all these peptides are important for the fast immobilization of the prey will be a question of future investigations.

Kv1.2 is a channel, which has been identified in a whole variety of neuronal (Coleman *et al.*, 1999; McKinnon, 1989; Rasband and Trimmer, 2001; Rasband *et al.*, 2001; Stühmer *et al.*, 1989) and other cell types, like heart muscle (Po *et al.*, 1992, 1993) and smooth muscle (Albarwani *et al.*, 2003; Davies and Kozlowski, 2001; Kerr *et al.*, 2001). Since \square M-R11K is the only conotoxin identified so far to specifically block Kv1.2 K⁺ channels, this peptide might be useful as a tool for studying the biophysical properties of these channels as well as their physiological functions.

4.1.4. \square M-R11K mutants affect kinetics of binding

The functional effects of \square M-R11K mutants on the blocking activity were examined by measuring the kinetic parameters of the toxin binding to *TShal* channels. In nearly all cases, we observed that the lower affinities of \square M-R11K mutants is mainly due to an increase in dissociation rates and a decrease in the association rates.

From Table 3.5, the different \square M-R11K mutants can be classified into three groups according to the effects observed for the changes in the binding kinetics. The first group is composed of the critical, positively charged, residues (R10, K18 and R19), which showed the biggest reduction in binding affinity compared to other alanine mutants. Although the charge was conserved, the mutant K18R/R19K has a $K^{(0)}$ value close to that of the wild-type. This indicates that the positive charge is important at both positions, but the specific nature of the side chain is not critical for the interaction as we noticed from the alanine walking experiments. For an electrostatic interaction, charge alterations should be manifested in changes of the association rate of the toxin. Indeed, mutations decreasing the net charge of well-studied scorpion toxins CTX (Park and Miller., 1992; Goldstein *et al.*, 1994) and Iberitoxin (Mullmann *et al.*, 1999), decreased the toxin on-rates. Our experiments showed that the group of the positively charged residues affected the on-rates more than the residues of other groups. Therefore, it is clear that the functional effect of these residue is predominated by direct electrostatic interactions.

The second group composed mainly from the hydrophobic residues, which affected the equilibrium block by major increase in off-rates, an effect also noticed in previous studies on CTX (Stampe *et al.*, 1992; Stampe *et al.*, 1994). These residues are located on the middle

region of the toxin and may play an indirect but important role in binding. This group is located in the joint region of the the flexible N-terminus arm formed by the first 11 residues, which might be important to facilitate the docking of the \square M-RIIIK to the pore region of the channel. The third group is composed mainly from polar residues that are located bordering the first two groups. These residues had small effect on the binding kinetics and may play supportive rule by polar binding within the toxin peptide.

The Leu side chain as the first residue of \square M-RIIIK most likely contributes in hydrophobic interaction(s) with hydrophobic residues in the pore region of *TSha1* channel. Such property has never been represented *at least* among conotoxins targeting K^+ channels characterized up to date. The Leu1 shows tolerance toward substituting the side chain with positively charged or another hydrophobic residue, whereas, replacement of the Leu1 with negatively charged residue or masking the N-terminus charge were not compatible with toxin binding. On the other hand, the substitution of Leu1 with aromatic amino acids (Phe or Tyr) resulted in a reduction of the $K^{(o)}$ values, about 80- to 140- fold. This is mainly due to increased off-rates, about 54- and 80-fold, respectively, and may be correlated with the bulky size of both Phe and Tyr residues.

4.1.5. \square M-RIIIK mutants do not interact with Nav1.4 sodium channel

Despite the structural similarity, \square M-RIIIK and \square -GIIIA show no overlap in pharmacological specificity. Our experiments on \square M-RIIIK WT and analogs showed no inhibition to ionic currents carried by Nav1.4 channels expressed in *Xenopus* oocytes (Fig. 3.10). These results are consistent with previous studies that showed no blocking of Nav1.4-mediated currents by \square M-RIIIK WT (Ferber *et al.*, 2003). Structural-functional studies on \square -GIIIA identified a critical residue believed to functionally occlude the external pore region of Nav1.4 channels (Becker *et al.*, 1992; French, *et al.*, 1996; Hui *et al.*, 2002). In contrast, \square M-RIIIK lack this critical Arg13 residue but, equivalently, has a hydroxylated proline at position 15 (Table 3.6). We found no functional effect of \square M-RIIIK mutants at Hyp15 position, upon introducing positively charged residue (O15K and O15R), on Nav1.4-mediated currents. Instead, Hyp15 mutants showed different binding affinities toward *TSha1*-mediated currents, reflected mainly by increased off rates. Interestingly, the binding affinity was two times bigger for O15K compared with O15A toxin analog by almost two times but still 6 times less potent than the \square M-RIIIK WT (see Table 3.6).

4.2. \square M-R11K: novel structure among conotoxins

4.2.1. Structure of \square M-conotoxin R11K

The three-dimensional structure of conotoxin \square M-R11K (Fig. 4.1) was determined by using NMR spectroscopy by Carlomagno and coworkers at the Max-Planck Institute for Biophysical Chemistry (Göttingen, Germany).

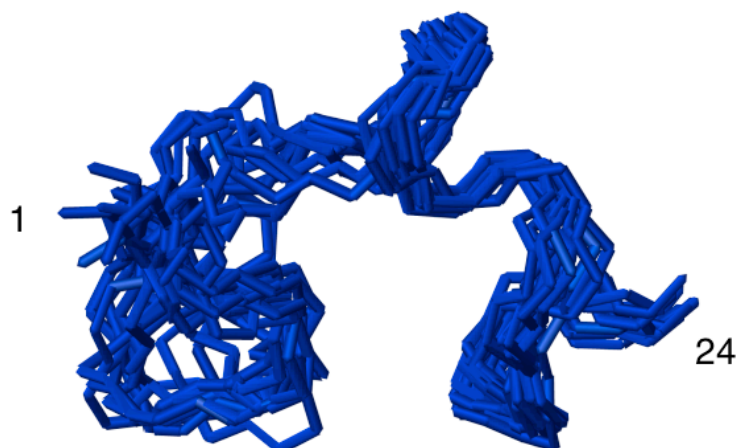


FIGURE 4.1. Superimposition of the 13 lowest-energy structures of \square M-R11K. Residues 1-11 have a high degree of flexibility, while residues 12-24 are well-defined.

The solution conformation of \square M-R11K differs substantially from that of \square -PVIIA, the only other structurally characterized conotoxin that interacts with the K^+ channels. While the two conotoxins share common binding sites on the *Shaker* K^+ channel (Shon *et al.*, 1998; Ferber *et al.*, 2003), they dramatically differ in the disulfide bond pattern, secondary structure elements, and charge distribution. \square M-R11K is encoded by a gene belonging to the M-superfamily, while \square -PVIIA belongs to the O-superfamily (see Fig. 1.5; Terlau and Olivera, 2004). The latter superfamily includes \square -conotoxins, which are targeted to voltage-gated Ca^{2+} channels.

4.2.2. Comparison between \square M-R11K and members of M-superfamily

The most well-characterized member of the M-superfamily is \square -conotoxin G11A, an extremely specific blocker of the Nav1.4 voltage gated Na^+ channel. The structure of \square M-R11K is much more similar to that of \square -G11A than to that of \square -PVIIA. Clearly, the shared class III Cys pattern of \square M-R11K and \square -G11A is the dominant determinant of the overall structure. Despite the structural similarity, \square M-R11K and \square -G11A show no overlap in pharmacological specificity at all.

The overall shape of α M-R11K is that of a disk with dimensions of 15X13 Å. The three dimensional structure of α M-R11K (Fig. 4.2, red ribbon) is very similar to that of the Na⁺ channel blockers α -conotoxins G11A and G11B (Fig. 4.2, blue ribbon) in the C-terminal region of residues 12-24 (Lancelin, *et al.*, 1991; Wakamatsu *et al.*, 1992; Hill *et al.*, 1996). On the other hand, the structure of α M-R11K significantly differs from that of α -G11A in residues 1-11. The N-terminal region of α -G11A consists of very tight turns (residues 2-5 and 5-8) which position the N-terminal tail in the opposite direction with respect to the C-terminus (Fig. 4.2B). Conversely, the N-terminal region of α M-R11K consists of an extended tail terminated by Cys4 followed by a wide loop between Cys5 and Leu11. In α M-R11K, the N-terminal tail protrudes into solution almost perpendicular to the flat surface of the peptide and to the C-terminal end (Fig. 4.2B).

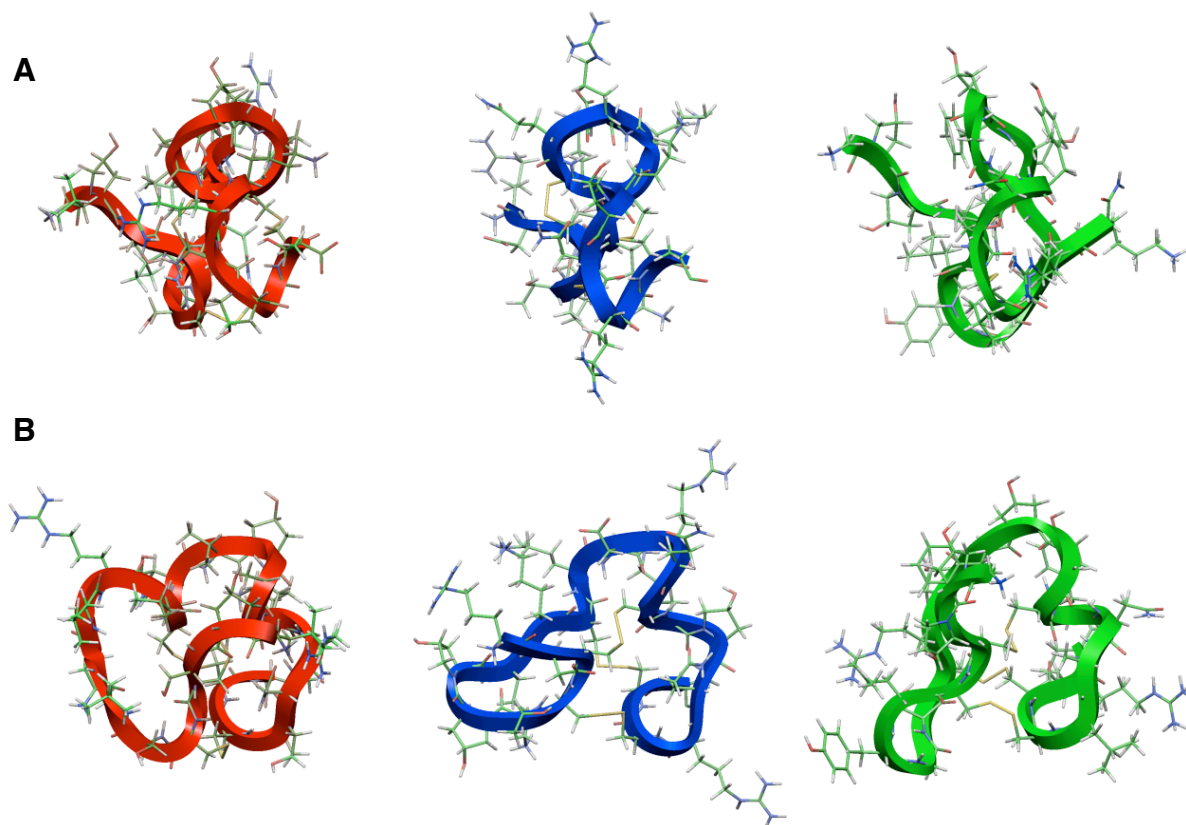


FIGURE 4.2. The three-dimensional NMR structures of M superfamily representatives (A) Comparison of the structures of α M-conotoxin R11K (red ribbon), α -conotoxin G11A (blue ribbon), and α -conotoxin P11F (green ribbon). The N-terminus is on the left side and the C-terminus on the right side for each peptide. The structure of the three peptides is very similar in the C-terminal part, while the N-terminal part shows conspicuous differences. (B) Same as panel A after a rotation of 90°. This orientation was chosen to highlight the different position of the N-terminal tail in the three peptides.

Recently, the three-dimensional structures of two α -conotoxins, α -P11E and α -P11F, antagonists of the nicotinic acetylcholine receptor, have been determined in solution by NMR

(Fig. 4.2A, B, green ribbon) (Van Wagoner *et al.*, 2003a; Van Wagoner *et al.*, 2003b). The disulfide bond pattern of these small peptides is homologous to that of both α M-R11K and α -G11A, although their natural receptor belongs to a different superfamily, the ligand-gated ion channels. The fold of the C-terminal part of α -P11F is similar to that observed for both α M-R11K and α -G11A, with two helical turns involving the last three cysteine residues. However, the N-terminal part of α -P11F differs in structure from both α M-R11K and α -G11A. Furthermore, unlike conotoxins α M-R11K and α -G11A, α -P11F has the form of a lens rather than a disk (Fig. 4.2B).

α M-R11K, the Na⁺ channel blocker α -G11A, and the noncompetitive antagonist of nicotinic acetylcholine receptors α -P11F all share a common class III Cys pattern. The structural features of the three peptides are very similar toward the C-terminus, where all three conotoxins are folded in two distorted helical turns (Fig. 4.2). However, toward the N-terminus, the three peptides show substantial differences in both structure and dynamics. While α -G11A and α -P11F have a well-defined backbone folded in a series of turns, α M-R11K is highly flexible in the region of residues 1-11. We suggest that the differences in the three-dimensional form, provided by the structural heterogeneity at the N-terminus, and in the surface charge distribution are an important determinant of target selectivity.

4.3. Identification of α M-R11K pharmacophore

4.3.1. α M-R11K pharmacophore is *not* organized around a dyad motif

The structural divergences between α M-R11K and α -P11A pose the intriguing question of whether the mechanism of the K⁺ channel conductance block of the two toxins significantly differs. Despite their differences in size, amino acid sequence, structure, and biological origin, all other well-characterized toxins (e.g., dendrotoxin from snakes and various scorpion and sea anemone toxins), including α -P11A, share a number of convergent features. The key amino acid determinants for the interaction with the K⁺ channel are localized on one side of the toxin surface, and the pharmacophore is formed by a hydrophobic-positively charged amino acid dyad motif.

Encouraged by the similarity in the mechanisms of interaction with the K⁺ channels of structurally and phylogenetically different peptides, we expected \square M-conotoxin RIIIK to fit in the common framework and to interact with K⁺ channels by a dyad-based pharmacophore. Conversely, the structural and mutational analyses described above indicate that \square M-RIIIK does not fit the established paradigm. \square M-RIIIK is a relatively flat, disk shaped molecule. The important amino acid determinants for binding are not clustered on the toxin surface into a clearly defined pharmacophore (Fig. 3.7). Most importantly, \square M-RIIIK does not appear to have a dyad motif composed of a hydrophobic amino acid and a lysine residue.

Our conclusion that a dyad does *not* exist is based on two sets of experimental data. First, the structure shows no hydrophobic residue within 6 Å of a positively charged residue. Second, we found that substitutions of aromatic residues for Leu1, the functionally most important hydrophobic amino acid in \square M-RIIIK, are tolerated even less than a substitution to Alanine. Furthermore, and most unexpectedly, substitution of a positive-charged amino acid gave an affinity close to that of the wild-type peptide. In fact, the Leu1 substitution with the smallest effect on the affinity of the peptide is an arginine (L1R) and not isoleucine (see Table 3.4). An affinity similar to that for the L1R substitution was observed for the methionine substitution (L1M). Since methionine is a smaller residue than arginine and on the other hand the lysine substitution (L1K) leads to a larger reduction in the affinity of the peptide than the L1R substitution, it is likely, that a combination of size-dependent hydrophobic and electrostatic interactions involving the first residue of this peptide, is important for binding to the channel. Moreover, L1H experiments showed that for the function of the toxin mutations of the Leu1 are more tolerant to positive than negative charged side chains demonstrated by the different toxin affinities at different pH. These observations are consistent with the kinetic analysis that Leu1 position was incompatible with aromatic and acidic side chains or capping the positively charged N-terminus.

Taken together, all these results are completely inconsistent with Leu1 being the hydrophobic partner in a dyad. Interestingly, the dyad hypothesis is challenged in a recent publication by Mouhat *et al.* (2004), who showed that the K24-Y33 functional dyad of the scorpion toxin Pi1 is not indispensable for recognition and binding to the voltage-gated Kv1.2 potassium channel. This conclusion, drawn from the observation of a partial but specific current reduction after application of the mutant [A24,A33]-Pi1, lacking the

functional dyad, confirms our results and opens the way to considering different possible mechanisms for the blockade of K⁺ channels.

4.3.2. \square M-RIIIK pharmacophore is a planar ring of four residues

The localization of the functionally critical amino acids on the three-dimensional structure of \square M-RIIIK is shown in Fig. 3.7B. The four most important residues (Leu1, Arg10, Lys18, and Arg19) and the seven residues of medium importance are distributed well across the whole molecule, as opposed to the commonly found structural motif for K⁺ channel blockers that contains a dyad of a positively charged residue and a hydrophobic residue. The separation of key residues in \square M-RIIIK resembles the properties observed for Na⁺ channel blocker \square -GIIIA more than other K⁺ channel-targeted toxins. However, all functionally relevant residues can be localized on a surface of 12 Å X 9 Å (Fig.3.7B, *right panel*), with the most important residues (in red) being situated at the edges and the residues of medium relevance (in yellow) in the middle of the surface. On the opposite side of the peptide (Fig.3.7B; *left panel*), no residue seems to be essential for function.

The charge distributions on the surfaces of \square M-RIIIK, \square -GIIIA, and \square -PVIIA are substantially different. In \square M-RIIIK, most of the positive charges are distributed at the edges of the peptide face containing the functionally essential amino acids (Fig. 4.3A, B). It is noteworthy that in \square M-RIIIK all determinants for binding contain a positive charge, and that all positively charged residues are necessary for binding. This ring of positive charges could be used as an anchor for residues of the K⁺ channel loops. In \square -GIIIA and \square -PVIIA, the distribution of both charges and binding determinant residues on the peptide surface is more homogeneous than in \square M-RIIIK. In \square -GIIIA, however, a ring of positive charges could be similarly identified at the height of R19 and R1 (Fig. 4.3C, D). In contrast to the case for \square M-RIIIK, a functionally highly relevant residue in \square -GIIIA, R13, sticks out from the surface defined by this ring and is probably projected into the channel pore.

In \square M-RIIIK, no additional positively charged residue sticks out from the surface defined by the ring of positively charged residues Leu1, Arg10, Lys18, and Arg19. This observation, together with the fact that \square M-RIIIK lacks a functional dyad, does not support the model of a positively charged side chain occluding the channel pore. On the contrary, the even distribution of Leu1, Arg10, Lys18, and Arg19 at the edges of the peptide face containing all

functionally relevant residues suggests that conotoxin \square M-R11IK may block the channel by covering the pore as a lid.

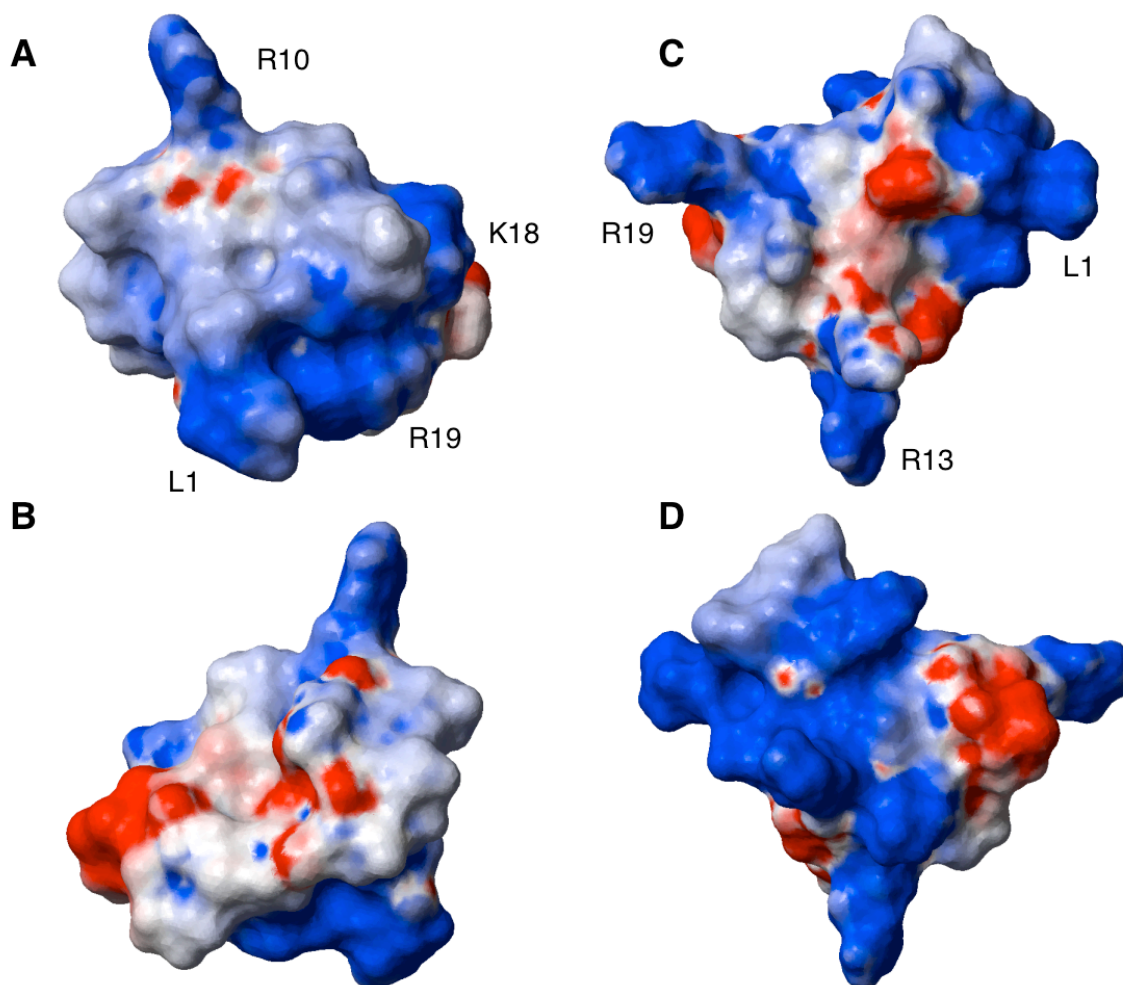


FIGURE 4.3. Electrostatic surface potential for \square M-R11IK (A and B) and \square -G11IA (C and D). Intense blue and red regions correspond to charges of 1.0 and -1.0 or greater, respectively. The surface potential was calculated with the AvgCharge algorithm of MOLMOL 2k•2.

This pharmacophore model represents a novel mechanism of K^+ channel block that has not been found in any other K^+ channel-targeted peptide characterized to date. The recent paper by Mouhat *et al.* (2004) demonstrates the presence of a basic ring in scorpion toxin Pi1 that might be similar to the one described here, indicating that a similar pharmacophore has been independently evolved by cone snails and scorpions. Mutation and docking data reveal the importance of a cooperative electrostatic interaction of the basic residues of this ring in scorpion toxin Pi1 with side chains of the turret region of the channel.

These results reinforce our proposition of a different model of peptide channel interaction that is not centered on a functional dyad. In a recent review of the interaction of several biodiverse scorpion toxins to K^+ channels (Rodriguez *et al.*, 2003), three different binding modes have been proposed: internal mode, involving residues at the “turret region”, the pore helix, and the selectivity filter of the channel; intermediate mode, involving residues at the turret region and the bottom of the vestibule of the channel; and external mode, involving residues that are distant from the channel selectivity filter. This idea is supported by the observation that scorpion toxin BmTx3 can block A-type K^+ and *Herg* currents using two different faces (Huys *et al.*, 2004), suggesting the existence of two different binding modes (Xu *et al.*, 2003). The pharmacophore model that we propose for the interaction of \square M-RIIIK with the *TShal* K^+ channel most likely resembles the intermediate binding mode. The structure function study reported here is broadly significant because \square M-RIIIK is at the unique intersection between structural similarity and similar target specificity.

We have provided direct evidence that \square M-RIIIK and \square -PVIIA, which both inhibit the same K^+ channel subtypes, are both structurally divergent and mechanistically dissimilar. In contrast, \square M-RIIIK is structurally highly similar to genetically related conotoxins (i.e., \square -conotoxin GIIIA and \square -conotoxin PIIF), which have a completely different target specificity (K^+ channels, Na^+ channels, and Ach receptors). This provides a potential framework for understanding both molecular convergence and divergence in ion channel-targeted ligands.

4.4. Mutant cycle analysis

A mutant cycle analysis was used to identify the individual interactions of the residues important for \square M-RIIIK binding with selected amino acids in the pore region of *TShal* K^+ channel. From the changes in binding energies, spatial restraints for the interacting surfaces were calculated to build a model of \square M-RIIIK binding to the *TShal* K^+ channel.

4.4.1. *TShal* mutant channels

Based on previous extensive site-directed studies on *Shaker* K⁺ channel and homologous sequences of mammalian Kv1 channel, 15 point-mutations were selected at seven positions within the P-loop of *TShal* channel in the turret region, the pore helix and the bottom of the vestibule of the channel (Fig. 3.12). Due to the electrostatic and hydrophobic nature of the \square M-R111K-channel interactions, we focused on hydrophobic and negative charged residues as targets for mutagenesis in the selected regions.

In general, some mutantions (S351K, E354K, E354Q and M375I) resulted in a decreased affinity of \square M-R111K of about ≥ 2 -fold, whereas, P349K and M375L mutations resulted in a decreased affinity of \square M-R111K of < 2 -fold. The rest, V376T, E348S and E348K showed no significant changes in the sensitivity to wild-type toxin. One additional mutation, M375K was not sensitive to \square M-R111K and therefore not useful for the cycling analysis. These mutants also affected the activation kinetics as shown in Fig. 3.14, and further work will address the functional effect of those mutants on the binding affinity (Fig. 3.13). For the *TShal* mutants investigated, there is a trend of decreasing the toxin affinity as we scan the loop from the turret region to the Met375 position, close to the selectivity filter. The toxin showed substantial decrease in affinity of binding at Val376 position, almost reaching the wild-type value. This indicates that \square M-R111K binds to the turret and pore helix regions but most likely not deep in the vestibule.

In comparison, among the key amino acids that affect the affinity of other *Shaker* K⁺ channel ligands are Lys427 (Glu354 in *TShal*), and Thr449 (Val376). In previous work, \square M-R111K interaction with a number of mutants of the *Shaker* potassium channel were assessed (Ferber *et al.*, 2003). The results for two different amino acid substitutions (K427D, and T449Y) showed strikingly different effects; T449Y, was found to be much more resistant to \square M-R111K. In contrast, the K427D mutant exhibited about a 10-fold greater affinity for the toxin than was observed for the wild-type *Shaker* channel. These observations are consistent with our findings that \square M-R111K interacts with negative residues in the turret region and that strongly reduce the binding affinity due to bulky sized residues at position 449 in *Shaker* channels.

4.4.2. Determining IC_{50} and $\Delta\Delta G$ values of the mutant cycle analysis

We performed mutant cycle analysis using the functional *TShal* mutants that showed sensitivity to ΔM -RIIIK (see Table 3.7). From the toxin mutants available, we used the residues, which have been shown to be important for binding. The IC_{50} values of the interacting toxin-channel pairs showed variable affinities reflecting the co-operative binding of several residues contributed from all Δ -subunits of the channel.

The IC_{50} values from Table 3.9 were used to calculate the Δ -values and obtain the coupling energies, $\Delta\Delta G$, between amino acid residues of the toxin and the amino acid residues within the pore region of *TShal*. The mutant ΔM -RIIIK peptides (with single amino acid substitutions) were tested against eight different mutant *TShal* channel isoforms. The highest Δ value scored was for the R10A-E354K pair of 0.06, which is equivalent to a $\Delta\Delta G$ value of 6.97 KJ/mol. This indicates a strong interaction between Arg10 (toxin) and Glu354 (channel) residues (see Fig. 3.15). For the other toxin-ion channel pairs, we observed the following possible interactions: Glu348 (toxin)-Arg10, Lys18 and N-terminus of Leu1 (Fig. 3.16); Pro249-Leu1, Lys18 and R10A; Ser351-R10A, K18A and R19A; Glu354-L1I, R10A, K18A, R19A and K18R/R19K mutants; Met375-Leu1 and Arg19 and Val376-Leu1. From the $\Delta\Delta G$ -values, the spatial restraints between the interacting surfaces can be calculated in order to build the model of ΔM -RIIIK docking to the *TShal* K^+ channel can be obtained (see Rauer *et al.*, 1999).

4.4.3. The lid docking model of ΔM -RIIIK-*TShal*

Docking calculations have been performed in the lab of Dr. Carlomagno at the Max-Planck-Institute for Biophysical Chemistry (Göttingen, Germany; Fig. 3.4). The docking model was derived from experimental mutant cycle data using the three-dimensional structure of the toxins as a template and the structure of *TShal* channels, which was modified from KcsA solved structure (Doyle *et al.*, 1998). The docking model shows a novel behavior in which the toxin blocks as a lid on the outer vestibule of the channel (Fig. 4.4). This lid is anchored by a positive charged ring formed by Arg10, Lys18 and R19 as three arms, which interact with the turret region. A fourth arm, started by the Leu1, is perpendicular to the triad ring and formed electrostatic interactions by the free N-terminus charge. There, Leu1 interact with a hydrophobic pocket made of Pro349, M375 and Val376.

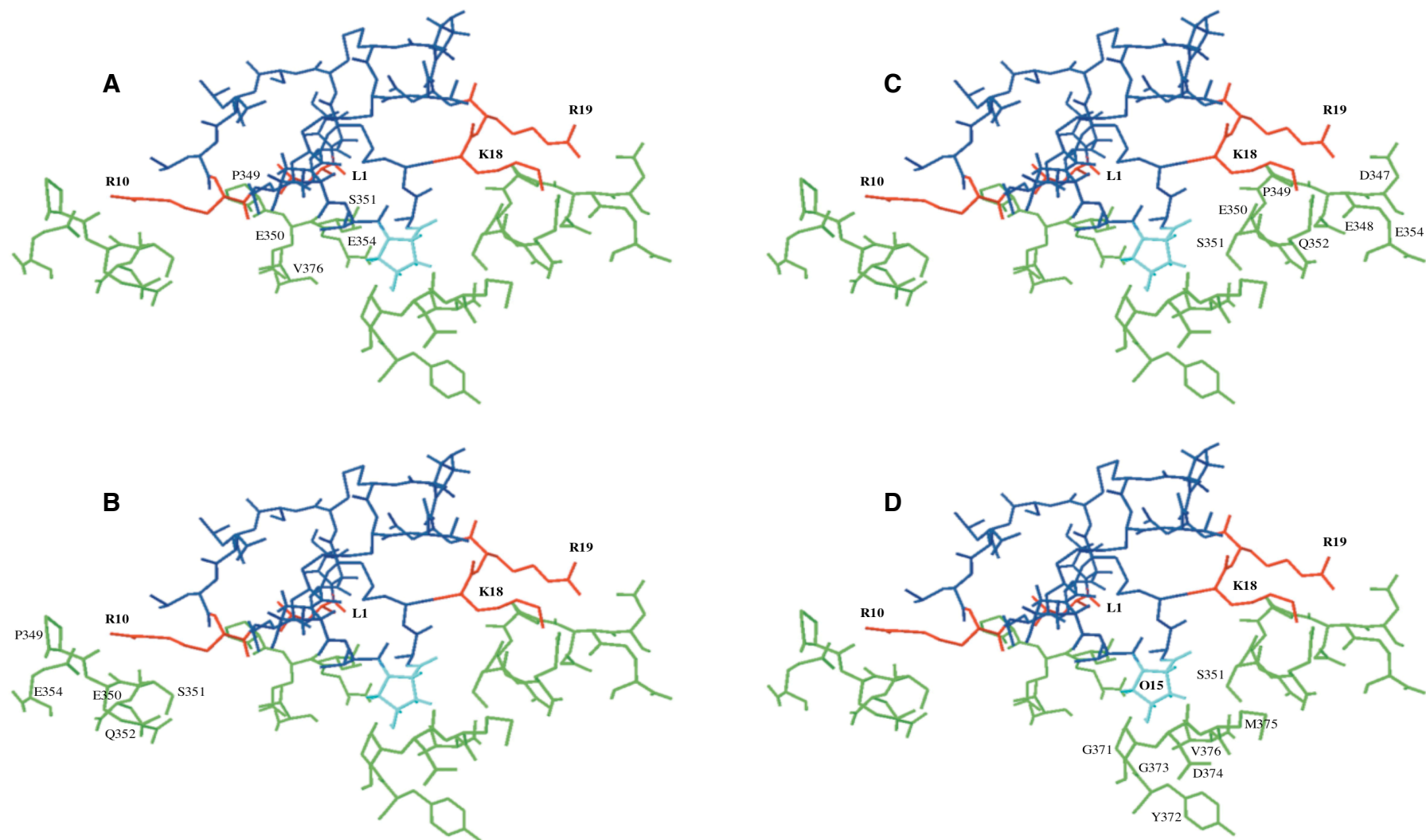


FIGURE 4.4. Close-view of \square M-R11IK-*TShal* docking model obtained from mutant cycle analysis. **A)** L1 residue of \square M-R11IK interacts with *TShal* vestibule residues: P349, E350, S351, E354 and V376. The residues E348 and M375 were removed for simplicity. **B)** R10 residue of \square M-R11IK interacts with *TShal* vestibule residues: P349, E350, S351, Q352 and E354. E348 was removed for simplicity. **C)** K18 and R19 residues of \square M-R11IK interact with *TShal* vestibule residues: D347, E348, P349, E350, S351, Q352 and E354. **D)** The orientation of \square M-R11IK docking showed O15 residue facing *TShal* vestibule residues: D374, M375 and V376. The selectivity filter of *TShal* K⁺ channel is represented by G371, Y372 and G373. \square M-R11IK pharmacophore is shown in red color, O15 in cyan and the rest in blue, while the homotetramers of *TShal* pore vestibule are represented by green.

Furthermore, the resulting model allowed the assignments of additional contacts between the toxin and the channel: Arg10 is close to Asp347, Glu350 and Gln352, whereas Leu1 and Lys18 are close to Gln352 in separated monomers. The models were also analyzed to identify additional contacts detected in the mutant cycle experiments, which could contribute to better define the structure of the toxin-channel complex. It was found that Hyp15 is close to Asp374 near the center of the pore.

According to the docking model calculations, two potential orientations of the peptide within the ion channel pore are possible. The data mutant cycle analysis indicate that \square M-RIIK docks in a position where Hyp15 faces the Val376 residue of *TSha1* channel (Fig. 4.5A). This orientation was confirmed by landscape population energy calculations performed by NMR group. Nevertheless, the second orientation cannot be ruled out (Fig. 4.5B).

On the basis of the kinetic analysis of the binding, Hyp15 residue is involved in occluding the ion channel pore (as carried by equivalent residue Arg13 of \square -GIIA) but still can sense some electrostatic interactions with the pore region. This observation supports our view of \square M-RIIK docking in which the Hyp15 residue faces the conducting pathway of the channel pore but does *not* occlude the external vestibule of the *TSha1* channel. Proline hydroxylation is the second most common post-translational modification observed in conotoxins (Craig, 2000).

The binding of \square M-RIIK to *TSha1* channel is stabilized by electrostatic and hydrophobic interactions between the toxin and the channel. It is clear that the pharmacophore of \square M-RIIK is not organized around a dyad motif but possess is a ring of basic residues, which resemble some scorpion K^+ toxins such as Tc32 (for review, see Mouhat *et al.*, 2004). In comparison, a docking model of \square -PVIIA into the KcsA crystal structure was assessed (Jacobsen *et al.*, 2000; Moran, 2001). The model of \square -PVIIA binding is based on the dyad model proposed by Duplais *et al.* (1997). The model assumed that Lys25 of \square -PVIIA is in the vicinity of Met448 and Phe9 of the toxin can be positioned close to Thr449 of the adjacent subunit of the channel pore vestibule. In this orientation, Lys7 of \square -PVIIA is facing toward the ion channel pore.

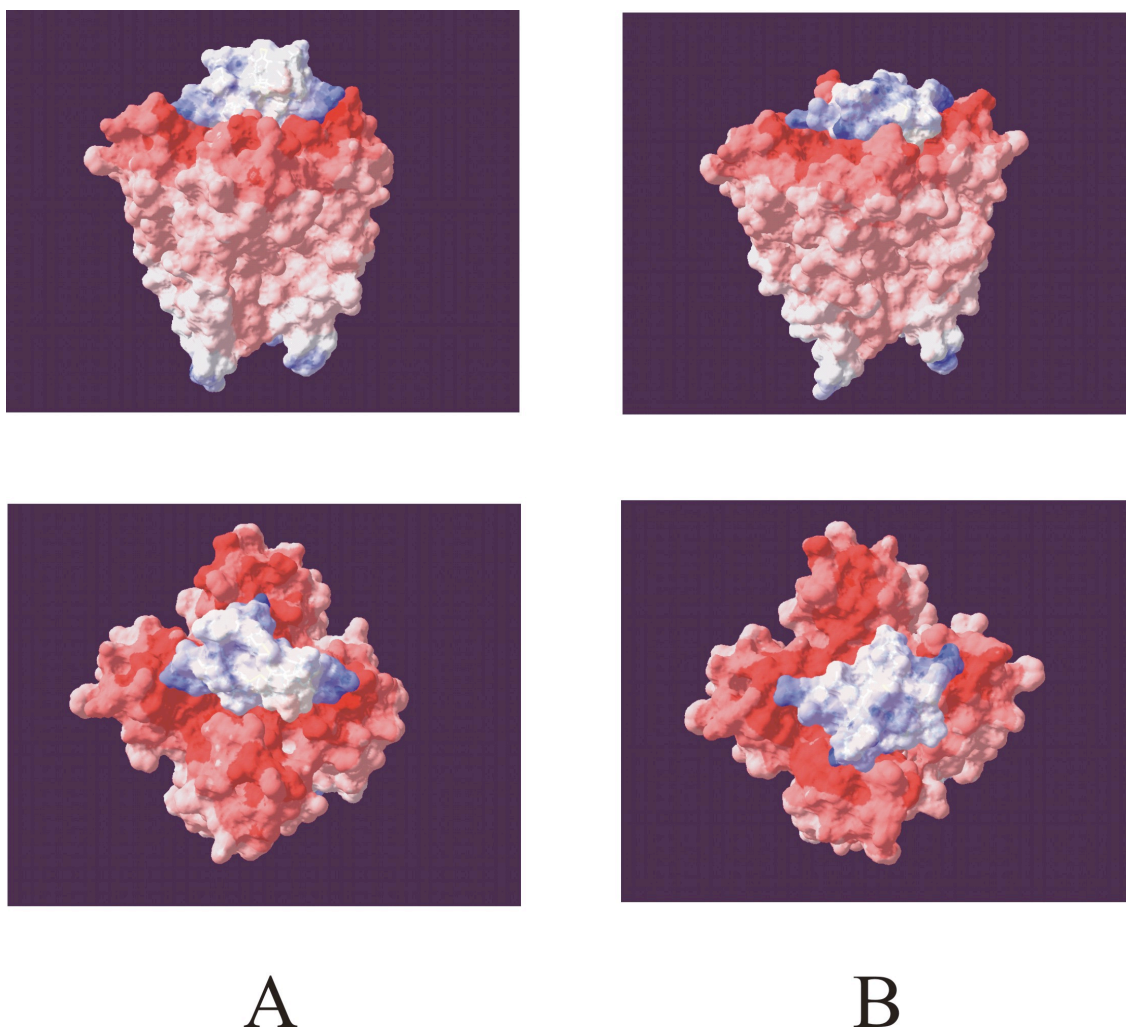


FIGURE 4.5. Orientation of \square M-R111K-*TShal* (Lid) docking model obtained from mutant cycle analysis. **A)** The most probable orientation of \square M-R111K interaction to *TShal* vestibule region. This model is built on the assumption that toxin residue Hyp15 faces the pore region of the channel. **B)** The less probable (but not rolled out) orientation of \square M-R111K interaction to *TShal* vestibule region. This model is built on the assumption that toxin residue Hyp13 faces the pore region of the channel.

On the other hand, \square -GIIIA binds superficially in the pore of Nav1.4 channels as a result of the summed effects of numerous relatively weak toxin-pore interactions (Li *et al.*, 2001). Since, the Na^+ channel pore is asymmetrical (Chiamvimonvat *et al.*, 1996; Li *et al.*, 1999), \square -CTX most likely binds in a single high-affinity orientation, whereas pore-blocking K^+ channel toxins bind in a four-fold off-axis fashion. The pattern of \square -GIIIA- Na^+ channel interactions, when interpreted in light of the known three-dimensional toxin structure, provides the first experimental evidence that the four Na^+ channel domains are arranged in a clockwise configuration when viewed from the extracellular side (Dudley *et al.*, 2000; Li *et al.*, 2001). The results also suggest that \square -GIIIA docks like an inverted pyramid with R13

reaching the deep pore region at a tilted angle with respect to the central pore axis. Both docking models of α -GIIIA and α -PVIIA differ from that of α M-RIIIK, in the case of the latter, no occluding residue is needed to block the channel.

In Summary, we were able to identify the model of α M-RIIIK binding to the *TSha1* K⁺ channel. The model shows that the toxin binds on the outer vestibule of the channel by a ring of three basic residues as a lid. The docking orientation of the model was revealed in which Hyp15 faces the vestibule of the channel but not occluding the pore. This "lid" model is novel among K⁺ channel antagonists.

CHAPTER FIVE: Summary

Venomous organisms have evolved an amazing variety of polypeptide neurotoxins interacting with different potassium (K^+) channels. Despite the structural divergence of the peptides interacting with the voltage-gated Kv1 subfamily of K^+ channels (such as the *Shaker* channel from *Drosophila*), a convergent functional feature has been identified. All these peptides seem to share a dyad motif composed of a lysine and a hydrophobic amino acid residue, usually a phenylalanine or a tyrosine. Neurotoxin peptides from the venomous cone snails (“conotoxins”) are well-known, highly subtype-selective ligands that interact with a variety of different voltage-gated and ligand-gated ion channel targets. Recently, \square M-conotoxin RIIIK (\square M-RIIIK) was described to block the *Shaker* K^+ channel in a state-dependent manner. The teleost homologue of *Shaker*, the trout *TShal* K^+ channel, is the highest-affinity target of \square M-RIIIK yet identified. Interestingly, the 24-amino acid sequence of \square M-RIIIK contains three positively charged residues but no aromatic side chain.

In the present study, we described the structural and functional parameters important for the binding of \square M-RIIIK with the *TShal* K^+ channels. An extensive mutational analysis was assessed with the aim to identify the functionally important residues of the toxin. Analogues of \square M-RIIIK containing alanine substitutions at each amino acid position except for the cysteine’s were used. The affinity of the alanine isoforms was functionally assayed by two-electrode voltage clamp measurements using *Xenopus* oocytes expressing *TShal* K^+ channel. It is shown that several mutations affect the affinity and kinetics of \square M-RIIIK binding to *TShal* channels. In contrast, \square M-RIIIK analogs did not show binding affinity to Nav1.4. The mutational analysis indicated that four amino acids (Leu1, Arg10, Lys18, and Arg19), which are located as a basic ring on the peptide, are essential for K^+ channel binding. Following the hypothesis that Leu1, the major hydrophobic amino acid determinant for binding, serves as the hydrophobic partner of a dyad motif, we investigated the effect of several mutations of Leu1 on the biological function of \square M-RIIIK. Surprisingly, both the structural and functional analysis results are clearly indicating that \square M-RIIIK lacks the dyad motif found in the other K^+ channel-targeted conopeptides characterized to date. The basic ring of \square M-RIIIK resembles that of the most recently described in some scorpion K^+ antagonists.

A mutant cycle analysis was used to identify the individual interactions of the residues important for \square M-RIIIK binding with selected amino acids in the pore region of *TSha1* K⁺ channel. From the changes in binding energies, spatial restraints for the interacting surfaces were calculated to build a model for the binding of \square M-RIIIK to *TSha1* channels. The docking model revealed a novel type of binding in which the toxin blocks the outer vestibule of the channel as a lid. This lid is anchored by a positive charged ring formed by Arg10, Lys18 and R19 as three arms, which interact with the turret region of the ion channel pore. In the turret region, Glu354 plays an important role in the electrostatic interactions with the triad ring. A fourth arm, composed of the N-terminal part of the peptide, is perpendicular to the triad ring and forms electrostatic interactions by its free N-terminus charge. There, Leu1 interacts with a hydrophobic pocket made of Pro349, Met375 and Val376. The docking orientation of the model indicates that Hyp15 faces the vestibule of the channel but is not occluding the pore. This "lid" model is novel among K⁺ channel antagonists.

Furthermore, the affinity of \square M-RIIIK for different mammalian potassium channels of the Kv1 family was investigated. It shows that \square M-RIIIK is the first conotoxin described to block human Kv1.2 potassium channels, whereas the other members of the Kv1 family tested are not affected by the peptide. The binding of \square M-RIIIK to Kv1.2 channels is state dependent with an IC₅₀ for the closed state of about 200 nM and for the open state of about 400 nM at a test potential of 0 mV. The Kv1.2 channel is known to be present in a variety of neurons, and in heart and smooth muscle. Therefore, \square M-RIIIK might be useful as a tool for studying the biophysical properties of these channels as well as their physiological functions.

CHAPTER SIX: References

- Albarwani, S., Nemetz, L. T., Madden, J. A., Tobin, A. A., England, S. K., Pratt, P. F., Rusch, N. J., (2003) Voltage-gated K⁺ channels in rat small cerebral arteries: molecular identity of the functional channels. *J. Physiol*, **551**: 751-763.
- Anderson, A. J., Harvey, A. L., Rowan, E. G. and Strong, P. N. (1988) Effects of charybdotoxin, a blocker of Ca²⁺-activated K⁺ channels, on motor nerve terminals. *Br. J. Pharmacol.*, **95**:1329-1335.
- Armstrong, C. M. and Bezanilla, F. (1977) Inactivation of the sodium channel. II. Gating current experiments. *J. Gen. Physiol.*, **70**: 567-590.
- Armstrong, C. M. and Hille, B. (1998) Voltage-gated ion channels and electrical excitability. *Neuron*, **20**:371-380.
- Avdonin, V., Nolan, B., Sabatier, J.-M., De Waard, M., Hoshi, T., 2000. Mechanisms of maurotoxin action on *Shaker* potassium channel. *Biophys. J.* ,**79**: 776-787.
- Baumgartner, W., Islas, L. and Sigworth, F. J. (1999) Two-electrode voltage clamp of *Xenopus* oocytes: voltage errors and compensation for local current flow. *Biophys. J.*, **77**: 1980-1991.
- Becker, S., Prusak-Sochaczewski, E., Zamponi, G., Beck-Sickinger, A.G., Gordon, R. D. and French, R. J. (1992) Action of derivatives of α -conotoxin GIIIA on sodium channels. Single amino acid substitutions in the toxin separately affect association and dissociation rates. *Biochemistry*, **31**:8229-8238.
- Catterall, W. A., Chandy, K. G., Clapham, D. E., Gutman, G. A., Hofmann, F., Harmar, A. J., Abernethy, D. R. and Spedding, M. (2003) International union of pharmacology: approaches to the nomenclature of voltage-gated ion Channels. *Pharmacol Rev*, **55**:573-574.
- Char-Chang, S., Coghlan, M., Sullivan, J. P. and Gopalakrishnan, M. (2000) Potassium channels: molecular defects, diseases, therapeutic opportunities. *Pharmacol. Rev.*, **52**:557-593.
- Chiamvimonvat, N., Pérez-García, M. T., Tomaselli, G.F. and Marbán, E. (1996). Control of ion flux and selectivity by negatively charged residues in the outer mouth of rat sodium channels. *J. Physiol.*, **491**:51-59.
- Coleman, S. K., Newcombe, J., Pryke, J., Doyle, J. O. (1999) Subunit composition of Kv1 channels in human CNS. *J. Neurochem*, **73**: 849–858.

- Covarrubias, M., Wei, A. A., Salkoff, L. (1991) *Shaker*, *Shal*, *Shab*, and *Shaw* express independent K⁺ current systems. *Neuron*, **7**:763-773.
- Craig, A. G., Bandyopadhyay, P. and Olivera, B. M. (1999) Post-translationally modified peptides from *Conus* venoms. *Eur J Biochem*, **264**: 271-275.
- Craig, A. G., Zafaralla, G., Cruz, L. J., Santos, A. D., Hillyard, D. R., Dykert, J., Rivier, J. E., Gray, W. R., Imperial, J., Delacruz, R. G., Sporning, A., Terlau, H., West, P. J., Yoshikami, D. and Olivera, B. M. (1998) An *O*-glycosylated neuroexcitatory *Conus* peptide. *Biochemistry*, **37**: 16019-16025.
- Craig, A.G. (2000) The characterization of conotoxins. *J. Toxicol. Toxin Rev.*, **19**: 53-93.
- Cruz, L. J. and White, J. (1995) Clinical toxicology of *Conus* snail stings. In: *Clinical Toxicology of Animal Venoms*, ed. Meier, J. and White, J., Boca Raton FL, CRC Press, pp: 117-127.
- Cruz, L. J., Gray, W. R., Olivera, B. M., Zeikus, R. D., Kerr, L., Yoshikami, D., and Moczydlowski, E. (1985) *Conus geographus* toxins that discriminate between neuronal and muscle sodium channels. *J. Biol. Chem.*, **260**: 9280-9288.
- Dauplais, M., Lecoq, A., Song, J., Cotton, J., Jamin, N., Gilquin, B., Roumestand, C., Vita, C., de Medeiros, C. L. C., Rowan, E., Harvey, A. L. and Ménez, A. (1997) On the Convergent Evolution of Animal Toxins *J. Biol. Chem.*, **272**: 4302-4309.
- Davies, A. R., and Kozłowski, R. Z. (2001) Kv channel subunit expression in rat pulmonary arteries. *Lung*, **179**: 147-161.
- Doyle, D. A., Cabral, J. M., Pfuetzner, R. A., Kuo, A., Gulbis, J. M., Cohen, S. L., Chait, B. T., and MacKinnon, R. (1998) The structure of the potassium channel: molecular basis of K⁺ conduction and selectivity. *Science*, **280**: 69-77.
- Dudley, S.C., Jr., Todt, H., Lipkind, G. and Fozzard, H.A. (1995) A α -conotoxin-insensitive Na⁺ channel mutant: possible localization of a binding site at the outer vestibule. *Biophys. J.*, **69**:1657-1665.
- England, L. J., Imperial, J., Jacobsen, R., Craig, A. G., Gulyas, J., Akhtar, M., Rivier, J., Julius, D. and Olivera, B. M. (1998) Inactivation of a serotonin-gated ion channel by a polypeptide toxin from marine snails. *Science*, **281**: 575-578.
- Eriksson, M. A. L. and Roux, B. (2002) Modeling the Structure of Agitoxin in Complex with the Shaker K⁺ Channel: A Computational Approach Based on Experimental Distance Restraints Extracted from Thermodynamic Mutant Cycles. *Biophys. J.*, **83**: 2595-2609.
- Fan, C. X., Chen, X. K., Zhang, C., Wang, L. X., Duan, K. L., He, L. L., Cao, Y., Liu, S. Y., Zhong, M. N., Ulens, C., Tytgat, J., Chen, J. S., Chi, C. W. and Zhou, Z. (2003) A novel

- conotoxin from *Conus betulinus*, ω -BtX, unique in cysteine pattern and in function is a specific BK channel modulator. *J. Biol. Chem.*, **278**: 12624-12633.
- Ferber, M., Sporning, A., Jeserich, G., DeLaCruz, R., Watkins, M., Olivera, B. M. and Terlau, H., (2003) A novel *Conus* peptide ligand for K⁺ channels. *J. Biol. Chem.*, **278**: 2177-2183.
- French, R. J., Prusak-Sochaczewski, E., Zamponi, G.W., Becker, S., Kularatna, A.S. and Horn, R. (1996) Interactions between a pore-blocking peptide and the voltage sensor of the sodium channel: an electrostatic approach to channel geometry. *Neuron*, **16**:407-413.
- Gao, Y.-D. and Garcia, M. (2003) Interaction of agitoxin2, charybdotoxin, and iberitoxin with potassium channels: Selectivity between voltage-gated and Maxi-K⁺ channels. *Proteins*, **52**: 146-154.
- Gilquin, B., Racapé, J., Wrisch, A., Visan, V., Lecoq, A., Grissmer, S., Ménez, A. and Gasparini, S. (2002) Structure of the BgK-Kv1.1 complex based on distance restraints Identified by double mutant cycles. *J. Biol. Chem.*, **277**: 37406-37413.
- Goldin, A. L. (1992) Maintenance of *Xenopus laevis* and oocyte injection. *Methods Enzymol.*, **207**: 266-279.
- Goldstein, S. A., Pheasant, D. J., Miller, C. (1994) The charybdotoxin receptor of a *Shaker* K⁺ channel: peptide and channel residues mediating molecular recognition. *Neuron*, **12**:1377-1388.
- Gurdon, J. B., Lane, C. D., Woodland, H. R. and Marbaix, G. (1971) Use of frog eggs and oocytes for the study of messenger RNA and its translation in living cells. *Nature* **233**:177-182.
- Heinemann, S. H. (1995) Guide to data acquisition and analysis. In: *Single-Channel Recording*. Sakmann, B. and Neher, E., New York and London, Plenum Press. Chapt. 3: 53- 91.
- Hidalgo, P. and Mackinnon. R. (1995) Revealing the architecture of a K⁺ channel pore through mutant cycles with a peptide inhibitor. *Science*, **268**: 307-310.
- Hill, J. M., Alewood, P. F., and Craik, D. J. (1996) Three-dimensional solution structure of ω conotoxin GIIIB, a specific blocker of skeletal muscle sodium channels. *Biochemistry*, **35**: 8824-8835.
- Hille, B. (2001) *Ionic channels of excitable membranes*, Sinauer, Sunderland, MA. USA.
- Hodgkin, A. L. and Huxley, A. F. (1952) A quantitative description of membrane current and its application to conduction and excitation in nerve. *J. Physiol. (Lond.)*, **117**: 500-544.
- Hopkins, C., Grilley, M., Miller, C., Shon, K., Cruz, L. J., Gray, W. R., Dykert, J., Rivier, J., Yoshikami, D. and Olivera, B. M. (1995) A new family of *Conus* peptides targeted to the

- nicotinic acetylcholine receptor. *J. Biol. Chem.*, **270**: 22361-22367.
- Hoshi, T., Zagotta, W. N. and Aldrich, R. W. (1990) Biophysical and molecular mechanisms of Shaker potassium channel inactivation. *Science*, **250**: 533-538.
- Hui, K., Lipkind, G., Fozzard, H.A and French, R. J. (2002) Electrostatic and steric contributions to block of the skeletal muscle sodium channel by α -conotoxin. *J. Gen. Physiol.*, **119**:45-54.
- Huys, I., Xu, C.-Q., Wang, C.-Z., Vacher, H., Martin-Eauclaire, M.-F., Chi, C.-W., and Tytgat, J. (2004) BmTx3, a scorpion toxin with two putative functional faces separately active on A-type K⁺ and Herg currents, *Biochem. J.*, **378**: 745-752.
- Ishii, T. M., Zerr, P., Xia, X., Bond, C. T., Maylie, J. and Adelman, J. P. (1998) Site-directed mutagenesis. *Meth. Enzymol.*, **293**: 53-88.
- Jacobsen, R. B. E., Koch, D., Lange-Malecki, B., Stocker, M., Verhey, J., Van Wagoner, R. M., Vyazovkina, A., Olivera, B. M. and Terlau, H. (2000) Single amino acid substitutions in α -conotoxin PVIIA disrupt interaction with the *Shaker* K⁺ Channel. *J. Biol. Chem.*, **275**: 24639- 24644.
- Jiang, Y., Lee, A., Chen, J., Cadene, M., Chait, B. T. and MacKinnon, R. (2002) Crystal structure and mechanism of a calcium-gated potassium channel. *Nature*, **417**: 515-522.
- Jiang, Y., Lee, A., Chen, J., Vanessa, R., Cadene, M., Chait, B. T. and MacKinnon, R. (2003) X-ray structure of a voltage-dependent K⁺ channel. *Nature*, **423**: 33-41.
- Kaufenstein, S., Huys, I., Lamthanh, H., Stöcklin, R., Sotto, F., Ménez, A., Tytgat, J. and Mebs, D. A. (2003) novel conotoxin inhibiting vertebrate voltage-sensitive potassium channels. *Toxicon*, **42**: 43-52.
- Kerr, P. M., Clement-Chomienne, O., Thorneloe, K. S., Chen, T. T., Ishii, K., Sontag, D. P., Walsh, M. P., Cole, W. C. (2001) Heteromultimeric Kv1.2-Kv1.5 channels underlie 4-aminopyridine- sensitive delayed rectifier K⁺ current of rabbit vascular myocytes. *Circ. Res.*, **89**: 1038-1044.
- Kohn, A. J., Saunders, P. R. and Wiener, S. (1960) Preliminary studies on the venom of the marine snail *Conus*. *Ann. N.Y. Acad. Sci.*, **90**: 706-725.
- Krieg, P. A. and Melton, D. A. (1987) *In vitro* RNA synthesis with SP6 RNA polymerase. *Meth. Enzymol.*, **155**: 397-415.
- Lancelin, J. M., Kohda, S., Tate, Y., Yanagawa, T., Satake, A. M., and Inagaki, F. (1991) Tertiary structure of α -conotoxin GIIIA in aqueous-solution. *Biochemistry*, **30**: 6908-6916.

- Lewis, R. S. and Cahalan, M. D. (1995) Potassium and calcium channels in lymphocytes. *Annu. Rev. Immunol.*, **13**: 623-653.
- Li, R. A., Velez, P., Chiamvimonvata, N., Tomasellia, G. F. and Marbán, E. (1999) Charged residues between the selectivity filter and S6 segments contribute to the permeation phenotype of the sodium channel. *J. Gen. Physiol.*, **115**: 81-92.
- Li, R. A., Ennis, I.L., French, R. J., Dudley Jr., S. C., Tomaselli, G. F. and Marbán, E. (2001). Clockwise domain arrangement of the sodium channel revealed by α -conotoxin (GIIIA) docking orientation. *J. Biol. Chem.*, **276**:11072-11077.
- Liman, E. R., Tytgat, J. and Hess, P. (1992) Subunit stoichiometry of a mammalian K⁺ channel determined by construction of multimeric cDNAs. *Neuron*, **9**:861-871.
- MacKinnon, R. and Miller, C. (1988) Mechanism of charybdotoxin block of the high-conductance, Ca²⁺- activated K⁺ channel. *J. Gen. Physiol.*, **91**: 335-349.
- MacKinnon R. and Miller, C. (1989) Mutant potassium channels with altered binding of charybdotoxin, a pore-blocking peptide inhibitor. *Science*, **245**:1382-1385.
- MacKinnon, R. (1991) Determination of the subunits stoichiometry of a voltage-activated potassium channel. *Nature*, **350**: 232-235.
- MacKinnon, R. (2003) Potassium channels. *FEBS Lett.*, **555**: 62-65.
- MacKinnon, R., Heginbotham, L. and Abramson, T. (1990) Mapping the receptor site for charybdotoxin, a pore-blocking potassium channel inhibitor. *Neuron*, **5**: 767-771.
- McIntosh, J. M., Santos, A. D., and Olivera, B. M. (1999) *Conus* peptides targeted to specific nicotinic acetylcholine receptor subtypes. *Annu Rev Biochem*, **68**: 59-88.
- Methfessel, C., Witzemann, V., Takahashi, T., Mishina, M., Numa, S., and Sakmann, B. (1986) Patch clamp measurements on *Xenopus laevis* oocytes: currents through endogenous channels and implanted acetylcholine receptor and sodium channels. *Pflugers Arch.*, **407**: 577-588.
- Miller, C. (1995) The charybdotoxin family of K⁺ channel-blocking peptides. *Neuron*, **15**: 5-10.
- Moran, O. (2001) Molecular simulation of the interaction of α -PVIIA with the *Shaker* potassium channel pore. *Eur. Biophys. J.*, **30**: 528-536.
- Mouhat S., Mosbah, A., V. Visan, Wulff. H., Delepierre, M., H. Darbon, Grissmer, S., De Waard, M. and Sabatier, J. (2004) The 'functional' dyad of scorpion toxin Pi1 is not itself a prerequisite for toxin binding to the voltage-gated Kv1.2 potassium channels. *Biochem. J.*, **377**: 25-36.

- Mullmann, T. J., Munujos, P., Garcia, M. L. and Giangiacomo, K. M. (1999) Electrostatic mutations in Iberitoxin as a unique tool for probing the electrostatic structure of the Maxi-K Channel outer vestibule. *Biochemistry*, **38**: 2395-2402.
- Nguyen, T. D. and Jeserich, G. (1998) Molecular structure and expression of *Shaker* type potassium channels in glial cells of trout CNS. *J. Neurosci. Res.*, **57**:284-292.
- Nguyen, T. D., Rabe, H. Terlau, H. and Jeserich, G. (2000) Isolation and heterologous expression of two genomic clones encoding *Shaker*-related potassium channels of trout CNS. *J. Neurosci. Res.*, **60**: 174-183.
- Olivera, B. M. (1997) E.E. Just Lecture 1996, *Conus* venom peptides, receptor and ion channel targets and drug design: 50 million years of neuropharmacology. *Mol. Biol. Cell*, **8**: 2101-2109.
- Olivera, B. M. (2002) *Conus* venom peptides: reflections from the biology of clades and species. *Annu. Rev. Ecol. Syst.*, **33**: 25-42.
- Olivera, B. M. and Cruz, L. J. (2001) Conotoxins, in retrospect. *Toxicon*, **39**: 7-14.
- Olivera, B. M., Gray, W. R., Zeikus, R., McIntosh, J. M., Varga, J., Rivier, J., De Santos, V. and Cruz, L. J. (1985) Peptide neurotoxins from fishhunting cone snails. *Science*, **230**: 1338-1343.
- Olivera, B. M., McIntosh, J. M., Cruz, L. J., Luque, F. A. and Gray, W. R. (1984) Purification and sequence of a presynaptic peptide toxin from *Conus geographus* venom. *Biochemistry*, **23**: 5087-5090.
- Olivera, B. M., Rivier, J., Clark, C., Ramilo, C. A., Corpuz, G. P., Abogadie, F. C., Mena, E., Woodward, S. R., Hillyard, D. R. and Cruz, L. J. (1990) Diversity of *Conus* neuropeptides. *Science*, **249**: 257-263.
- Park, C. and Miller, C. (1992) Interaction of charybdotoxin with permeant ions inside the pore of a K⁺ channel. *Neuron*, **9**: 307-313.
- Po, S., Roberds, S., Snyders, D. J., Tamkun, M. M. and Bennett, P. B. (1993) Heteromultimeric assembly of human potassium channels. Molecular basis of a transient outward current? *Circ. Res.*, **72**: 1326-1336.
- Po, S., Snyders, D. J., Baker, R., Tamkun, M. M., Bennett, P. B. (1992) Functional expression of an inactivating potassium channel cloned from human heart. *Circ. Res.*, **71**: 732-736.
- Pongs, O., Kecskemethy, N., Müller, R., Krah-Jentgens, I., Baumann, A., Kiltz, H. H., Canal, I., Llamazares, S., and Ferrus, A. (1988) *Shaker* encodes a family of putative potassium channel proteins in the nervous system of *Drosophila* *EMBO J*, **7**:1087-1096.

- Ranganathan, R., Lewis, J. H. and MacKinnon, R. (1996) Special localization of the K⁺ channel selectivity filter by mutant cycle-based structure analysis. *Neuron*, **16**: 131-139.
- Rasband, M. N. and Trimmer, J.S., (2001) Subunit composition and novel localization of K⁺ channels in spinal chord. *J. Comp. Neurol.*, **429**: 166-176.
- Rasband, M. N., Park, E. W., Vanderah, T. W., Lai, J., Porreca, F. and Trimmer, J. S., (2001) Distinct potassium channels on painsensing neurons. *Proc. Natl Acad. Soc.* **98**: 13373–13378.
- Rauer, H., Pennington, M., Cahalan, M. and Chandy, K. G. (1999) Structural conservation of the pores of calcium-activated and voltage-gated potassium channels determined by a sea anemone toxin. *J. Biol. Chem.*, **274**: 21885-21892.
- Rettig, J., Heinemann, S. H., Wunder, F., Lorra, C., Parcej, D. N., Dolly, J. O. and Pongs, O. (1994) Inactivation properties of voltage-gated K⁺ channels altered by presence of β -subunit. *Nature*, **369**: 289-294.
- Röckel, D., Korn, W. and Kohn, A. J. (1995). *Manual of the Living Conidae*. Verlag Christa Hemmen Wiesbaden, Germany.
- Rodriguez de la Vega, R. C., Merino, E., Becerril, B., and Possani, L. D. (2003) Novel interactions between K⁺ channels and scorpion toxins, *Trends Pharmacol. Sci.i*, **24**: 222-227.
- Rudy, B. (1988) Diversity and ubiquity of K⁺ channels. *Neuroscience*, **25**: 729-749.
- Sambrook, J., and Russell, D. W. (2001) *Molecular Cloning: A Laboratory Manual*, Third Edition, Cold Spring Harbor Laboratory Press, Cold Spring Harbor, NY
- Savarin, P., Guennegues, M., Gilquin, B., Lamthanh, H., Gasparini, S., Zinn-Justin, S. and Ménez, A. (1998) Three-dimensional structure of kappa-conotoxin PVIIA, a novel potassium channel-blocking toxin from cone snails. *Biochemistry*, **37**: 5407-5416.
- Scanlon, M. J., Naranjo, D., Thomas, L., Alewood, P. F., Lewis, R. J., Craik, D. J. (1997) Solution structure and proposed binding mechanism of a novel potassium channel toxin kappa-conotoxin PVIIA. *Structure*, **5**:1585-1597.
- Schreiber, G. and Fersht, A. R. (1995) Energetics of protein-protein interactions: analysis of the barnase-barstar interface by single mutations and double mutant cycles. *J. Mol. Biol.*, **248**: 478-486.
- Shen, N., V. and Pfaffinger, P. J. (1995) Molecular recognition and assembly sequences involved in the subfamily-specific assembly of voltage-gated K⁺ channel subunit proteins. *Neuron*, **14**: 625-633.

- Shon, K., Stocker, M., Terlau, H., Stühmer, W., Jacobsen, R., Walker, C., Grilley, M., Watkins, M., Hillyard, D. R., Gray, W. R. and Olivera, B. M. (1998) ω -conotoxin PVIIA: A peptide inhibiting the *Shaker* K⁺ channel. *J. Biol. Chem.*, **273**: 33-38.
- Sokolova, O., Kolmakova-Partensky, L. and Grigorieff, N. (2001) Three-dimensional structure of a voltage-gated potassium channel at 2.5 nm resolution. *Structure*, **9**: 215-220.
- Srinivasan, K. N., Sivaraja, V., Huys, I., Sasaki, T., Cheng, B., Kumar, T. K. S., Sato, K., Tytgat, J., Yu, C., Ching San, B. C., Ranganathan, S., Bowie, J. H., Kini, R. M. and Gopalakrishnakone, P. (2002) ω -hefutoxin1, a novel toxin from the scorpion *Heterometrus fulvipes* with unique structure and function - Importance of the functional diad in potassium channel selectivity. *J. Biol. Chem.*, **277**: 30040-30047.
- Stampe, P., Kolmakova-Partensky, L. and Miller, C. (1992) Mapping hydrophobic residues of the interaction surface of charybdotoxin. *Biophys J.*, **62**: 8-9.
- Stampe, P., Kolmakovapartensky, L. and Miller, C. (1994) Intimations of K⁺ channel structure from a complete functional map of the molecular-surface of charybdotoxin. *Biochemistry*, **33**, 443-450.
- Stühmer, W. (1992) Electrophysiological recordings from *Xenopus* oocytes. *Meth. Enzymol.*, **207**: 319-339.
- Stühmer, W. (1998) Electrophysiologic recordings from *Xenopus* oocytes. *Meth. Enzymol.*, **293**: 280-300.
- Stühmer, W. and Parekh, A. B. (1995) Electrophysiological recordings from *Xenopus* oocytes. In: *Single channel recording*. Sakmann, B. and Neher, E., New York and London, Plenum Press, Chapt: **15**: 341-355.
- Stühmer, W., Ruppersberg, J. P., Schröter, K. H., Sakmann, B., Stocker, M., Giese, K. P., Perschke, A., Baumann, A. and Pongs, O. (1989) Molecular basis of functional diversity of voltage-gated potassium channels in mammalian brain. *EMBO J.* **11**: 3235-3244.
- Sudarslal, S., Singaravadelan, G., Ramasamy, P. Ananda, K. Sarma, S. P., Sikdar, S. K., Krishnan, K. S. and Balaram, P. (2004) A novel 13 residue acyclic peptide from the marine snail, *Conus monile*, targets potassium channels. *Biochem. Biophys. Res. Comm.*, **317**: 682-688.
- Tempel, B. L., Papazian, D. M., Schwarz, T. L., Jan, Y. N. and Jan, L. Y. (1987) Sequence of probable potassium-channel component encoded at the *Shaker* locus of *Drosophila*. *Science*, **237**:770-775.
- Terlau, H. and Stühmer, W. (1998) Structure and function of voltage-gated ion channels. *Naturwissenschaften*, **85**: 437-444.

- Terlau, H., Boccaccio, A., Olivera, B. M. and Conti, F. (1999) The block of *Shaker* K⁺ channels by α -conotoxin PVIIA is state dependent. *J. Gen. Physiol.*, **114**: 125-140.
- Terlau, H., Shon, K., Grilley, M., Stocker, M., Stühmer, W. and Olivera, B. M. (1996) Strategy for rapid immobilization of prey by a fish-hunting cone snail. *Nature*, **381**: 148-151.
- Terlau, H. and Olivera, B. M. (2004) Conus venoms: a rich source of novel ion channel-targeted peptides. *Physiol. Rev.*, **84**: 41-68.
- Van Wagoner, R. M., Jacobsen, R. B., Olivera, B. M., and Ireland, C. M. (2003a) Characterization and three-dimensional structure determination of α -conotoxin PIIIF, a novel noncompetitive antagonist of nicotinic acetylcholine receptors, *Biochemistry*, **42**: 6353-6362.
- Van Wagoner, R. M., and Ireland, C. M. (2003b) An improved solution structure for α -conotoxin PIIIE, *Biochemistry*, **42**: 6347-6352.
- Vassilev, P. M., Scheuer, T. and Catterall, W. A. (1988) Identification of an intracellular peptide segment involved in sodium channel inactivation. *Science*, **241**: 1658-1661.
- Villmann, C., Bull, L. and Hollmann, M. (1997) Kainate binding proteins possess functional ion channel domains. *J Neurosci*, **17**:7634-7643.
- Wakamatsu, K., Kohda, D., Hatanaka, H., Lancelin, J. M., Ishida, Y., Oya, M., Nakamura, H., Inagaki, F., and Sato, K. (1992) Structure-activity relationships of α -conotoxin GIIIA: structure determination of active and inactive sodium-channel blocker peptides by NMR and simulated annealing calculations, *Biochemistry*, **31**: 12577-12584.
- West, J. W., Patton, E. D., Scheuer, T., Wang, Y. and Goldin, A. L. (1992) A cluster of hydrophobic amino acid residues required for fast Na⁺-channel inactivation. *Pro. Natl. Acad. Sci. USA*, **89**: 1091.
- Woodward, S. R., Cruz, L. J., Olivera, B. M. and Hillyard, D. R. (1990) Constant and hypervariable regions in conotoxin propeptides. *EMBO J*, **1**: 1015-1020.
- Xu, C.-Q., Zhu, S.-Y., Chi, C.-W., and Tytgat, J. (2003) Turret and pore block of K⁺ channels: what is the difference? *Trends Pharmacol. Sci.* **24**, 446-448.
- Zagotta, W. N., Hoshi, T. and Aldrich, R. W. (1990) Restoration and inactivation in mutants of *Shaker* potassium channels by a peptide derived from *ShB*. *Science*, **250**: 568-571.

ACKNOWLEDGEMENT

I would like to thank the two referees of the thesis; Prof. Venugopalan Ittekkot and Prof. Heinrich Terlau and the committee members of the thesis defense, Prof. Claudio Richter and Prof. Michael Koch, for their time and efforts. My grateful thanks to Prof. Walter Stühmer for his generosity and invaluable logistic support. I am greatly indebted to Prof. Heinrich Terlau for his direct support and his invaluable advice. He was a great group leader and patient co-advisor. Without him, this work would not be possible.

I would like to acknowledge my colleagues in the group of Molecular and Cellular Neuropharmacology at the Max-Planck-Institute for Experimental Medicine in Göttingen for their collaboration and solidarity. In our group, special thanks to Dr. Michael Ferber for his assistant help, technical support and practical work in this project. The technical assistance of Annett Sporning, Mona Honemann, Nina Strüver and Tanja Nilsson is greatly appreciated. My sincere thanks for my colleagues Drs.: Anna Boccaccio, Rocio Finol, Dietlind Koch, Martina Blashke and Manuel Gebauer for their endless support and kindness. To all my friends and colleagues in the department of Molecular Biology and Neuronal signaling at Max-Planck-Institute, my deep appreciation for wonderful friendship and research atmosphere. I would like to express my sincere gratefulness to Ute Rust and Svea Viola Dettmer for unconditional assistance with the management of never ending paperwork and kindness.

My especial grateful to the co-operative groups involved in this work: the lab of Prof. Jean Rivier (Salk Institute, San Diego, USA), the lab of Prof. Baldomero Olivera (Salt Lake City, Utah, USA), the group of Dr. Teresa Carlomagno, in the department of Prof. Griesinger (MPIBC, Göttingen, Germany). I owe a special thank to Prof. R. J. French for his helpful discussions during this project. This work was funded by the Biofuture Prize from the German Ministry of Education and Research (Förderkennzeichen: 0311859) and by the Max-Planck-Gesellschaft.

I am especially grateful to my parents, brothers, sisters and relatives for their continuous support and love. To all my friends...love you all and keep blooming in the sky...

Ahmed Al-Sabi'

September, 25th, 2004

Curriculum Vitae et studiorum

Ahmed Nafi' (Sulaiman) Mohd. Al-Sabi'

- 22.11. 1974: Born in Kuwait
- 1981-1985: Ground school, AL-Razi School, Salmeyah, Kuwait.
- 1985-1989: Middle school, Al-Jareer school, Medan-Hawalli, Kuwait.
- 1989-1990: Secondary school, Al-Rhomaythiyah school, Al-Rhomaythiyah, Kuwait.
- 1990-1991: Secondary school, Idoon school, Irbid, Jordan.
- 1991-1993: Secondary high school, Irbid High School, Irbid, Jordan.
- 1993: General Secondary Education Irbid High School, Irbid, Jordan.
- 1993-1997: B.Sc. in Biological Sciences (Department of Biological Sciences-Yarmouk University-Irbid) Major: Biological Sciences.
- 1997-2001: M.Sc. in Biology (Department of Biological Sciences-Yarmouk University-Irbid-Jordan) Major: Biological Sciences-Marine Biology.
Thesis: Sponges in the Jordanian coastline of the Gulf of Aqaba (Jordan)
- 2001-2004: PhD. Student at the Max-Planck Institute for Experimental Medicine, department of Molecular Biology of Neuronal signals by Prof. Dr. Walter Stühmer; supervised by Prof. Dr. Heinrich Terlau, Göttingen, Germany.
Thesis: Structural and functional studies of α M-conotoxin RIIK interaction with *Shaker*-related potassium channels from trout fish (*TShal*).